WT-1317 (EX)
EXTRACTED VERSION

OPERATION REDWING

40985

Project 2.63
Characterization of Fallout

Pacific Proving Grounds
May-July 1956

Headquarters Field Command
Defense Atomic Support Agency
Sandia Base, Albuquerque, New Mexico

March 15, 1961

NOTICE

This is an extract of WT-1317, which remains classified SECRET/RESTRICTED DATA as of this date.

Extract version prepared for:

Director
DEFENSE NUCLEAR AGENCY
Washington, D.C. 20305

1 JUNE 1982

Approved for public release; distribution unlimited.

TABLE 2.3 STATION LOCATIONS IN THE ATOLL AREA

Station	Shot Cherokee North Latitude and East Longitude		Shot Zuni North Latitude and East Longitude		Shot Flathead North Latitude and East Longitude		Shot Navajo North Latitude and East Longitude		Shot Tewa North Latitude and East Longitude	
	deg	min	deg	min	deg	min	deg	min	deg	min
YFNB 13 (E)	11	35.3	11	40.0	11	40.0	11	39.1	11	37.5
	165	31.2	165	17.2	165	17.2	165	16.2	165	27.0
YFNB 29 (G,H)	11	37.5	11	37.5	11	37.5	11	36.2	11	37.4
	165	27.0	165	27.0	165	27.0	165	29.8	165	14.2
How Island (F) *	148,320 N		148,320 N		148,320 N		148,320 N		148,320 N	
	167,360 E		167,360 E		167,360 E		167,360 E		167,360 E	
How Island (K) *	148,450 N		148,450 N		148,450 N		148,450 N		148,450 N	
	167,210 E		167,210 E		167,210 E		167,210 E		167,210 E	
George Island (L) *	168,530 N		168,530 N		168,530 N		168,530 N		168,530 N	
	131,250 E		131,250 E		131,250 E		131,250 E		131,250 E	
William Island (M) *	109,030 N		109,030 N		109,030 N		—		—	
	079,540 E		079,540 E		079,540 E		—		—	
Charlie Island (M) *	—		—		—		172,150 N		172,150 N	
	—		—		—		081,150 E		081,150 E	
Raft-1 (P)	11	35.1	11	35.1	11	35.1	11	35.1	11	35.1
	165	27.6	165	27.6	165	27.6	165	27.6	165	27.6
Raft-2 (R)	11	34.6	11	34.6	11	34.6	11	34.6	11	34.6
	165	22.2	165	22.2	165	22.2	165	22.2	165	22.2
Raft-3 (S)	11	35.4	11	35.4	11	35.4	11	35.4	11	35.4
	165	17.2	165	17.2	165	17.2	165	17.2	165	17.2
Skiff-AA	12	06.1	12	06.1	12	06.1	12	05.4	12	05.4
	164	47.0	164	47.0	164	47.0	164	44.9	164	44.9
Skiff-BB	12	11.6	12	11.6	12	11.6	12	11.5	12	11.5
	165	10.0	165	10.0	165	10.0	165	07.5	165	07.5
Skiff-CC	12	11.3	12	11.3	12	10.7	12	11.8	12	11.8
	165	23.0	165	23.0	165	17.6	165	20.9	165	20.9
Skiff-DD	12	11.5	12	11.5	12	11.5	12	11.5	12	11.5
	165	40.0	165	40.0	165	40.0	165	40.0	165	40.0
Skiff-EE	12	11.3	12	11.3	12	11.3	12	11.3	12	11.3
	165	57.3	165	57.3	165	57.3	165	57.3	165	57.3
Skiff-FF	12	02.4	12	02.4	12	03.5	12	02.4	12	02.4
	166	15.5	166	15.5	166	14.2	166	15.5	166	15.5
Skiff-GG	11	57.8	11	57.8	11	57.8	—	—	12	01.1
	165	13.8	165	13.8	165	13.8	—	—	165	10.2
Skiff-HH	12	01.3	12	01.3	12	02.0	12	02.0	12	02.0
	165	22.9	165	22.9	165	21.6	165	21.6	165	21.6
Skiff-KK	12	02.0	12	02.0	12	02.0	12	02.0	12	02.0
	165	40.0	165	40.0	165	40.0	165	40.0	165	40.0
Skiff-LL	12	02.0	12	02.0	12	02.0	12	02.0	12	02.0
	165	58.0	165	58.0	165	58.0	165	58.0	165	58.0
Skiff-MM	11	52.8	11	52.8	11	52.8	11	52.7	11	52.7
	164	58.4	164	58.4	164	58.4	164	56.0	164	56.0
Skiff-PP	11	52.0	—	—	11	50.5	11	52.0	11	52.0
	165	22.8	—	—	165	23.9	165	22.8	165	22.8
Skiff-RR	11	51.0	11	51.0	11	53.3	11	52.3	11	52.3
	165	40.0	165	40.0	165	35.2	165	39.7	165	39.7
Skiff-SS	11	50.0	11	50.0	11	51.1	—	—	—	—
	165	58.0	165	58.0	165	58.0	—	—	—	—
Skiff-TT	11	50.8	11	50.8	11	50.8	11	50.8	11	50.8
	166	15.0	166	15.0	166	15.0	166	15.0	166	15.0
Skiff-UU	11	42.5	11	42.5	11	42.5	—	—	—	—
	165	47.5	165	47.5	165	47.5	—	—	—	—
Skiff-VV	11	21.7	11	21.7	—	—	—	—	—	—
	165	19.5	165	19.5	—	—	—	—	—	—
Skiff-WW	—	—	—	—	—	—	—	—	11	43.2
	—	—	—	—	—	—	—	—	165	11.5
Skiff-XX	—	—	—	—	—	—	—	—	11	41.2
	—	—	—	—	—	—	—	—	164	55.1
Skiff-YY	—	—	—	—	—	—	—	—	11	54.0
	—	—	—	—	—	—	—	—	164	36.4

* Holmes and Narver coordinates.

TABLE 2.4 SHIP LOCATIONS AT TIMES OF PEAK ACTIVITY

The symbols t_a and t_c represent the times of arrival and cessation of fallout, respectively; t_p is the time of peak observed ionization rate.

Station	Shot Cherokee			Shot Zuni			Shot Flathead			Shot Navajo			Shot Tewa		
	Time	North Latitude and East Longitude		Time	North Latitude and East Longitude		Time	North Latitude and East Longitude		Time	North Latitude and East Longitude		Time	North Latitude and East Longitude	
	TSD, hr	deg	min	TSD, hr	deg	min	TSD, hr	deg	min	TSD, hr	deg	min	TSD, hr	deg	min
YAG 40	6 (t_a) *	12	40.0	3.4 (t_a)	12	22.0	8.0 (t_a)	12	19.7	6.0 (t_a)	12	12.3	4.4 (t_a)	12	04.5
(A, B)		164	20.0		165	45.8		165	20.8		165	08.8		164	44.8
	9 (t_p) *	12	40.0	4.3	12	22.0	11.6	12	23.2	6.6	12	12.0	6.2	12	04.5
		164	35.0		165	37.0		165	31.2		165	11.0		164	46.9
				4.8	12	22.0	12.8	12	34.7	7.3	12	11.0	7.2 (t_p)	12	06.0
					165	30.3		165	34.0		165	10.0		164	49.2
				5.3	12	22.5	13.8	12	26.0	9.2	12	13.0	8.2	12	06.4
					165	24.5		165	37.1		165	04.3		164	53.0
				5.8	12	22.0	17.0 (t_p)	12	31.9	11.1	12	11.0	8.5 (t_c)	12	06.2
					165	19.0		165	43.5		165	04.8		164	52.8
				6.3	12	23.0	22 (t_c)	12	41.8	12.1	12	12.0			
					165	15.4		165	54.3		165	04.8			
				6.7 (t_p)	12	23.5				12.3 (t_p)	12	12.2			
					165	15.7					165	04.2			
				7.4 (t_c)	12	24.4				13.1	12	13.0			
					165	16.2					165	01.0			
										16 (t_c)	12	09.9			
											164	59.5			
YAG 39	10 (t_a) *	13	18.0	12 (t_a)	13	00.6	4.5 (t_a)	12	04.2	2.3 (t_a)	12	01.8	2.0 (t_a)	12	05.6
(C)		163	42.0		165	02.2		165	23.4		165	18.3		165	12.0
	12 (t_p) *	12	20.0	12.6	13	00.6	5.1	12	04.7	4.6	11	59.7	2.2	12	03.5
		163	40.0		165	03.0		165	18.0		165	20.0		165	12.0
				14.6	12	53.0	6.1	12	06.0	5.6	12	01.7	2.7	12	04.0
					165	02.8		165	25.0		165	19.5		165	13.1
				16.1	13	00.0	8.1	12	03.0	6.0 (t_p)	11	59.3	4.7	12	01.5
					165	07.1		165	26.0		165	20.7		165	18.0
				17.6	13	03.8	10.1	12	07.0	6.6	11	57.0	5.0 (t_p)	12	01.6
					165	00.0		165	27.0		165	22.0		165	18.2
				18.6	13	00.4	11.0 (t_p)	12	05.6	8.6	12	02.0	5.3 (t_c)	12	01.8
					165	00.6		165	27.0		165	20.0		165	18.3
				19.6	12	58.0	12.1	12	04.0	9.6	11	59.0			
					165	08.0		165	27.0		165	19.0			
				20.6	12	59.0	13 (t_c)	12	05.1	11.6	11	58.0			
					165	01.2		165	27.8		165	20.0			
				21.6	13	00.6				12.6	11	57.0			
					165	10.7					165	18.0			
				24.6	13	00.0				14.6	11	55.0			
					165	11.4					165	23.5			

TABLE 2.4 CONTINUED

The symbols t_a and t_c represent the times of arrival and cessation of fallout, respectively; t_p is the time of peak observed ionization rate.

Station	Shot Cherokee			Shot Zuni			Shot Flathead			Shot Navajo			Shot Tewa		
	Time	North Latitude and East Longitude		Time	North Latitude and East Longitude		Time	North Latitude and East Longitude		Time	North Latitude and East Longitude		Time	North Latitude and East Longitude	
	TSD, hr	deg	min	TSD, hr	deg	min	TSD, hr	deg	min	TSD, hr	deg	min	TSD, hr	deg	min
YAG 39				25 (t_p)	13	00.8				15 (t_c)	12	00.1			
(C)					165	10.6					165	20.1			
				26.6	13	03.0									
					165	08.0									
				29 (t_c)	13	02.4									
					165	10.7									
LST 611	20 (t_p) †	14	20.0	18 (t_p) †	13	41.5	6.6 (t_a)	12	06.9	3.0 (t_a)	11	38.2	7.0 (t_a)	12	27.8
(D)		163	40.0		164	22.0		164	40.0		164	39.5		164	40.5
							7.3	12	00.0	3.6	11	35.0	7.2	12	25.8
								164	40.0		164	40.0		164	38.9
							7.6	12	00.0	4.4	11	33.7	10.2	12	24.0
								164	42.0		164	41.8		164	48.3
							8.3	12	01.6	5.1	11	35.6	12.2	12	25.5
								164	43.5		164	41.5		164	49.0
							9.1 (t_p)	12	02.0	6.1 (t_p)	11	34.1	13.2	12	25.0
								164	47.0		164	42.4		164	50.5
							12.6	12	03.0	7.1	11	34.8	13.6 (t_p)	12	25.3
								165	01.0		164	41.5		164	50.4
							15.6	12	05.0	7.6	11	37.2	14 (t_c)	12	25.4
								165	13.0		164	41.0		164	50.3
							18.2	11	46.0	10.1	11	35.8			
								165	08.0		164	39.5			
							20 (t_c)	11	47.4	12.1	11	34.2			
								165	16.2		164	39.6			
										12.9	11	33.7			
											164	38.7			
										13 (t_c)	11	33.9			
											164	38.8			

* Questionable value; activity near background level.

† Predicted value; no fallout occurred.

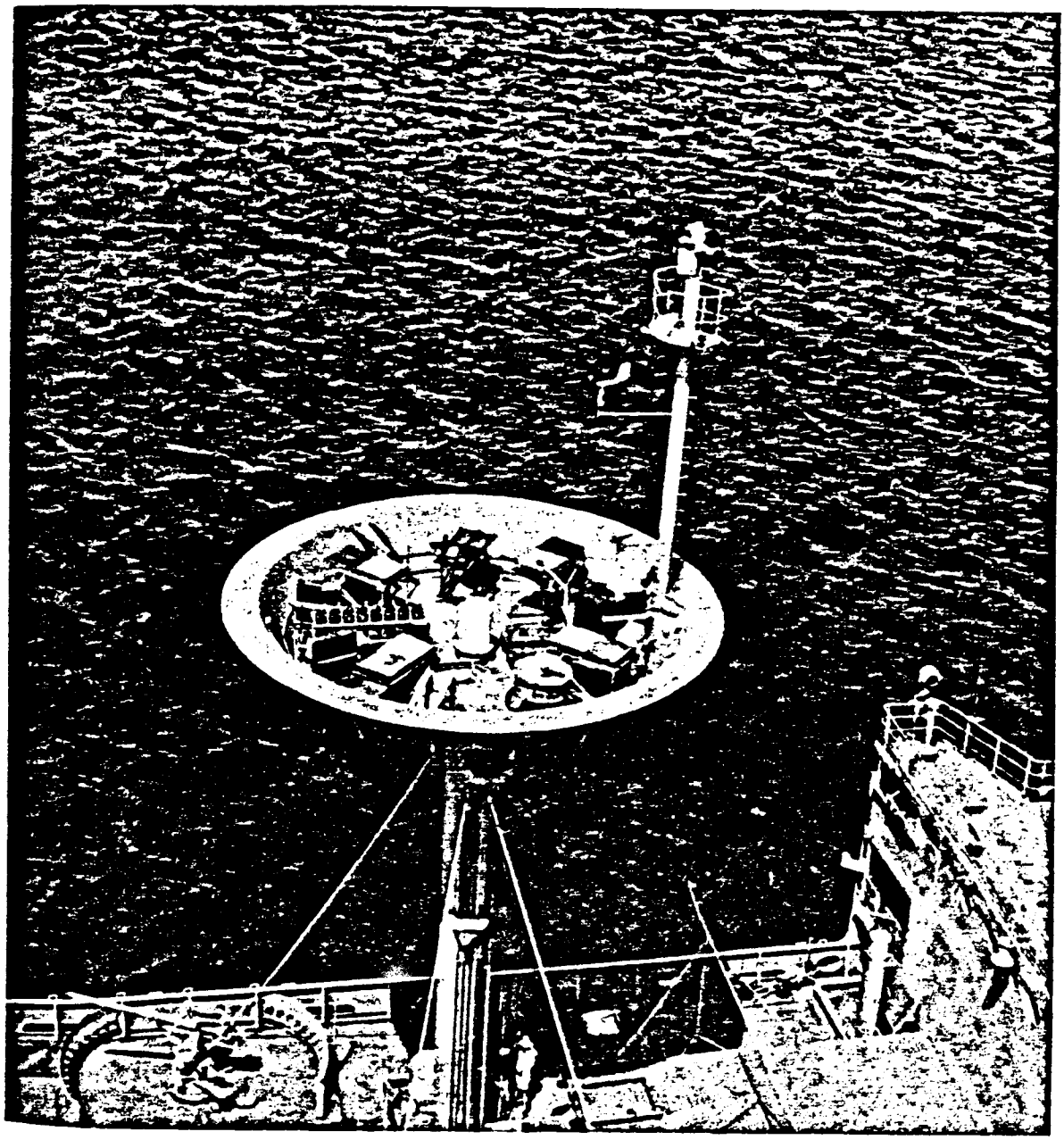

Figure 2.1 Aerial view of major sampling array.

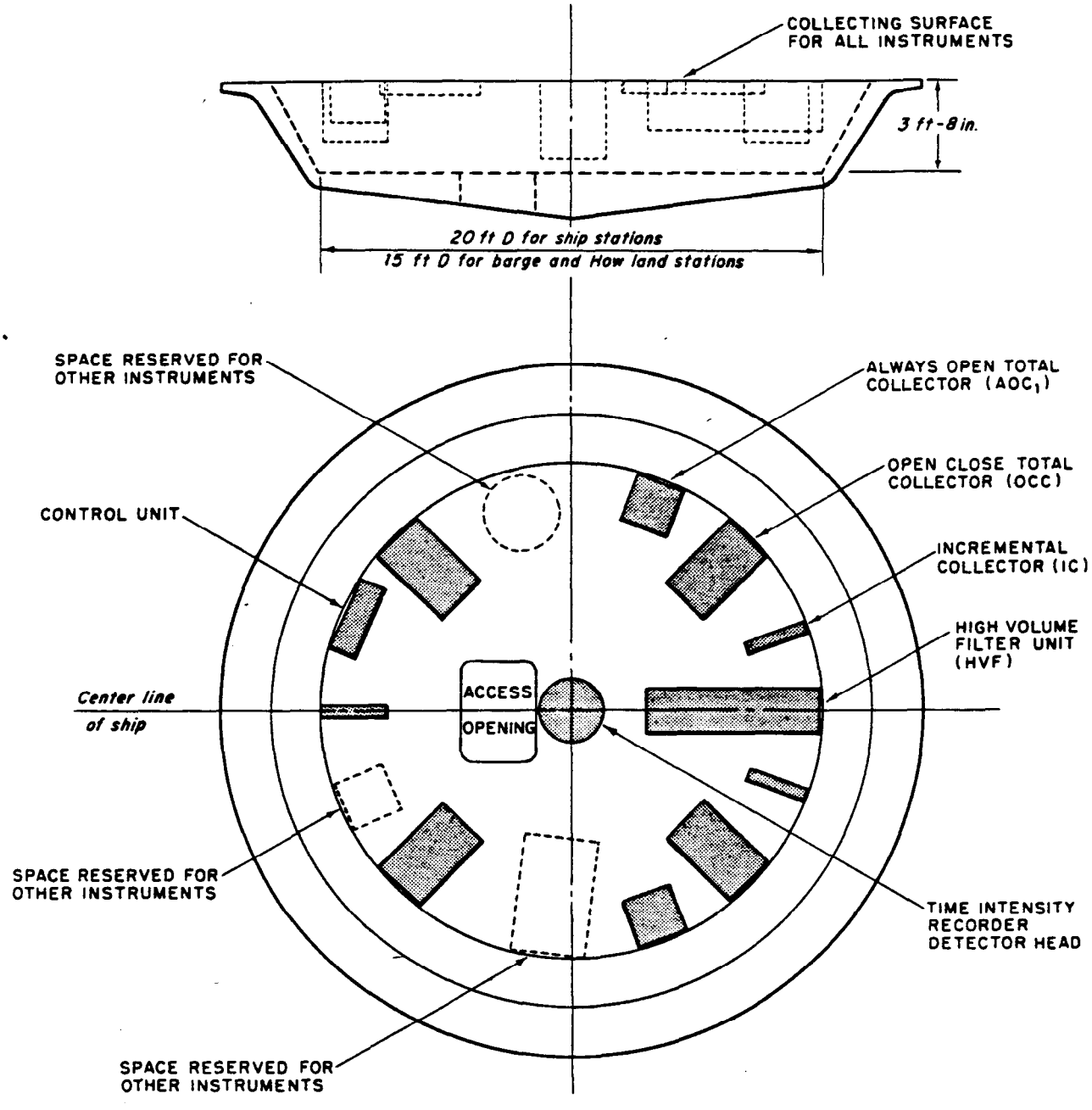

Figure 2.2 Plan and elevation of major sampling array.

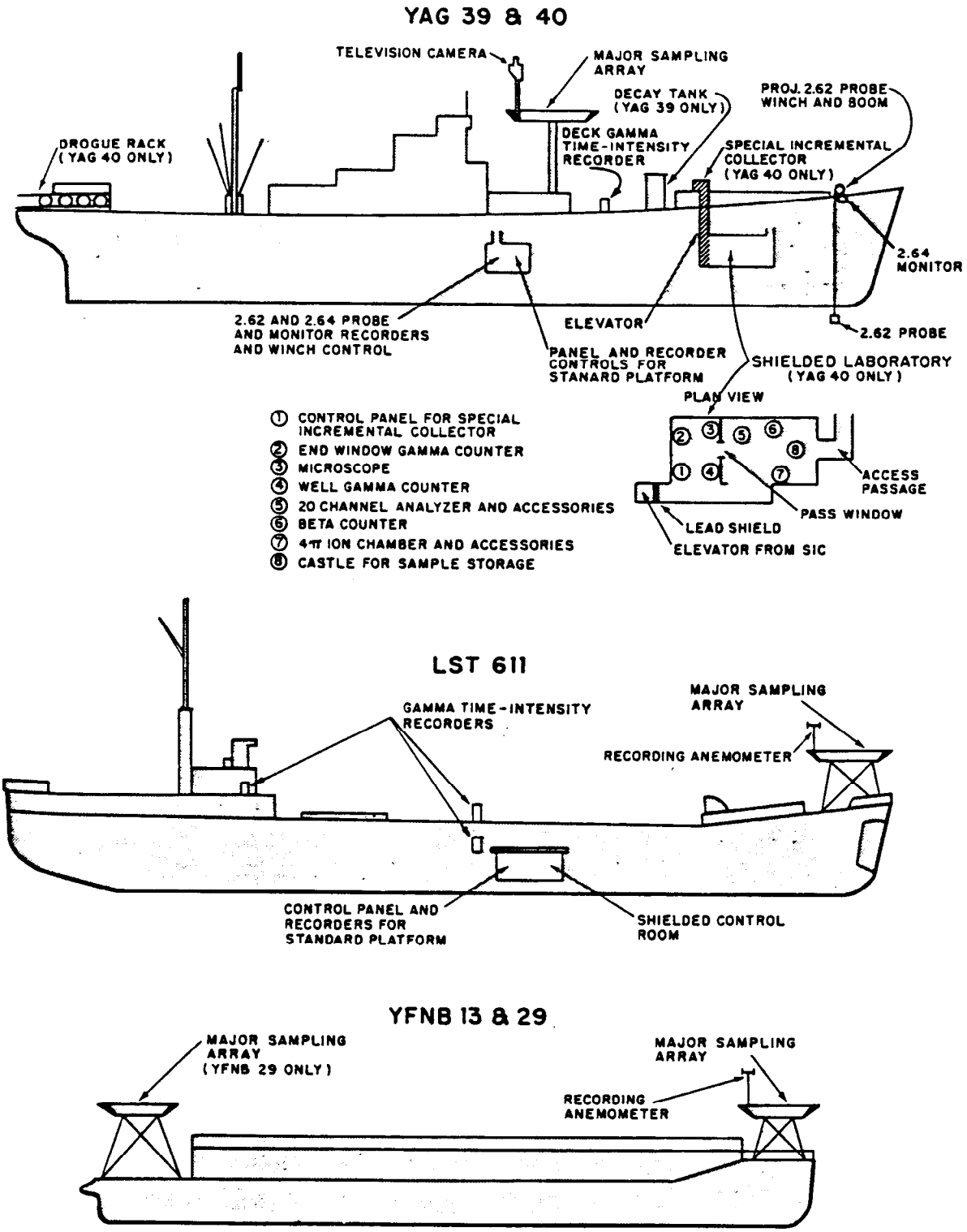

Figure 2.3 Ship and barge stations.

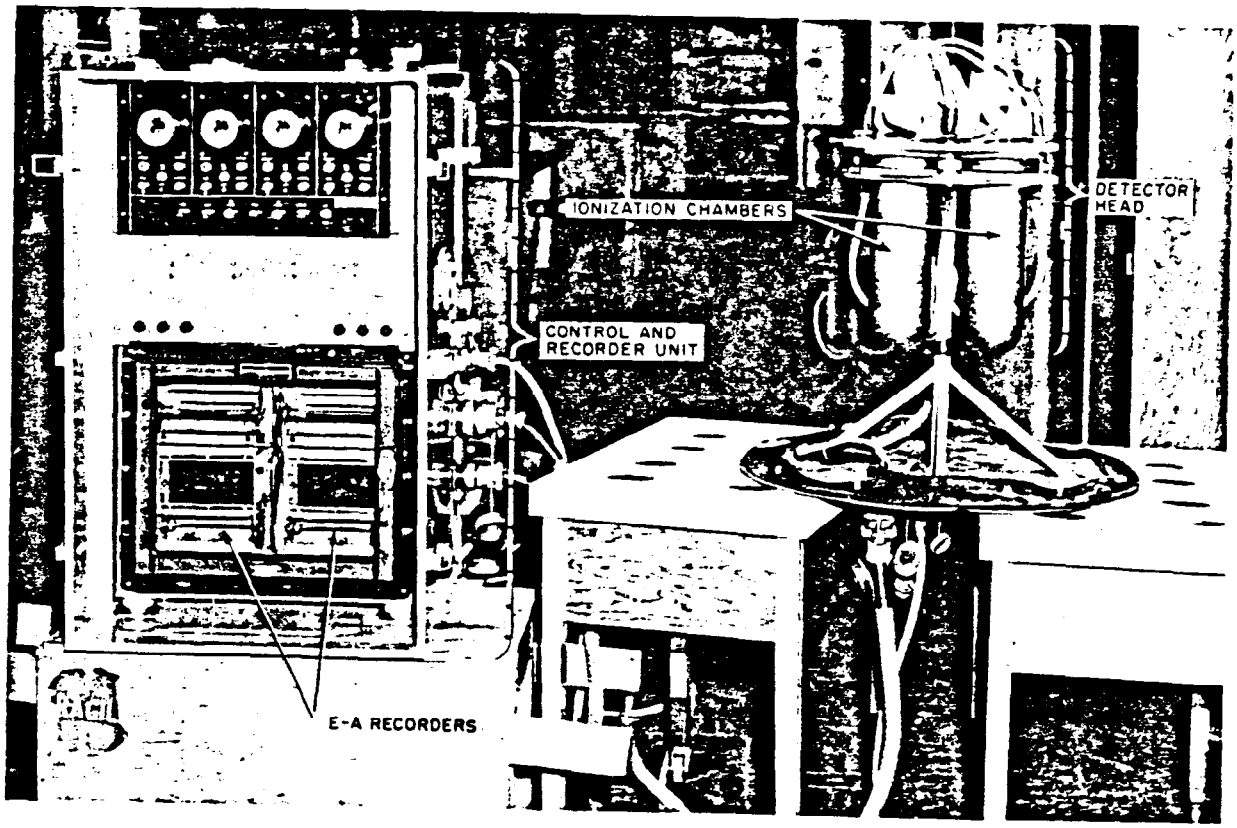

Figure 2.4 Functional view of gamma time-intensity recorder (TIR).

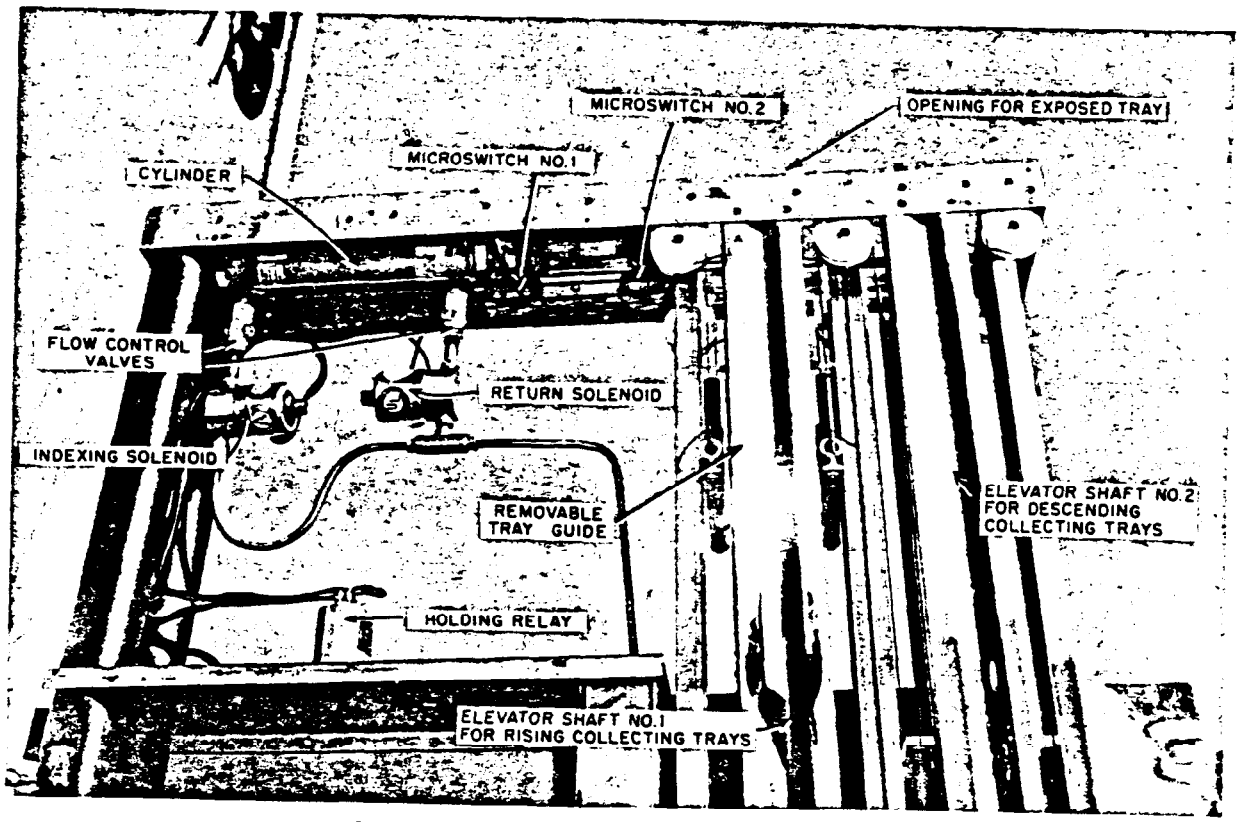

Figure 2.5 Functional view of incremental collector (IC).

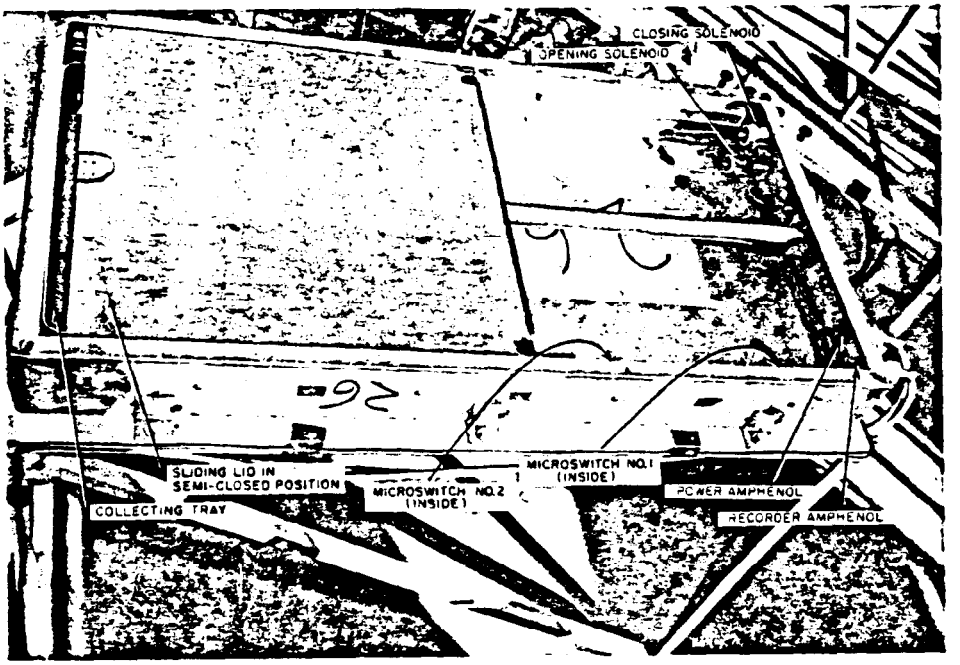

Figure 2.6 Functional view of open-close total collector (OCC).

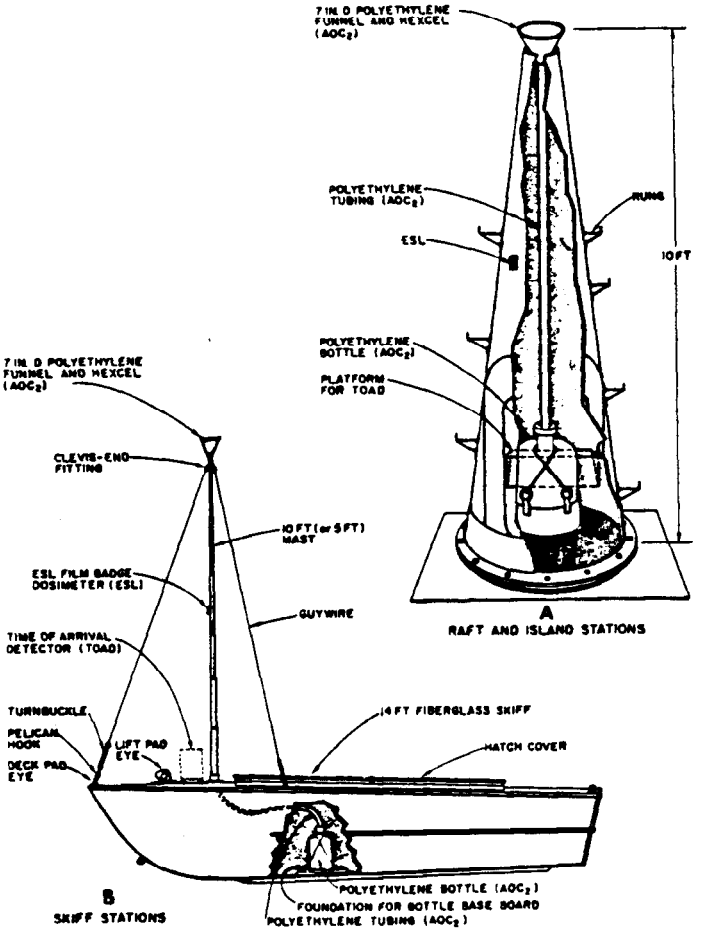

Figure 2.7 Minor sampling array.

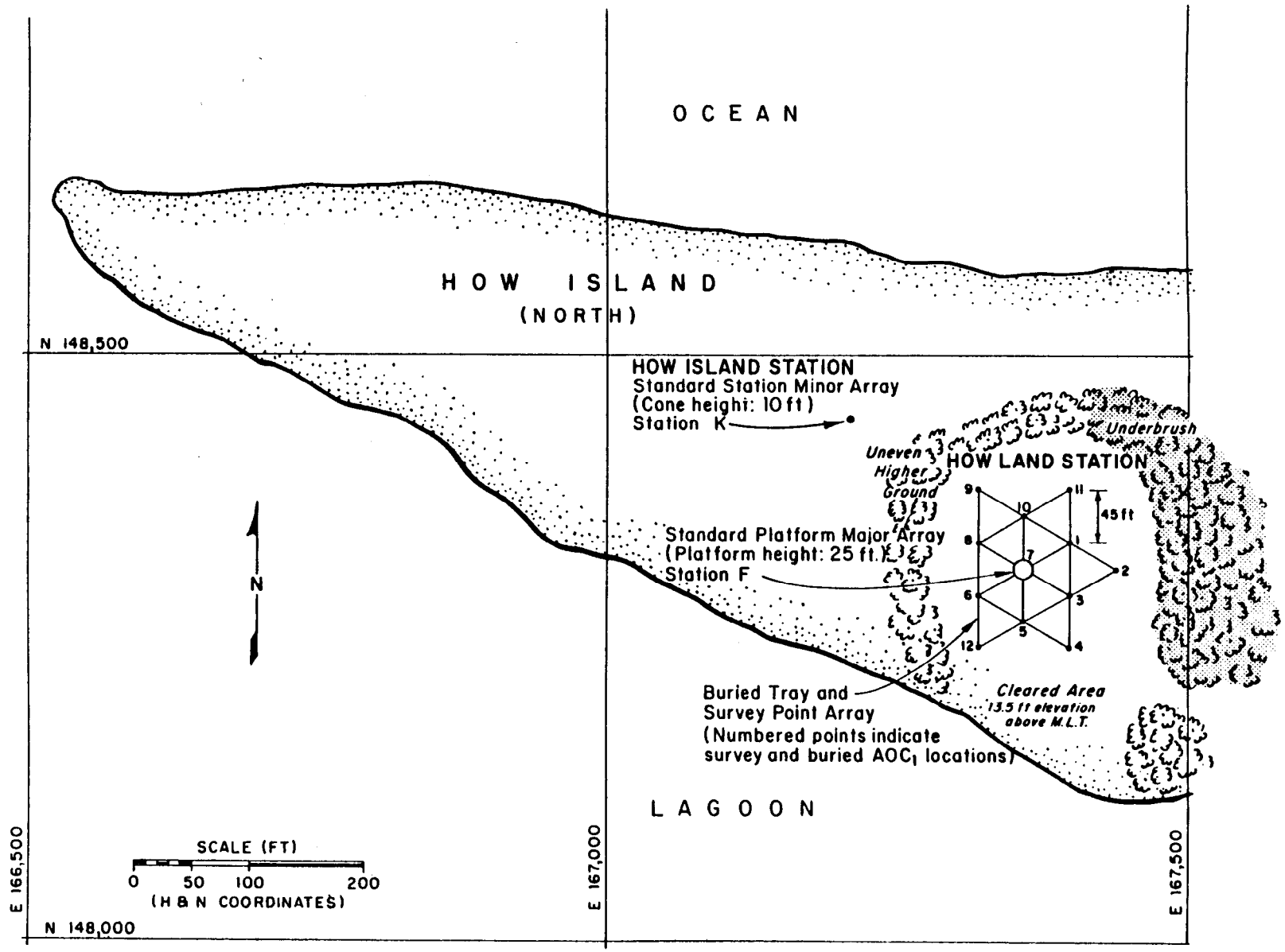

Figure 2.8 Location map and plan drawing of Site How.

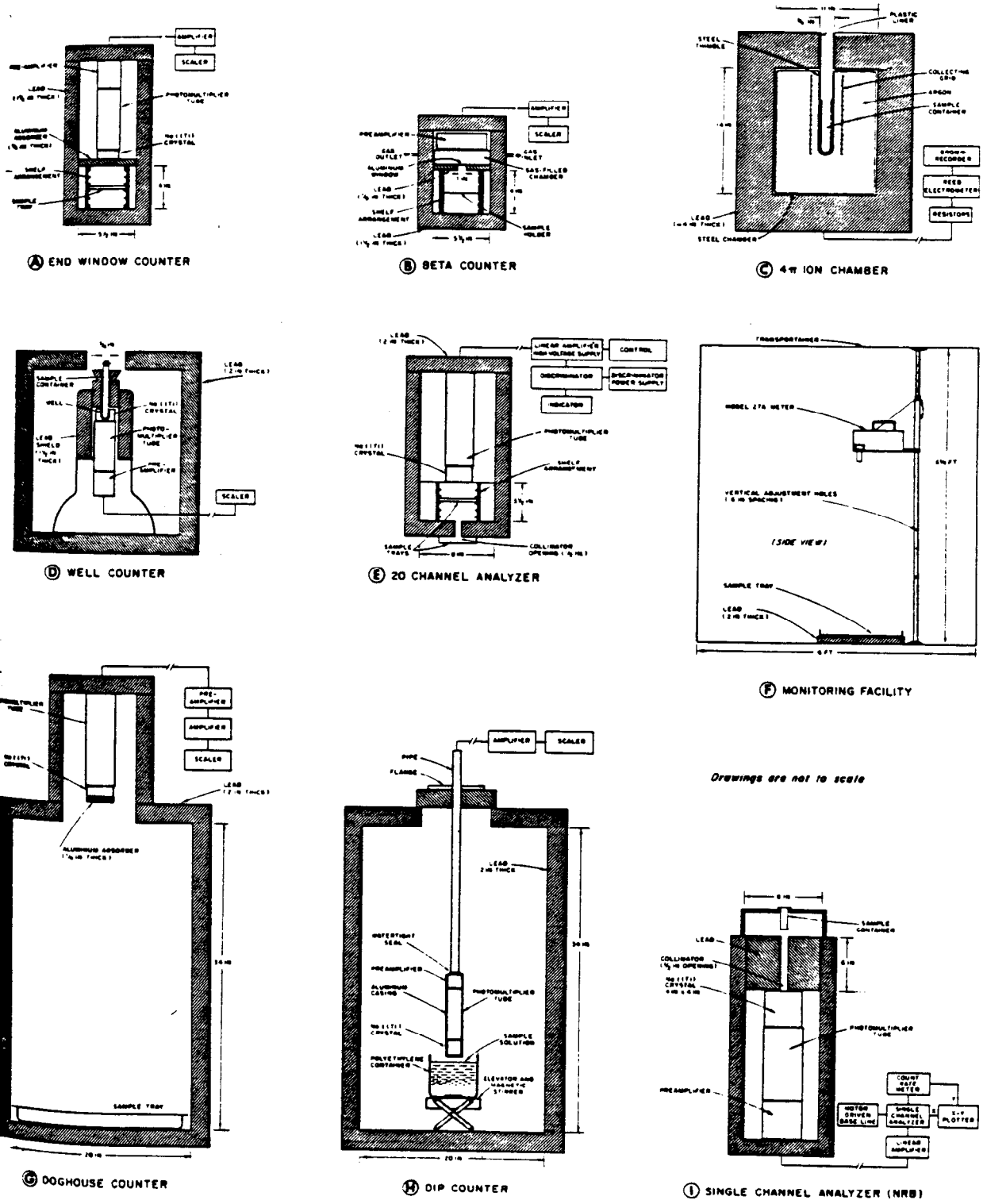

Figure 2.9 Counter geometries.

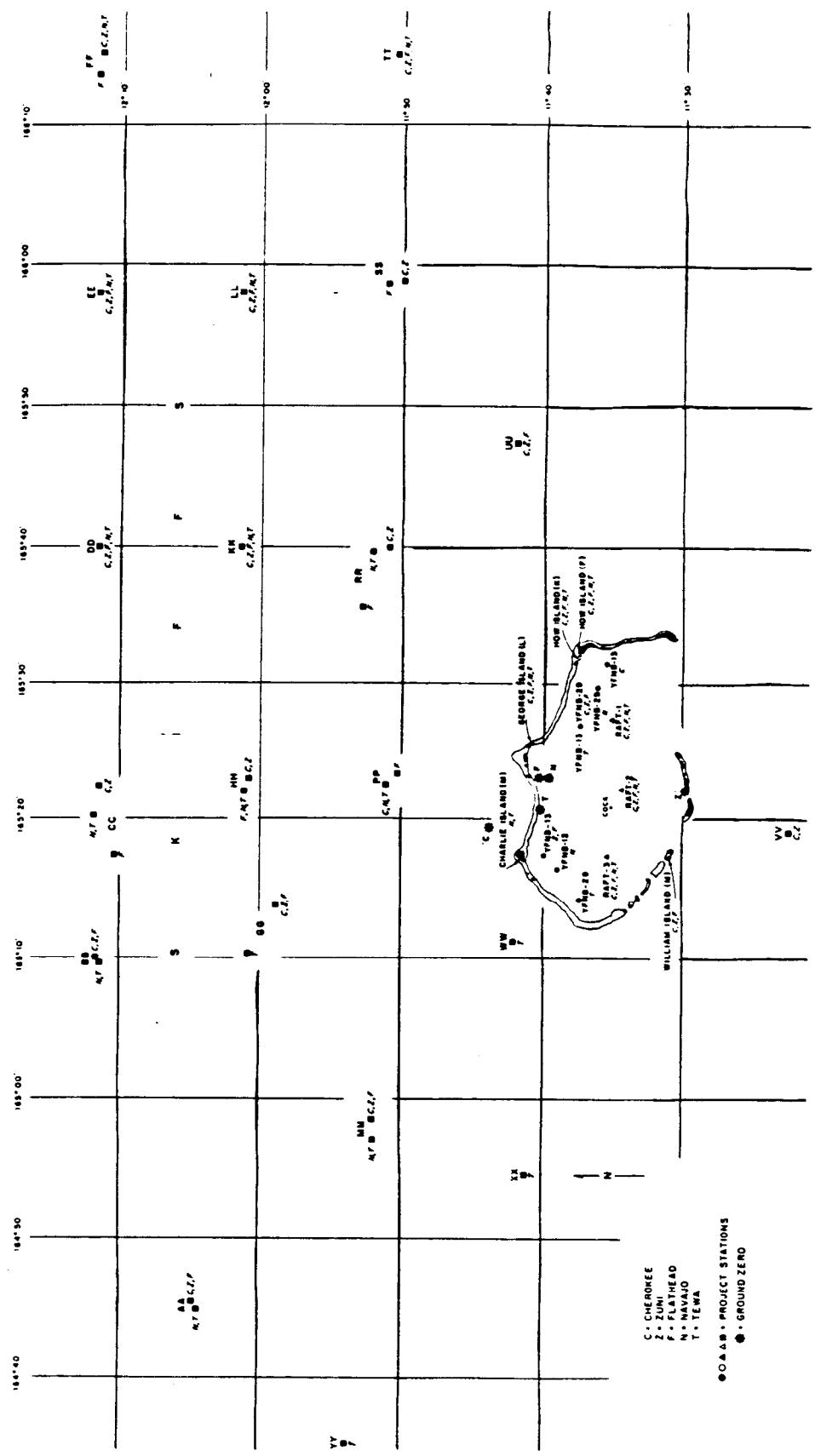

Figure 2.10 Station locations in the atoll area.

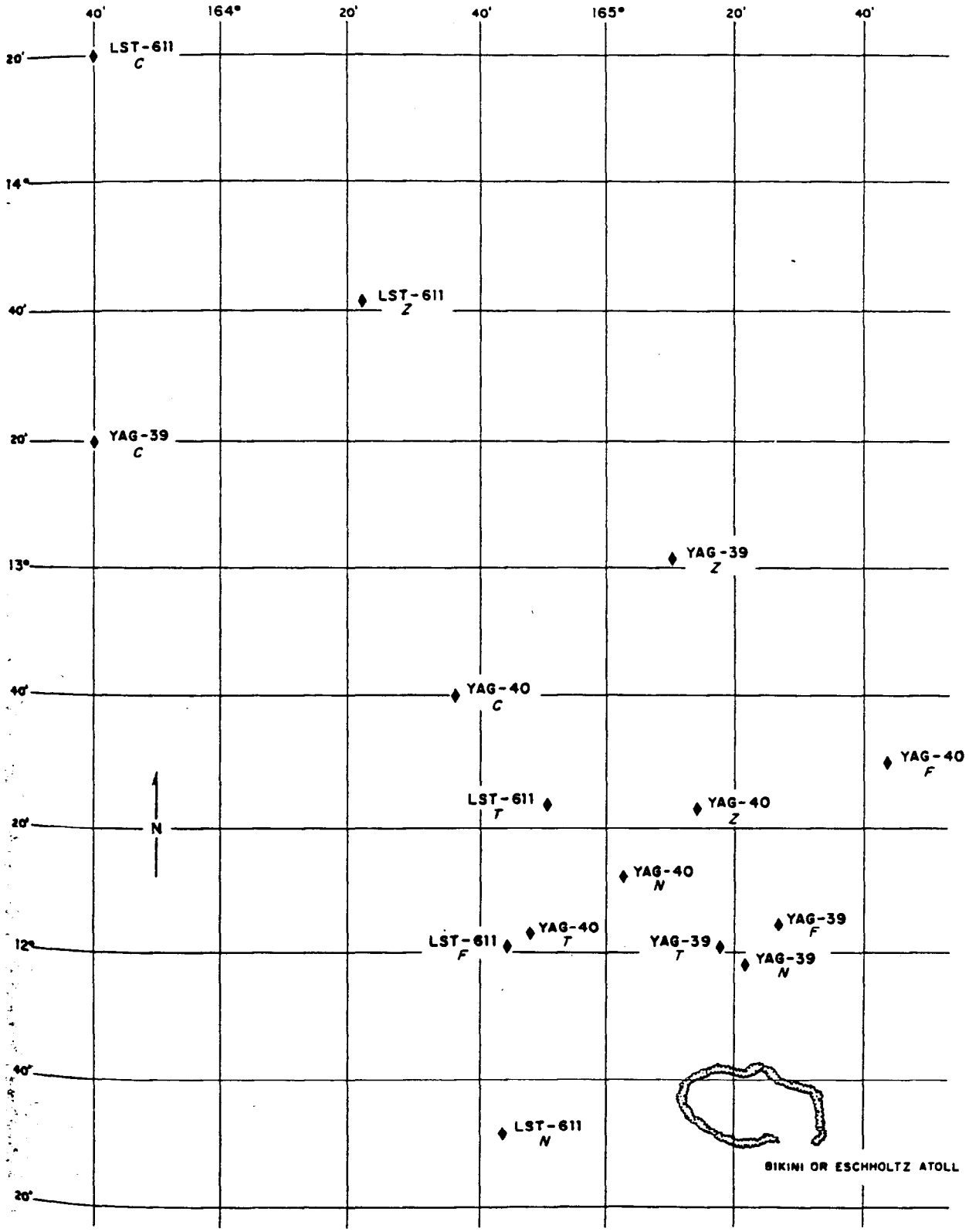

Figure 2.11 Ship locations at times of peak activity.

Chapter 3
RESULTS

3.1 DATA PRESENTATION

The data has been reduced and appears in comprehensive tables (Appendix B) that summarize certain kinds of information for all shots and stations. The text itself contains only derived results.

In general, the details of calculations, such as those involved in reducing gross gamma spectra to absolute photon intensities or in arriving at R-values, have not been included. Instead, original data and final results are given, together with explanations of how the latter were obtained and with references to reports containing detailed calculations.

Results for the water-surface Shots Flathead and Navajo, and the land-surface and near-land-surface Shots Zuni and Tewa, are presented in four categories: fallout-buildup characteristics (Section 3.2); physical, chemical, and radiochemical characteristics of the contaminated material (Section 3.3); its radionuclide composition and radiation characteristics (Section 3.4); and correlations of results (Section 4.3). Appendix B contains all reduced data for these shots separated into three types: that pertaining to the buildup phase (Section B.1); information on physical, chemical, and radiological properties (Section B.2); and data used for correlation studies (Section B.3).

Measurements and results for Shot Cherokee, an air burst during which very little fallout occurred, are summarized in Section 4.1.

Unreduced data are presented in Section B.4.

Each of the composite plots of TIR readings and IC tray activities presented in the section on buildup characteristics may be thought of as constituting a general description of the surface radiological event which occurred at that station. In this sense the information needed to complete the picture is provided by the remainder of the section on particle-size variation with time and mass-arrival rate, as well as by the following sections on the activity deposited per unit area, the particulate properties of the contaminated material, its chemical and radiochemical composition, and the nature of its beta- and gamma-ray emissions. Penetration rates and activity profiles in the ocean extend the description to subsurface conditions at the YAG locations. The radiological event that took place at any major station may be reconstructed in as much detail as desired by using Figures 3.1 through 3.4 as a guide and referring to the samples from that station for the results of interest. Each sample is identified by station, collector, and shot in all tables and figures of results, and the alphabetical and numerical designations assigned to all major array collectors are summarized in Figure A.1.

Throughout the treatment which follows, emphasis has been placed on the use of quantities such as fissions per gram and R^{99} values, whose variations show fundamental differences in fallout properties. In addition, radiation characteristics have been expressed in terms of unit fissions wherever possible. As a result, bias effects are separated, certain conclusions are made evident, and a number of correlations become possible. Some of the latter are presented in Sections 3.3, 3.4, and 4.3.

3.2 BUILDUP CHARACTERISTICS

3.2.1 Rate of Arrival. Reduced and corrected records of the ionization rates measured by one TIR and the sample activities determined from one IC at each major array station are plotted against time since detonation (TSD) in Figures 3.1 through 3.4 for Shots Flathead, Navajo,

Zuni, and Tewa. Numerical values are tabulated in Tables B.1 and B.2. Because the records of the TIR's and the deck (D-TIR) are plotted for the YAG's, the measurements made by the TIR's in the standard platform (P-TIR) have been included in Appendix B. The records of the IC's with shorter collection intervals have been omitted, because they show only the greater variability in the fine structure of the other curves and do not cover the entire fallout period.

TIR readings have been adjusted in accordance with the calibration factors applying to the four ionization chambers present in each instrument, and corrected to account for saturation loss over all ranges. (The adjustments were made in accordance with a private communication from H. Rinnert, NRDL, and based upon Co^{60} gamma rays incident on an unobstructed chamber, normal to its axis.) Recorder speeds have also been checked and the time applying to each reading verified. In those cases where saturation occurred in the highest range, readings have been estimated on the basis of the best information available and the curves dotted in on the figures.

It is pointed out that these curves give only approximate air-ionization rates. Because of the varying energy-response characteristics of each ionization chamber, and internal shielding effects resulting from the construction of the instrument, TIR response was nonuniform with respect both to photon energy and direction, as indicated in Figures A.2 through A.4. The overall estimated effect was to give readings as much as 20 percent lower than would have been recorded by an ideal instrument. (Measurements were made on the YAG 39 and YAG 40 during all four shots with a Cutie Pie or T1B hand survey meter held on top of an operating TIR. The TIR's indicated, on the average, 0.85 ± 25 percent of the survey meter readings, which themselves indicate only about 75 percent of the true dose rate 3 feet above a uniformly distributed plane source (Reference 17). Total doses calculated from TIR curves and measured by film-pack dosimeters (ESL) at the same locations are compared in Section 4.3.5.)

Detailed corrections are virtually impossible to perform, requiring source strength and spectral composition as functions of direction and time, combined with the energy-directional response characteristics of each chamber. It is also pointed out that these sources of error are inherent to some degree in every real detector and are commonly given no consideration whatsoever. Even with an ideal instrument, the measured dose rates could not be compared with theoretical land-equivalent dose rates because of irregularities in the distribution of the source material and shielding effects associated with surface conditions. However, a qualitative study of the performance characteristics of ship, barge, and island TIR's indicated that all performed in a manner similar for the average numbers of fissions deposited and identical radionuclide compositions.

The exposure interval associated with each IC tray has been carefully checked. In those cases where the time required to count all of the trays from a single instrument was unduly long, activities have been expressed at a common time of H+12 hours. Background and coincidence loss corrections have also been made.

The time interval during which each tray was exposed is of particular importance, not only because its midpoint fixes the mean time of collection, but also because all tray activities in counts per minute (counts/min) have been normalized by dividing by this interval, yielding counts per minute per minute of exposure (counts/min^2). Such a procedure was necessary, because collection intervals of several different lengths were used. The resulting quantity is an activity-arrival rate, and each figure shows how this quantity varied over the successive collection intervals at the reference time, or time when the trays were counted. If it can be established that mass is proportional to activity, these same curves can be used to study mass-arrival rate with time (Section 3.2.3, Shots Flathead and Navajo); if, on the other hand, the relationship of mass to activity is unknown, they may be used for comparison with curves of mass-arrival rate constructed by some other means (Section 3.2.3, Shots Zuni and Tewa).

Thus, while each point on a TIR curve expresses the approximate gamma ionization rate produced at that time by all sources of activity, the corresponding time point on the IC curve gives the decay-corrected relative rate at which activity was arriving. Both complementary kinds of information are needed for an accurate description of the radiological event that took place at a given station and are plotted together for this reason—not because they are comparable in any other way.

The activities of the IC trays have not been adjusted for sampling bias, although some undoubtedly exists, primarily because its quantitative effects are unknown. Relative rates may still be derived if it is assumed that all trays are biased alike, which appears reasonable for those cases in which wind speed and direction were nearly constant during the sampling period (Section 4.3.2). More extensive analysis would be required to eliminate uncertainties in the remaining cases.

It should also be mentioned that IC trays with alternating greased-disk and reagent-film collecting surfaces were intentionally used in all of the collectors for Shots Flathead and Navajo —with no detectable difference in efficiency for the resulting fallout drops—and of necessity for Shot Tewa. The late move of Shot Tewa to shallow water produced essentially solid particle fallout, for which the efficiency of the reagent film as a collector was markedly low. Thus, only the greased-disk results have been plotted for the YAG 40 in Figure 3.4, although it was necessary to plot both types for some of the other stations. Trays containing reagent-film disks, all of which were assigned numbers between 2994 and 3933, may be distinguished by reference to Table B.2. A few trays, designated by the prefix P, also contained polyethylene disks to facilitate sample recovery.

3.2.2 Times of Arrival, Peak Activity, and Cessation. The times at which fallout first arrived, reached its peak, and ceased at each major array station are summarized for all shots in Table 3.1. Peak ionization rates are also listed for convenient reference. Time of arrival detector (TOAD) results, covering all minor array stations and providing additional values for the major stations in the atoll area, are tabulated in Table 3.2.

The values given in Table 3.1 were derived from Figures 3.1 through 3.4, and the associated numerical values in Tables B.1 and B.2, by establishing certain criteria which could be applied throughout. These are stated in the table heading; while not the only ones possible, they were felt to be the most reasonable in view of the available data.

Arrival times (t_a) were determined by inspection of both TIR and IC records, the resulting values being commensurate with both. Because the arrival characteristics varied, arrival could not be defined in some simple way, such as "1 mr/hr above background." The final values, therefore, were chosen as sensible-arrival times, treating each case individually. It should be mentioned that, within the resolving power of the instruments used, no time difference existed between the onset of material collections on the IC trays and the toe of the TIR buildup curve. The IC's on the ships were manually operated and generally were not triggered until the arrival of fallout was indicated by the TIR or a survey meter, thus precluding any arrival determination by IC; those at the unmanned stations, however, triggered automatically at shot time, or shortly thereafter, and could be used. The SIC on the YAG 40 also provided usable data, ordinarily yielding an earlier arrival time than IC B-7 on the same ship. In order to conserve trays, however, the number exposed before fallout arrival was kept small, resulting in a larger time uncertainty within the exposure interval of the first active tray.

Once defined, times of peak activity (t_p) could be taken directly from the TIR curves. Because peaks were sometimes broad and flat, however, it was felt to be desirable to show also the time interval during which the ionization rate was within 10 percent of the peak value. Examination of these data indicated that $t_p \sim 2t_a$; this point is discussed and additional data are presented in Reference 18.

Cessation time (t_c) is even more difficult to define than arrival time. In almost every case, for example, fallout was still being deposited at a very low rate on the YAG 40 when the ship departed station. Nevertheless, an extrapolated cessation time which was too late would give an erroneous impression, because 90 or 95 percent of the fallout was down hours earlier. For this reason, IC-tray activities measured at a common time were cumulated and the time at which 95 percent of the fallout had been deposited read off. A typical curve rises abruptly, rounds over, and approaches the total amount of fallout asymptotically. Extrapolated cessation times were estimated primarily from the direct IC plots (Figures 3.1 through 3.4), supplemented by the cumulative plots, and the TIR records replotted on log-log paper. It must be emphasized

that the cessation times reported are closely related to the sensitivity of the measuring systems used and the fallout levels observed.

All values for time of arrival given in Table 3.2 were determined from TOAD measurements. They were obtained by subtracting the time interval measured by the instrument clock, which started when fallout arrived, from the total period elapsed between detonation and the time when the instrument was read.

Because the TOAD's were developed for use by the project and could not be proof-tested in advance, certain operational problems were encountered in their use; these are reflected by Footnotes §, ¶ and † in Table 3.2. Only Footnote † indicates that no information was obtained by the units; however, Footnotes § and ¶ are used to qualify questionable values. Because the TOAD's from the barge and island major stations were used elsewhere after Shot Flathead, Footnote * primarily expresses the operational difficulties involved in servicing the skiffs and keeping them in place.

The fact that a station operated properly and yet detected no fallout is indicated in both tables by Footnote ‡. In the case of the major stations, this means that the TIR record showed no measurable increase and all of the IC trays counted at the normal background rate. For the minor stations, however, it means that the rate of arrival never exceeded 20 mr/hr per half hour, because the radiation trigger contained in the TOAD was set for this value.

3.2.3 Mass-Arrival Rate. A measure of the rate at which mass was deposited at each of the major stations during Shots Zuni and Tewa is plotted in Figure 3.5 from data contained in Table B.4; additional data are contained in Table B.6. Corresponding mass-arrival rates for Shots Flathead and Navajo may be obtained, where available, by multiplying each of the IC-tray activities (count/min^2) in Figures 3.1 and 3.2 by the factor, micrograms per square feet per hour per counts per minute per minute, [μg/(ft^2-hr-count/min^2)]. For the YAG 40, YAG 39, and LST 611, the factor is 0.0524 for Shot Flathead and 0.701 for Shot Navajo. For the YFNB 29, the factor is 0.343 for Shot Flathead. For the YFNB 13 and How-F, the factor is 3.69 for Shot Navajo.

The former values of mass-arrival rate, micrograms per square foot per hour [μg/(ft^2/hr)], were calculated from the particle-size distribution studies in Reference 19, discussed in more detail in Section 3.2.4. The number of solid particles in each size increment deposited per square foot per hour was converted to mass by assuming the particles to be spheres with a density of 2.36 gm/cm^3. Despite the fact that a few slurry particles might have been present (Section 3.3.1), these values were then summed, over all size increments, to obtain the total mass-arrival rate for each tray, or as a function of time since detonation (TSD). These results may not be typical for the geographic locations from which the samples were taken, because of collector bias (Section 4.3.2).

Because this result will be affected by any discrepancy between the number of particles of a certain size, which would have passed through an equal area in free space had the tray not been present, and the number ultimately collected by the tray and counted, both sampling bias (Section 4.3.2) and counting error (Section 3.2.4) are reflected in the curves of Figure 3.5. For this reason they, like the curves of Section 3.2.1, are intended to provide only relative-rate information and should not be integrated to obtain total-mass values, even over the limited periods when it would be possible to do so. The total amount of mass (mg/ft^2) deposited at each major station, determined from chemical analysis of OCC collections, is given in Table 3.16.

The constants to be used for the water-surface shots follow from the slurry-particle sodium chloride analyses in Reference 31 and were derived on the basis of experimentally determined values relating well-counter gamma activity to sodium chloride weight in the deposited fallout. These values and the methods by which they were obtained are presented in Section 3.3.2. The factors were calculated from the ratio of counts per minute per minute (count/min^2) for the IC-tray area to counts per minute per gram [(counts/min)/gm] of NaCl from Table 3.12. The grams of NaCl were converted to grams of fallout, with water included, in the ratio of 1/2.2; and the gamma well counts from the table were expressed as end-window gamma counts by use of the ratio 1/62. An average value of specific activity for each shot was used for the ship stations,

while a value more nearly applicable for material deposited from 1 to 3 hours after detonation was used for the barge and island stations.

It is to be noted that the insoluble solids of the slurry particles (Section 3.3.2) were not included in the conversion of grams of NaCl to grams of fallout. Even though highly active, they constituted less than 2 to 4 percent of the total mass and were neglected in view of measurement errors up to ±5 percent for sodium chloride, ±15 percent for specific activity, and ±25 percent for water content.

3.2.4 Particle-Size Variation. The way in which the distribution of solid-particle sizes varied over the fallout buildup period at each of the major stations during Shots Zuni and Tewa is shown in Figures 3.6 through 3.9. The data from which the plots were derived are tabulated in Table B.3, and similar data for a number of intermediate collection intervals are listed in Table B.5. All of the slurry particles collected over a single time interval at a particular location during Shots Flathead and Navajo tended to fall in one narrow size range; representative values are included in Table 3.12.

The information contained in Tables B.3 through B.6 and plotted in the figures represents the results of studies described in detail in Reference 19. All IC trays were inserted in a fixed setup employing an 8-by-10-inch-view camera and photographed with a magnification of 2., soon after being returned to NRDL. Backlighting and low-contrast film were used to achieve maximum particle visibility. A transparent grid of 16 equal rectangular areas was then superimposed on the negative and each area, enlarged five times, printed on 8-by-10-inch paper at a combined linear magnification of 10.

Since time-consuming manual methods had to be used in sizing and counting the photographed particles, three things were done to keep the total number as small as possible, consistent with good statistical practice and the degree of definition required. (1) The total number of trays available from each collector was reduced by selecting a representative number spaced at more or less equal intervals over the fallout-buildup period. Reference was made to the TIR and IC curves (Figures 3.1 to 3.4) during the selection process, and additional trays were included in time intervals where sharp changes were indicated. (2) Instead of counting the particles in all areas of heavily loaded trays, a diagonal line was drawn from the most dense to the least dense edge and only those areas selected which were intersected by the line. (3) No particles smaller than 50 microns in diameter were counted, this being arbitrarily established as the size defining the lower limit of significant local fallout. (The lower limit was determined from a fallout model, using particle size as a basic input parameter (Section 4.3.1). Particles down to ~20 microns in diameter will be present, although the majority of particles between 20 and 50 microns will be deposited at greater distances than those considered.)

Actual sizing and counting of the particles on the selected ten times enlargements was accomplished by the use of a series of gages consisting of four sets of black circular spots of the same magnification, graduated in equal-diameter increments of 5, 10, 30, and 100 microns. These were printed on a sheet of clear plastic so that the largest spot which could be completely inscribed in a given particle area could be determined by superimposition. Thus, all of the particle sizes listed refer to the diameter of the maximum circle which could be inscribed in the projected area of the particle. A preliminary test established that more-consistent results could be achieved using this parameter than the projected diameter, or diameter of the circle equal to the projected area of the particle.

A number of problems arose in connection with the counting procedure: touching particles were difficult to distinguish from single aggregates; particles which were small, thin, translucent, or out of focus were difficult to see against the background; particles falling on area borderlines could not be accurately sized and often had to be eliminated; some elongated particles, for which the inscribed-circle method was of questionable validity, were observed; a strong tendency existed to overlook particles smaller than about 60 microns, because of the graininess of the print and natural human error. Most of these problems were alleviated, however, by having each print processed in advance by a specially trained editor. All particles to be counted were first marked by the editor, then sized by the counter.

Once the basic data, consisting of the number of particles in each arbitrary size interval between 50 and 2,600 microns, were obtained for the selected trays, they were normalized to a 1-micron interval and smoothed, to compensate in part for sample sparsity, by successive applications of a standard smoothing function on a digital computer. These, with appropriate unit conversions, are the results listed in Tables B.3 and B.5: the numbers of particles, within a 1-micron interval centered at the indicated sizes, collected per hour for each square foot of surface.

Figures 3.6 through 3.9 show how the concentration of each particle size varied over the buildup period by providing, in effect, successive frequency distributions on time-line sections. The curves representing the 92.5- and 195-micron particles have been emphasized to bring out overall trends and make the figures easier to use. Measures of central tendency have been avoided, because the largest particles which make the most-significant contribution to the activity are not significantly represented in the calculation of the mean particle size, while the small particles which make the greatest contribution in the calculation of the mean particle size are most subject to errors from counting and background dust deposits. It should also be remembered that sampling bias is present and probably assumes its greatest importance for the small particles.

Plots of pure background collections for the ship and barge stations resemble the plot of the YAG 39 data for Shot Zuni, but without the marked peaks in the small particles or the intrusions of the large particles from below, both of which are characteristic of fallout arrival. This is not necessarily true for the How land station, however, where such features may result from disturbances of the surface dust; the series of peaks at about 4 hours during Shot Zuni, for example, appears to be the result of too close an approach by a survey helicopter.

3.2.5 Ocean Penetration. Figure 3.10 shows the general penetration behavior of fallout activity in the ocean for Shot Navajo, a water-surface shot, and Shot Tewa, resembling a land-surface shot. These simplified curves show a number of successive activity profiles measured during and after the fallout period with the oceanographic probe (SIO-P) aboard the YAG 39 and demonstrate the changing and variable nature of the basic phenomena. The best estimates of the rate at which the main body of activity penetrated at the YAG 39 and YAG 40 locations during Shots Flathead, Navajo, and Tewa are summarized in Table 3.3, and the depths at which this penetration was observed to cease are listed in Table 3.4. The data from which the results were obtained are presented in graphical form in Figure B.1; reduced-activity profiles similar to those shown in Figure 3.10 were used in the preparation of the plots. Estimates of the maximum penetration rates observed for Shots Zuni, Navajo, and Tewa appear in Table 3.5.

The values tabulated in Reference 20 represent the result of a systematic study of measured profiles for features indicative of penetration rate. Various shape characteristics, such as the depth of the first increase in activity level above normal background and the depth of the juncture of the gross body of activity with the thin body of activity below, were considered; but none was found to be applicable in every case.

The concept of equivalent depth was devised so that: (1) all the profile data (i.e., all the curves giving activity concentration as a function of depth) could be used, and (2) the results of the Project 2.63 water-sampling effort could be related to other Program 2 studies, in which the determination of activity per unit volume of water near the surface (surface concentration) was a prime measurement. The equivalent depth is defined as the factor which must be applied to the surface concentration to give the total activity per unit water surface area as represented by the measured profile. Because the equivalent depth may be determined by dividing the planimetered area of any profile by the appropriate surface concentration, it is relatively independent of profile shape and activity level and, in addition, can utilize any measure of surface concentration which can be adjusted to the time when the profile was taken and expressed in the same units of activity measurement. Obviously, if the appropriate equivalent depth can be determined, it may be applied to any measurement of the surface concentration to produce an estimate of the activity per unit area when no other data are available.

The penetration rates in Table 3.3 were obtained by plotting all equivalent-depth points avail-

able for each ship and shot (Figure B.1), dividing the data into appropriate intervals on the basis of the plots, and calculating the slopes of the least-squares lines for these intervals. The maximum depths of penetration listed in Table 3.4 were derived from the same plots by establishing that the slopes did not differ significantly from zero outside of the selected intervals. Erratic behavior or failure of the probes on both ships during Shot Zuni and on the YAG 40 during Shot Flathead prevented the taking of data which could be used for equivalent-depth determinations. It did prove possible in the former case, however, to trace the motion of the deepest tip of the activity profile from the YAG 39 measurements; and this is reported, with corresponding values from the other events, as a maximum penetration rate in Table 3.5.

It is important to emphasize that the values given in Tables 3.3 and 3.4, while indicating remarkably uniform penetration behavior for the different kinds of events, refer only to the gross body of the fallout activity as it gradually settles to the thermocline. When the deposited material consists largely of solid particles, as for Shots Zuni and Tewa, it appears that some fast penetration may occur. The rates listed for these shots in Table 3.5 were derived from a fast-traveling component which may have disappeared below the thermocline, leaving the activity profile open at the bottom (Figure 3.10). On the other hand, no such penetration was observed for Shot Flathead and was questionable in the case of Shot Navajo. This subject is discussed further in Section 4.3.2, and estimates of the amount of activity disappearing below the thermocline are presented.

It is also important to note that the linear penetration rates given in Table 3.3 apply only from about the time of peak onward and after the fallout has penetrated to a depth of from 10 to 20 meters. Irregular effects at shallower depths, like the scatter of data points in the vicinity of the thermocline, no doubt reflect the influence both of differences in fallout composition and uncontrollable oceanographic variables. The ships did move during sampling and may have encountered nonuniform conditions resulting from such localized disturbances as thermal gradients, turbulent regions, and surface currents.

In addition to penetration behavior, decay and solubility effects are present in the changing activity profiles of Figure 3.10. The results of the measurements made by the decay probe (SIO-D) suspended in the tank filled with ocean water aboard the YAG 39 are summarized in Table 3.6. Corresponding values from Reference 15 are included for comparison; although similar instrumentation was used, these values were derived from measurements made over slightly different time intervals in contaminated water taken from the ocean some time after fallout had ceased.

Two experiments were performed to study the solubility of the activity associated with solid fallout particles and give some indication of the way in which activity measurements made with energy-dependent instruments might be affected. Several attempts were also made to make direct measurements of the gamma-energy spectra of water samples, but only in one case (Sample YAG 39-T-IC-D, Table B.20) was there enough activity present in the aliquot.

The results of the experiments are summarized in Figures 3.11 and 3.12. Two samples of particles from Shot Tewa, giving 4-π ionization chamber readings of 208×10^{-9} and 674×10^{-8} ma respectively, were removed from a single OCC tray (YAG 39-C-34 TE) and subjected to measurements designed to indicate the solubility rates of various radionuclides in relation to the overall solubility rate of the activity in ocean water.

The first sample (Method I) was placed on top of a glass-wool plug in a short glass tube. A piece of rubber tubing connected the top of this tube to the bottom of a 10-ml microburet filled with sea water. The sea water was passed over the particles at a constant rate, and equivolume fractions were collected at specified time intervals. In 23 seconds, 3 ml passed over the particles, corresponding to a settling rate of 34 cm/min—approximately the rate at which a particle of average diameter in the sample (115 microns) would have settled. The activity of each fraction was measured with the well counter soon after collection and, when these measurements were combined with the total sample activity, the cumulative percent of the activity dissolved was computed (Figure 3.11). Gamma-energy spectra were also measured on fractions corresponding roughly to the beginning (10 seconds), middle (160 seconds) and end (360 seconds) of the run (Figure 3.12). The time of the run was D+5 days.

On D+4 the second sample (Method II) was placed in a vessel containing 75 ml of sea water. After stirring for a certain time interval, the solution was centrifuged and a 50-λ aliquot removed from the supernate. This procedure was repeated several times over a 48-hour period, with the activity of each fraction being measured shortly after separation and used to compute the cumulative percent of the total activity in solution (Figure 3.11). The gamma spectrum of the solution stirred for 48 hours was also measured for comparison with the spectra obtained by Method I (Figure 3.12).

As indicated in Figure 3.11, more than 1 percent of the total activity went into solution in less than 10 seconds, followed by at least an additional 19 percent before equilibrium was achieved. This was accompanied by large spectral changes, indicating marked radionuclide fractionation (Figure 3.12); nearly all of the I^{131}, for example, appears to have been dissolved in 360 seconds.

The dip-counter activities of all water samples taken by Projects 2.63 and 2.62a are tabulated in Table B.32. Ocean background corrections have not been attempted but may be estimated for each shot at the YAG 39 and YAG 40 locations from the activities of the background samples collected just prior to the arrival of fallout. All other corrections have been made, however, including those required by the dilution of the designated 1,100-ml depth samples to the standard 2,000-ml counting volume. Normalized dip-counter decay curves for each event (Figure B.14), and the records of the surface-monitoring devices (NYO-M, Figures B.8 through B.13) are also included in Section B.4.

3.3 PHYSICAL, CHEMICAL, AND RADIOCHEMICAL CHARACTERISTICS

3.3.1 Solid Particles. All of the active fallout collected during Shot Zuni, and nearly all collected during Shot Tewa, consisted of solid particles which closely resembled those from Shot M during Operation Ivy and Shot 1 during Operation Castle (References 21 and 22). Alternate trays containing greased disks for solid-particle collection and reagent films for slurry-particle collection were used in the IC's during Shot Tewa. Microscopic examination of the latter revealed an insignificant number of slurry particles; these results are summarized in Table B.10. No slurry particles were observed in the Zuni fallout, although a small number may have been deposited.

As illustrated in Figure 3.13, the particles varied from unchanged irregular grains of coral sand to completely altered spheroidal particles or flaky agglomerates, and in a number of cases included dense black spheres (Reference 19). Each of these types is covered in the discussion of physical, chemical, radiochemical, and radiation characteristics which follows. Basic data for about 100 particles from each shot, selected at random from among those removed from the SIC trays in the YAG 40 laboratory, are included in Table B.34.

Physical and Chemical Characteristics. A number of irregular and spheroidal particles collected on the YFNB 29 during Shots Zuni and Tewa were thin-sectioned and studied under a petrographic microscope (Reference 23); some from Shot Zuni were also subjected to X-ray diffraction analysis (Table 3.7). Typical thin sections of both types of particles are presented in Figures 3.14, 3.15 and 3.16 for Shot Zuni and Figures 3.17 and 3.18 for Shot Tewa. Although the particles shown in the figures were taken from samples of close-in fallout, those collected 40 miles or more from the shot point by the SIC on the YAG 40 were observed to be similar, except for being smaller in size.

Both methods of analysis showed the great majority of irregular particles to consist of fine-grained calcium hydroxide, $Ca(OH)_2$, with a thin surface layer of calcium carbonate, $CaCO_3$ (Figure 3.17). A few, however, had surface layers of calcium hydroxide with central cores of unchanged coral ($CaCO_3$), and an even smaller number were composed entirely of unchanged coral (Figure 3.14). It is likely that the chemically changed particles were formed by decarbonation of the original calcium carbonate to calcium oxide followed by hydration to calcium hydroxide and subsequent reaction with CO_2 in the atmosphere to form a thin coat of calcium carbonate. Particles of this kind were angular in appearance and unusually white in color (Figure 3.13, A and G).

Many of the irregular particles from Shot Zuni were observed to carry small highly active

spherical particles 1 to 25 microns in diameter on their surfaces (Figures 3.13G and 3.15). Shot Tewa particles were almost entirely free from spherical particles of this kind, although a few with diameters less than 1 micron were discovered when some of the irregular particles were powdered and examined with an electron microscope. A few larger isolated spherical particles were also found in the Zuni fallout (Figures 3.13, B and H). Such particles varied in color from orange-red for the smallest sizes to opaque black for the largest sizes.

While these particles were too small to be subjected to petrographic or X-ray diffraction analysis, it was possible to analyze a number of larger particles collected during Shot Inca which appeared to be otherwise identical (Figure 3.19). The Inca particles were composed primarily of Fe_3O_4 and calcium iron oxide ($2\ CaO.Fe_2O_3$) but contained smaller amounts of Fe_2O_3 and CaO. Some were pure iron oxide but the majority contained calcium oxide in free form or as calcium iron oxide (Reference 24).

Most of the spheroidal particles consisted of coarse-grained calcium hydroxide with a thin surface layer of calcium carbonate (Figure 3.16). Nearly all contained at least a few grains of calcium oxide, however, and some were found to be composed largely of this material (Figure 3.18)—5 to 75 percent by volume. Although melted, particles of this kind probably underwent much the same chemical changes as the irregular particles, the principal difference being that they were incompletely hydrated. They varied in appearance from irregular to almost perfect spheres and in color from white to pale yellow (Figure 3.13, C, H, and K). Many had central cavities, as shown in Figure 3.16 and were in some cases open on one side.

Because of their delicacy, the agglomerated particles could not be thin-sectioned and had to be crushed for petrographic and X-ray diffraction analysis. They were found to be composed primarily of calcium hydroxide and some calcium carbonate. It has been observed that similar particles are formed by the expansion of calcium oxide pellets placed in distilled water, and that the other kinds of fallout particles sometimes change into such aggregates if exposed to air for several weeks. The particles were flaky in appearance, with typical agglomerated structures, and a transparent white in color (Figure 3.13, D, I, and J); as verified by examination of IC trays in the YAG 40 laboratory immediately after collection, they were deposited in the forms shown.

The densities of 71 yellow spheroidal particles, 44 white spheroidal particles, and 7 irregular particles from Shot Zuni were determined (Reference 25) using a density gradient tube and a bromoform-bromobenzene mixture with a range from 2.0 to 2.8 gm/cm^3. These results, showing a clustering of densities at 2.3 and 2.7 gm/cm^3, are summarized in Table 3.8. The yellow spheres are shown to be slightly more dense than the white, and chemical spot tests made for iron gave relatively high intensities for the former with respect to the latter. No density determinations were made for agglomerated particles, but one black spherical particle (Table 3.7) was weighed and calculated to have a density of 3.4 gm/cm^3.

The subject of size distribution has been covered separately in Section 3.2.4, and all information on particle sizes is included in that section.

Radiochemical Characteristics. Approximately 30 irregular, spheroidal and agglomerated particles from Shot Zuni were subjected to individual radiochemical analysis (Reference 26), and the activities of about 30 more were assayed in such a way that certain of their radiochemical properties could be inferred. A number of particles of the same type were also combined in several cases so that larger amounts of activity would be available. These data are tabulated in Tables B.7 and B.8.

Radiochemical measurements of Sr^{89}, Mo^{99}, Ba^{140}-La^{140} and Np^{239} were made. (All classified information such as the product/fission ratio for Np^{239}, which could not be included in Reference 26, and the limited amount of data obtained for Shots Tewa and Flathead were received in the form of a private communication from the authors of Reference 26.) For the most part, conventional methods of analysis (References 27 and 28) were used, although the amounts of Np^{239} and Mo^{99} (actually Tc^{99m}) were determined in part from photopeak areas measured on the single-channel gamma analyzer (Section 2.2 and Reference 29). The total number of fissions in each sample was calculated from the number of atoms of Mo^{99} present, and radiochemical results were expressed as R-values using Mo^{99} as a reference. (R-values, being defined as the ratio

of the observed amount of a given nuclide to the amount expected from thermal neutron fission of U^{235}, relative to some reference nuclide, combine the effects of fractionation and variations in fission yield and contain a number of experimental uncertainties. Values between 0.5 and 1.5 cannot be considered significantly different from 1.0.) Selected particles were also weighed so that the number of fissions per gram could be computed.

Radioactivity measurements were made in the gamma well counter (WC) and the 4-π gamma ionization chamber (GIC), both of which are described in Section 2.2. Because the efficiency of the former decreased with increasing photon energy, while the efficiency of the latter increased, samples were often assayed in both instruments and the ratio of the two measurements (counts per minute per 10^4 fissions to milliamperes per 10^4 fissions) used as an indication of differences in radionuclide composition.

It will be observed that the particles in Table B.7 have been classified according to color and shape. For purposes of comparing radiochemical properties, spheroidal and agglomerated particles have been grouped together and designated as "altered particles," while irregular particles have been designed "unaltered particles." The latter should not be interpreted literally, of course; it will be evident from the foregoing section that the majority of irregular particles have undergone some degree of chemical change. Particles were classified as altered if they exhibited the obvious physical changes of spheroidal or agglomerated particles under the optical microscope.

Radiochemical results for all altered and unaltered particles from Shot Zuni are summarized in Table 3.9, and activity ratios of the particles from this shot and Shot Tewa are compared in Table 3.10. The differences in radiochemical composition suggested in the tables are emphasized in Figure 3.20, which shows how the energy-dependent ratios (counts per minute per 10^4 fissions, milliamperes per 10^4 fissions and counts per minute per milliamperes) varied with time, and in Figure 3.21, wherein the data used for computing the R-values and product/fission (p/f) ratios (number of atoms of induced product formed per fission) in Tables B.7 and B.8 are presented graphically by plotting the numbers of atoms of each nuclide in a sample versus the number of atoms of Mo^{99}. Data obtained from calibration runs with neutron-irradiated U^{235} are plotted in the former for comparison; and the standard cloud sample data for Np^{239}, as well as those derived from the estimated device fission yields for Ba^{140} and Sr^{89}, are included in the latter.

It is interesting to note that these results not only establish that marked differences exist between the two types of particles, but also show the altered particles to be depleted in both Ba^{140}-La^{140} and Sr^{89}, while the unaltered particles are enriched in Ba^{140}-La^{140} and perhaps slightly depleted in Sr^{89}. The altered particles are also seen to be about a factor of 100 higher than the unaltered in terms of fissions per gram. When these R-values are compared with those obtained from gross fallout samples (Tables 3.17 and 3.21), it is further found that the values for altered particles resemble those for samples from the lagoon area, while the values for the unaltered particles resemble those from cloud samples.

Activity Relationships. All of the particles whose gamma activities and physical properties were measured in the YAG 40 laboratory (Table B.34), as well as several hundred additional particles from the incremental collectors on the other ships and barges, were studied systematically (Reference 30) in an attempt to determine whether the activities of the particles were functionally related to their size. These data are listed in Table B.9 and the results are plotted in Figures 3.22 and 3.23. Possible relationships between particle activity, weight, and density were also considered (Reference 25), using a separate group of approximately 135 particles collected on the YFNB 29 during Shots Zuni and Tewa and the YAG 39 during Shot Tewa only; Figures 3.24 and 3.25 show the results.

As implied by the differences in radiochemical composition discussed in the preceding section, marked differences exist in the gamma-radiation characteristics of the different types of particles. Compared with the variations in decay rate and energy spectrum observed for different particles collected at about the same time on the YAG 40 (Figures B.2, B.3 and B.4), altered particles show large changes relative to unaltered particles. Figures 3.26 and 3.27 from Reference 26 illustrate this point. The former, arbitrarily normalized at 1,000 hours, shows how

well-counter decay rates for the two types of particles deviate on both sides of the interval from 200 to 1,200 hours, and how the same curves fail to coincide, as they should for equivalent radionuclide compositions, when plotted in terms of 10^4 fissions. The latter shows the regions in which the primary radionuclide deficiencies exist.

The previous considerations suggest that particles should be grouped according to type for the study of activity-size relationships.

Figures 3.22 and 3.23 show the results of a study made in this way (Table B.9). A large number of the particles for which size and activity data were obtained in the YAG 40 laboratory during Shots Zuni and Tewa were first grouped according to size (16 groups, about 32 microns wide, from 11 to 528 microns), then subdivided according to type (irregular or angular, spheroidal or spherical, and agglomerated) within each size group. The distribution of activities in each size group and subgroup was considered and it was found that, while no regular distribution was apparent for the size group, the subgroup tended toward normal distribution. Median activities were utilized for both, but maximum and minimum values for the overall size group were included in Table B.9 to show the relative spread. It will be observed that activity range and median activity both increase with size.

Similar results for groups of particles removed from IC trays exposed aboard the YAG 39, LST 611, YFNB 13, and YFNB 29 during Shot Tewa are also included in Table B.9. These have not been plotted or used in the derivation of the final relationships, because the particles were removed from the trays and well-counted between 300 and 600 hours after the shot, and many were so near background that their activities were questionable. (This should not be interpreted to mean that the fallout contained a significant number of inactive particles. Nearly 100 percent of the particles observed in the YAG 40 laboratory during Shots Zuni and Tewa were active.)

In the figures, the median activity of each size group from the two sets of YAG 40 data has been plotted against the mean diameter of the group for the particles as a whole and several of the particle type subgroups. Regression lines have been constructed, using a modified least-squares method with median activities weighted by group frequencies, and 95-percent-confidence bands are shown in every case. Agglomerated particles from Shot Zuni and spheroidal particles from Shot Tewa have not been treated because of the sparsity of the data.

It should also be noted that different measures of diameter have been utilized in the two cases. The particles from both shots were sized under a low-power microscope using eyepiece micrometer disks; a series of sizing circles was used during Shot Zuni, leading to the diameter of the equivalent projected area D_a, while a linear scale was used for Shot Tewa, giving simply the maximum particle diameter D_m. The first method was selected because it could be applied under the working conditions in the YAG 40 laboratory and easily related to the method described in Section 3.2.4 (Figure B.5); the second method was adopted so that more particles could be processed and an upper limit established for size in the development of activity-size relationships.

The equations for the regression lines are given in the figures and summarized as follows: all particles, Shot Zuni, $A \propto D_a^{2.4}$, Shot Tewa, $A \propto D_m^{1.8}$; irregular particles, Shot Zuni, $A \propto D_a^{2.2}$, Shot Tewa, $A \propto D_m^{1.7}$; spheroidal particles, Shot Zuni, $A \propto D_a^{3.7}$; and agglomerated particles, Shot Tewa, $A \propto D_m^{2.1}$.

(Analogous relationships for Tewa particles from the YFNB 29 were derived on the basis of much more limited data in Reference 25, using maximum diameter as the measure of size. These are listed below; error not attributable to the linear regression was estimated at about 200 percent for the first two cases and 400 percent for the last: all particles, $A \propto D_m^{2.01}$; irregular particles, $A \propto D_m^{1.92}$; and spheroidal particles, $A \propto D_m^{3.37}$.)

It may be observed that the activity of the irregular particles varies approximately as the square of the diameter. This is in good agreement with the findings in Reference 23; the radioautographs in Figures 3.14 and 3.17 show the activity to be concentrated largely on the surfaces of the irregular particles. The activity of the spheroidal particles, however, appears to vary as the third or fourth power of the diameter, which could mean either that it is a true function of particle volume or that it diffused into the molten particle in a region of higher activity concentration in the cloud. The thin-section radioautographs suggest the latter to be true, showing the activity to be distributed throughout the volume in some cases (Figure 3.16) but confined to

the surface in others (Figure 3.18). It may also be seen that the overall variation of activity with size is controlled by the irregular particles, which appear to predominate numerically in the fallout (Table B.9), rather than by the spheroidal particles. Table 3.11 illustrates how the activity in each size group was divided among the three particle types.

No correlation of particle activity with density was possible (Figure 3.25) but a rough relationship with weight was derived for a group of Tewa particles from the YFNB 29 on the basis of Figure 3.24: $A \propto W^{0.7}$, where W refers to the weight in micrograms and nonregression error is estimated at ~140 percent (Reference 25). (An additional study was performed at NRDL, using 57 particles from the same source and a more stable microbalance. The resulting relation was: $A \propto W^{0.57}$.) This result is consistent with the diameter functions, because $D^2 \propto W^{2/3}$. The relative activities of the white and yellow spheroidal particles referred to earlier were also compared and the latter were found to be slightly more active than the former.

3.3.2 Slurry Particles. All of the fallout collected during Shots Flathead and Navajo consisted of slurry particles whose inert components were water, sea salts, and a small amount of insoluble solids. (Although IC and SIC trays containing greased disks were interspersed among those containing reagent films for shots, no isolated solid particles that were active were observed.) Large crystals displaying the characteristic cubic shape of sodium chloride were occasionally observed in suspension. The physical and chemical, radiochemical, and radiation characteristics of these particles are discussed below. Table B.35 contains representative sets of data, including data on particles collected on the YAG 40 and at several other stations during each shot.

Physical and Chemical Characteristics. Slurry particles have been studied extensively and are discussed in detail in Reference 31. The results of preliminary studies of the insoluble solids contained in such particles are given in Reference 32. Figure 3.28 is a photomicrograph of a typical deposited slurry droplet, after reaction with the chloride-sensitive reagent film surface. The chloride-reaction area appears as a white disk, while the trace or impression of the impinging drop is egg shaped and encloses the insoluble solids. The concentric rings are thought to be a Liesegang phenomenon. An electronmicrograph of a portion of the solids is shown in Figure 3.29, illustrating the typical dense agglomeration of small spheres and irregular particles.

The physical properties of the droplets were established in part by microscopic examination in the YAG 40 laboratory soon after their arrival, and in part by subsequent measurements and calculations. For example, the dimensions of the droplets that appeared on the greased trays provided a rapid approximation of drop diameter, but the sphere diameters reported in Table 3.12 were calculated from the amount of chloride (reported as NaCl equivalent) and H_2O measured later from the reagent films. It will be noted that particle size decreased very slowly with time; and that for any given time period, size distribution need not be considered, because standard deviations are small. Average densities for the slurry particles, calculated from their dimensions and the masses of NaCl and H_2O present, are also given in Table 3.12.

On the basis of the data in Table 3.12, and a calibration method for solids volume that involved the collection on reagent film of simulated slurry droplets containing aluminum oxide suspensions of appropriate diameter at known concentrations, it was estimated that the particles were about 80 percent NaCl, 18 percent H_2O, and 2 percent insoluble solids by volume. The latter were generally amber in color and appeared under high magnification (Figure 3.29) to be agglomerates composed of irregular and spherical solids ranging in size from about 15 microns to less than 0.1 micron in diameter. The greatest number of these solids were spherical and less than 1 micron in diameter, although a few were observed in the size range from 15 to 60 microns.

Chemical properties were determined by chloride reagent film, X-ray diffraction, and electron diffraction techniques. (The gross chemistry of slurry drops is of course implicit in the analyses of the OCC collections from Shots Flathead and Navajo (Table B.18); no attempt has been made to determine the extent of correlation.) The first featured the use of a gelatin film containing colloidal red silver dichromate, with which the soluble halides deposited on the film

react when dissolved in saturated, hot water vapor. The area of the reaction disk produced, easily measured with a microscope, is proportional to the amount of NaCl present (Reference 33). The values of NaCl mass listed in Table 3.12 were obtained by this method; the values of H_2O mass were obtained by constructing a calibration curve relating the volume of water in the particle at the time of impact to the area of its initial impression, usually well defined by the insoluble solids trace (Figure 3.28). Because the water content of slurry fallout varies with atmospheric conditions at the time of deposition, mass is expressed in terms of the amount of NaCl present; the weight of water may be estimated by multiplying the NaCl mass by 1.2, the average observed factor.

Conventional X-ray diffraction methods were used for qualitative analysis of the insoluble solids, stripped from the reagent film by means of an acrylic spray coating, and they were found to consist of calcium iron oxide ($2\ CaO \cdot Fe_2O_3$), oxides of calcium and iron, and various other compounds (Table 3.13). Some of these were also observed by electron diffraction.

Radiochemical Characteristics. Thirteen of the most-active slurry particles removed from the SIC trays in the YAG 40 laboratory during Shot Flathead were combined (Reference 26), and analyzed radiochemically in much the same way as the solid particles described earlier in Section 3.3.1. The sample was assayed in the gamma well counter (WC) and the 4-π gamma ionization chamber (GIC), then analyzed for Mo^{99}, Ba^{140}-La^{140}, Sr^{89}, and Np^{239}; total fissions, activity ratios, R-values and the product/fission ratio were computed as before. The results are presented in Table 3.14.

It may be seen that the product/fission ratio and $R^{99}(89)$ value are comparable with the values obtained for gross fallout samples (Tables 3.17, 3.18, and 3.21), and that the overall radionuclide composition resembles that of the unaltered solid particles. Slight depletion of both Ba^{140}-La^{140} and Sr^{89} is indicated.

Activity Relationships. Since the mass of slurry-particle fallout was expressed in terms of NaCl mass, it was decided to attempt to express activity relationships in the same terms. This was accomplished in two steps. First, the H+12-hours well-counter activities measured on the IC trays from the majority of the stations listed in Table 3.12 were summed to arrive at the total amounts of activity deposited per unit area (counts per minute per square foot). These values were then divided by the average specific activity calculated for each station (counts per minute per microgram NaCl) to obtain the total amount of NaCl mass deposited per unit area (micrograms NaCl per square foot). Results for Shot Flathead are plotted in Figure 3.30, and numerical values for both shots are tabulated in Table B.11; the Navajo results were not plotted because of insufficient data. (Figure 3.30 and Table B.11 have been corrected for recently discovered errors in the tray activity summations reported in Reference 31.)

While this curve may be used to estimate the amount of activity associated with a given amount of slurry-fallout mass in outlying areas, it must be remembered that the curve is based on average specific activity. It should also be noted that the unusually high values of NaCl mass obtained for the YFNB 29 during Shot Flathead have not been plotted. A correspondingly high value for the YFNB 13 during Shot Navajo appears in the table. These were felt to reflect differences in composition which are not yet well understood.

A preliminary effort was also made to determine the way in which the activity of slurry particles was divided between the soluble and insoluble phases. As illustrated in Figure 3.31, radioautographs of chloride reaction areas on reagent films from all of the Flathead collections and a few of the Navajo shipboard collections indicated that the majority of the activity was associated with the insoluble solids. This result was apparently confirmed when it was found that 84 percent of the total activity was removable by physical stripping of the insoluble solids; however, more careful later studies (private communication from N. H. Farlow, NRDL) designed to establish the amount of activity in solids that could not be stripped from the film, and the amount of dissolved activity in gelatin removed with the strip coating, decreased this value to 65 percent. It must be noted that the stripping process was applied to a Flathead sample from the YAG 40 only, and that solubility experiments on OCC collections from other locations at Shot Navajo (Reference 32) indicated the partition of soluble-insoluble activity may vary with collector location or time of arrival. The latter experiments, performed in duplicate, yielded

average insoluble percentages of 93 and 14 for the YAG 39 (two aliquots) and the YFNB 13 respectively.

While such properties of barge shot fallout as the slurry nature of the droplets, diameters, densities, and individual activities have been adequately measured, it is evident that more extensive experimentation is required to provide the details of composition of the solids, their contribution to the weight of the droplets, and the distribution of activity within the contents of the droplets.

3.3.3 Activity and Fraction of Device. An estimate of the total amount of activity deposited at every major and minor station during each shot is listed in Table 3.15. Values are expressed both as fissions per square foot and fraction of device per square foot for convenience. In the case of the major stations the weighted mean and standard deviation of measurements made on the four OCC's and two AOC_1's on the standard platform are given, while the values tabulated for the minor stations represent single measurements of AOC_2 collections. Basic data for both cases are included in Tables B.12 and B.14. (Tray activities were found to pass through a maximum and minimum separated by about 180 degrees when plotted against angular displacement from a reference direction; ten values at 20-degree intervals between the maximum and minimum were used to compute the mean and standard deviation (Section 4.3.2).)

The number of fissions in one OCC tray from each major station and one standard cloud sample was determined by radiochemical analysis for Mo^{99} after every shot (Reference 34). Because these same trays and samples had previously been counted in the doghouse counter (Section 2.2), the ratio of doghouse counts per minute at 100 hours could then be calculated for each shot and location, as shown in Table B.13, and used to determine the number of fissions in the remaining OCC trays (fissions per 2.60 ft^2, Table B.12). Final fissions per square foot values were converted to fraction of device per square foot by means of the fission yields contained in Table 2.1 and use of the conversion factor 1.45×10^{26} fissions/Mt(fission). (Slight discrepancies may be found to exist in fraction of device values based on Mo^{99}, because only interim yields were available at the time of calculation.)

Aliquots from some of the same OCC trays analyzed radiochemically for Mo^{99} were also measured on the dip counter. Since the number of fissions in the aliquots could be calculated and the fallout from Shots Flathead and Navajo was relatively unfractionated, the total number of fissions in each AOC_2 from these shots could be computed directly from their dip-counter activities using a constant ratio of fissions per dip counts per minute at 100 hours. Table B.14I gives the results.

Shot Zuni, and to a lesser extent Shot Tewa, fallout was severely fractionated, however, and it was necessary first to convert dip-counter activities to doghouse-counter activities, so that the more-extensive relationships between the latter and the fissions in the sample could be utilized. With the aliquot measurements referred to above, an average value of the ratio of doghouse activity per dip-counter activity was computed (Table B.15), and this used to convert all dip counts per minute at 100 hours to doghouse counts per minute at 100 hours (Table B.14II). The most appropriate value of fissions per doghouse counts per minute at 100 hours was then selected for each minor station, on the basis of its location and the time of fallout arrival, and the total number of fissions calculated for the collector area, 0.244 ft^2. Final fission per square foot values were arrived at by normalizing to 1 ft^2, and fraction of device per square foot was computed from the total number of device fissions as before.

Many of the results presented in this report are expressed in terms of 10^4 fissions. For example, all gamma- and beta-decay curves in Section 3.4 (Figures 3.34 to 3.38) are plotted in units of counts per second per 10^4 fissions, and the final ionization rates as a function of time for each shot (Figure 3.39) are given in terms of roentgens per hour per 10^4 fissions per square foot. Thus, the estimates in Table 3.15 are all that is required to calculate the radiation intensities which would have been observed at each station under ideal conditions any time after the cessation of fallout. It should be noted, however, that the effects of sampling bias have not been entirely eliminated from the tabulated values and, consequently, will be reflected in any quantity determined by means of them. Even though the use of weighted-mean collector values for the

major stations constitutes an adjustment for relative platform bias, the question remains as to what percent of the total number of fissions per unit area, which would have been deposited in the absence of the collector, were actually collected by it. This question is considered in detail in Section 4.3.2.

3.3.4 Chemical Composition and Surface Density. The total mass of the fallout collected per unit area at each of the major stations is summarized for all four shots in Table 3.16. Results are further divided into the amounts of coral and sea water making up the totals, on the assumption that all other components in the device complex contributed negligible mass. These values were obtained by conventional quantitative chemical analysis of one or more of the OCC tray collections from each station for calcium, sodium, chlorine, potassium, and magnesium (References 35 through 38); in addition analyses were made for iron, copper and uranium (private communication from C. M. Callahan and J. R. Lai, NRDL). The basic chemical results are presented in Tables B.16 and B.18. (Analyses were also attempted for aluminum and lead; possibly because of background screening, however, they were quite erratic and have not been included.)

The chemical analysis was somewhat complicated by the presence in the collections of a relatively large amount of debris from the fiberglass honeycomb (or hexcell) inserts, which had to be cut to collector depth and continued to spall even after several removals of the excess material. It was necessary, therefore, to subtract the weight of the fiberglass present in the samples in order to arrive at their gross weights (Table B.18I). The weight of the fiberglass was determined in each case by dissolving the sample in hydrochloric acid to release the carbonate, filtering the resultant solution, and weighing the insoluble residue. In addition, the soluble portion of the resin binder was analyzed for the elements listed above and subtracted out as hexcell contribution to arrive at the gross amounts shown (References 39 and 40). Aliquots of the solution were then used for the subsequent analyses.

It was also necessary to subtract the amount of mass accumulated as normal background. These values were obtained by weighing and analyzing samples from a number of OCC trays which were known to have collected no fallout, although exposed during the fallout period. Many of the trays from Shot Cherokee, as well as a number of inactive trays from other shots, were used; and separate mean weights with standard deviations were computed for each of the elements under ocean and land collection conditions (Tables B.16 and B.18).

After the net amount of each element due to fallout was determined, the amounts of original coral and sea water given in Table 3.16 could be readily computed with the aid of the source compositions shown in Table B.16. In most cases, coral was determined by calcium; however, where the sea water/coral ratio was high, as for the barge shots, the sea water contribution to the observed calcium was accounted for by successive approximation. Departure from zero of the residual weights of the coral and sea water components shown in Table B.18 reflect combined errors in analyses and compositions. It should be noted that all ± values given in these data represent only the standard deviation of the background collections, as propagated through the successive subtractions. In the case of Shot Zuni, two OCC trays from each platform were analyzed several months apart, with considerable variation resulting. It is not known whether collection bias, aging, or inherent analytical variability is chiefly responsible for these discrepancies.

The principal components of the device and its immediate surroundings, exclusive of the naturally occurring coral and sea water, are listed in Table B.17. The quantities of iron, copper and uranium in the net fallout are shown in Table B.18I to have come almost entirely from this source. Certain aliquots from the OCC trays used for radiochemical analysis were also analyzed independently for these three elements (Table B.18II). These data, when combined with the tabulated device complex information, allow computation of fraction of device; the calculations have been carried out in Section 4.3.4 for uranium and iron and compared with those based on Mo^{99}.

3.4 RADIONUCLIDE COMPOSITION AND RADIATION CHARACTERISTICS

3.4.1 Approach. If the identity, decay scheme, and disintegration rate of every nuclide in

a sample are known, then all emitted particle or photon properties of the mixture can be computed. If, in addition, calibrated radiation detectors are available, then the effects of the sample emissions in those instruments may also be computed and compared with experiment. Finally, air-ionization or dose rates may be derived for this mixture under specified geometrical conditions and concentrations.

In the calculations to follow, quantity of sample is expressed in time-invariant fissions, i.e., the number of device fissions responsible for the gross activity observed; diagnostically, the quantity is based on radiochemically assayed Mo^{99} and a fission yield of 6.1 percent. This nuclide, therefore, becomes the fission indicator for any device and any fallout or cloud sample. The computation for slow-neutron fission of U^{235}, as given in Reference 41, is taken as the reference fission model; hence, any $R^{99}(x)$ values in the samples differing from unity, aside from experimental uncertainty, represent the combined effects of fission kind and fractionation, and necessitate modification of the reference model if it is to be used as a basis for computing radiation properties of other fission-product compositions. (An R-value may be defined as the ratio of the amount of nuclide x observed to the amount expected for a given number of reference fissions. The notation $R^{99}(x)$ means the R-value of mass number x referred to mass number 99.)

Two laboratory instruments are considered: the doghouse counter employing a 1-inch-diameter-by-1-inch-thick NaI(Tl) crystal detector, and the continuous-flow proportional beta counter (Section 2.2). The first was selected because the decay rates of many intact OCC collections and all cloud samples were measured in this instrument; the second, because of the desirability of checking calculated decay rates independent of gamma-ray decay schemes. Although decay data were obtained on the 4-π gamma ionization chamber, response curves (Reference 42) were not included in the calculations. However, the calculations made in this section are generally consistent with the data presented in Reference 42. The data obtained are listed in Table B.26.

3.4.2 Activities and Decay Schemes. The activities or disintegration rates of fission products for 10^4 fissions were taken from Reference 41; the disintegration rates are used where a radioactive disintegration is any spontaneous change in a nuclide. Other kinds of activities are qualified, e.g., beta activity. (See Section 3.4.4.) Those of induced products of interest were computed for 10^4 fissions and a product/fission ratio of 1, that is, for 10^4 initial atoms (Reference 43).

Prepublication results of a study of the most-important remaining nuclear constants—the decay schemes of these nuclides—are contained in References 42 and 44. The proposed schemes, which provide gamma and X-ray photon energies and frequencies per disintegration, include all fission products known up to as early as ~45 minutes, as well as most of the induced products required. All of the following calculations are, therefore, limited to the starting time mentioned and are arbitrarily terminated at 301 days.

3.4.3 Instrument Response and Air-Ionization Factors. A theoretical response curve for the doghouse counter, based on a few calibrating nuclides, led to the expected counts/disintegration of each fission and induced product as a function of time, for a point-source geometry and 10^4 fissions or initial atoms (Reference 43). The condensed decay schemes of the remaining induced nuclides were also included. To save time, the photons emitted from each nuclide were sorted into standardized energy increments, 21 of equal logarithmic width comprising the scale from 20 kev to 3.25 Mev. The response was actually computed for the average energy of each increment, which in general led to errors no greater than ~10 percent.

Counting rates expected in the beta counter were obtained from application of the physical-geometry factor to the theoretical total-beta and positron activity of the sample. With a response curve essentially flat to beta E_{max} over a reasonably wide range of energies, it was not necessary to derive the response to each nuclide and sum for the total. Because the samples were essentially weightless point sources, supported and covered by 0.80 mg/cm^2 of pliofilm, scattering and absorption corrections were not made to the observed count rates; nor were gamma-ray contributions subtracted out. Because many of the detailed corrections are self-

canceling, it is assumed the results are correct to within ~20 percent. The geometries (or counts/beta) for Shelves 1 through 5 are given in Section A.2.

Air-ionization rates 3 feet above an infinite uniformly contaminated plane, hereafter referred to as standard conditions (SC), are based on the curve shown in Figure B.6, which was originally obtained in another form in Reference 7. The particular form shown here, differing mainly in choice of parameters and units, has been published in Reference 45. Points computed in Reference 46 and values extracted from Reference 47 are also shown for comparison. The latter values are low, because air scattering is neglected.

The ionization rate (SC) produced by each fission-product nuclide as a function of time for 10^4 reference fissions/ft^2 (Reference 17), was computed on a line-by-line basis; the induced products appear in Table B.19 for 10^4 fissions/ft^2 and a product/fission ratio of 1, with lines grouped as described for the doghouse-counter-response calculations.

The foregoing sections provide all of the background information necessary to obtain the objectives listed in the first paragraph of Section 3.4.1, with the exception of the actual radionuclide composition of the samples. The following sections deal with the available data and methods used to approximate the complete composition.

3.4.4 Observed Radionuclide Composition. Radiochemical R-values of fission products are given in Table 3.17 and observed actinide product/fission ratios appear in Table 3.18, the two tables summarizing most of the radiochemistry done by the Nuclear and Physical Chemistry, and Analytical and Standards Branches, NRDL (Reference 34).

The radiochemical results in Reference 34 are expressed as device fractions, using fission yields estimated for the particular device types. These have been converted to R-values by use of the equation:

$$R_{\theta}^{99}(x) = \frac{FOD_E(x)}{FOD(99)} \cdot \frac{FY_E(x)}{FY_{\theta}(x)}$$

Where $R_{\theta}^{99}(x)$ is the R-value of nuclide x relative to Mo^{99}; $FOD_E(x)$ and $FY_E(x)$ are respectively the device fraction and estimated yield of nuclide x reported in Reference 34, $FY_{\theta}(x)$ is the thermal yield of nuclide x, and FOD(99) is the device fraction by Mo^{99}. The thermal yields used in making this correction were taken from ORNL 1793 and are as follows: Zr^{95}, 6.4 percent; Te^{132}, 4.4 percent; Sr^{89}, 4.8 percent; Sr^{90}, 5.9 percent; Cs^{137}, 5.9 percent; and Ce^{144}, 6.1 percent. The yield of Mo^{99} was taken as 6.1 percent in all cases. The R-values for all cloud-sample nuclides were obtained in that form directly from the authors of Reference 34.

Published radiochemical procedures were followed (References 48 through 54), except for modifications of the strontium procedure, and consisted of two $Fe(OH)_3$ and $BaCrO_4$ scavenges and one extra $Sr(NO_3)_2$ precipitation with the final mounting as $SrCO_3$. Table 3.19 lists principally product/fission ratios of induced activities other than actinides for cloud samples; sources are referenced in the table footnotes.

Supplementary information on product/fission ratios in fallout and cloud samples was obtained from gamma-ray spectrometry (Tables B.20 and B.21) and appears in Table 3.20.

3.4.5 Fission-Product-Fractionation Corrections. Inspection of Tables 3.17 through 3.20, as well as the various doghouse-counter and ion-chamber decay curves, led to the conclusion that the radionuclide compositions of Shots Flathead and Navajo could be treated as essentially unfractionated. It also appeared that Shots Zuni and Tewa, whose radionuclide compositions seemed to vary continuously from lagoon to cloud, and probably within the cloud, might be covered by two compositions: one for the close-in lagoon area, and one for the more-distant ship and cloud samples. The various compositions are presented as developed, starting with the simplest. The general method and supporting data are given, followed by the results.

Shots Flathead and Navajo. Where fission products are not fractionated, that is, where the observed $R^{99}(x)$ values are reasonably close to 1 (possible large R-values among low-yield valley and right-wing mass numbers are ignored), gross fission-product properties may

be readily extracted from the sources cited. Induced product contributions may be added in after diminishing the tabular values (product/fission = 1) by the proper ratio. After the resultant computed doghouse-counter decay rate is compared with experiment, the ionization rate (SC) may be computed for the same composition. Beta activities may also be computed for this composition—making allowance for those disintegrations that produce no beta particles. The Navajo composition was computed in this manner, as were the rest of the compositions, once fractionation corrections had been made.

Shot Zuni. A number of empirical corrections were made to the computations for unfractionated fission products in an effort to explain the decay characteristics of the residual radiations from this shot. The lagoon-area composition was developed first, averaging available lagoon area R-values. As shown in Figure 3.32, R-values of nuclides which, in part at least, are decay products of antimony are plotted against the half life of the antimony precursor, using the fission-product decay chains tabulated in Reference 56. (Some justification for the assumptions are made that, after ~45 minutes, the R-values of all members of a given chain are identical, and related to the half life of the antimony precursor, then Figure 3.32 may be used to estimate R-values of other chains containing antimony precursors with different half lives. The R-value so obtained for each chain is then used as a correction factor on the activity (Reference 41) of each nuclide in that chain, or more directly, on the computed doghouse activity or ionization (SC) contribution (Table 3.21). The partial decay products of two other fractionating precursors, xenon and krypton, are also shown in Figure 3.32, and are similarly employed. These deficiencies led to corrections in some 22 chains, embracing 54 nuclides that contributed to the activities under consideration at some time during the period of interest. The R-value of I^{131} was taken as 0.03; a locally measured but otherwise unreported I^{133}/I^{131} ratio of 5.4 yields an I^{133} R-value of 0.16.

Although the particulate cloud composition might have been developed similarly, using a different set of curves based on cloud R-values, it was noticed that a fair relation existed between cloud and lagoon nuclide R-values as shown in Figure 3.33. Here $R^{99}(x)$ cloud/$R^{99}(x)$ lagoon is plotted versus $R^{99}(x)$ lagoon average. The previously determined lagoon chain R-values were then simply multiplied by the indicated ratio to obtain the corresponding cloud R-values. The dotted lines indicate the trends for two other locations, YAG 39 and YAG 40, although these were not pursued because of time limitations. It is assumed that the cloud and lagoon compositions represent extremes, with all others intermediate. No beta activities were computed for this shot.

Shot Tewa. Two simplifying approximations were made. First, the cloud and outer station average R-values were judged sufficiently close to 1 to permit use of unfractionated fission products. Second, because the lagoon-area fission-product composition for Shot Tewa appeared to be the same as for its Zuni counterpart except in mass 140, the Zuni and Tewa lagoon fission products were therefore judged to be identical, except that the Ba^{140}-La^{140} contribution was increased by a factor of 3 for the latter.

The induced products were added in, using product/fission ratios appropriate to the location wherever possible; however, the sparsity of ratio data for fallout samples dictated the use of cloud values for most of the minor induced activities.

3.4.6 Results and Discussion. Table B.22 is a compilation of the computed doghouse counting rates for the compositions described; these data and some observed decay rates are shown in Figures 3.34 through 3.37. All experimental doghouse-counter data is listed in Table B.23. Table B.24 similarly summarizes the Flathead and Navajo computed beta-counting rates; they are compared with experiment in Figure 3.38, and the experimental data are given in Table B.25. Results of the gamma-ionization or dose rate (SC) calculations for a surface concentration of 10^4 fissions/ft^2 are presented in Table 3.22 and plotted in Figure 3.39. It should be emphasized that these computed results are intended to be absolute for a specified composition

and number of fissions as determined by Mo^{99} content, and no arbitrary normalization has been employed to match theory and experiment. Thus, the curves in Figure 3.39, for instance, represent the best available estimates of the SC dose rate produced by 10^4 fissions/ft^2 of the various mixtures. The Mo^{99} content of each of the samples represented is identical, namely the number corresponding to 10^4 fissions at a yield of 6.1 percent. The curves are displaced vertically from one another solely because of the fractionation of the other fission products with respect to Mo^{99}, and the contributions of various kinds and amounts of induced products.

It may be seen that the computed and observed doghouse-counter decay rates are in fairly good agreement over the time period for which data could be obtained. The beta-decay curves for Shots Flathead and Navajo, initiated on the YAG 40, suggest that the computed gamma and ionization curves, for those events at least, are reasonably correct as early as 10 to 15 hours after detonation.

The ionization results may not be checked directly against experiment; it was primarily for this reason that the other effects of the proposed compositions were computed for laboratory instruments. If reasonable agreement can be obtained for different types of laboratory detectors, then the inference is that discrepancies between computed and measured ionization rates in the field are due to factors other than source composition and ground-surface fission concentration.

The cleared area surrounding Station F at How Island (Figure 2.8) offers the closest approximation to the standard conditions for which the calculations were made, and Shot Zuni was the only event from which sufficient fallout was obtained at this station to warrant making a comparison. With the calculated dose rates based on the average buried-tray value of $2.08 \pm 0.22 \times 10^{14}$ fissions/ft^2 (Table B.27) and the measured rates from Table B.28, (plotted in Figure B.7), the observed/calculated ratio varies from 0.45 at 11.2 hours to 0.66 from 100 to 200 hours, falling to an average of 0.56 between 370 and 1,000 hours. Although detailed reconciliation of theory and experiment is beyond the scope of this report, some of the factors operating to lower the ratio from an ideal value of unity were: (1) the cleared area was actually somewhat less than infinite in extent, averaging ~120 feet in radius, with the bulldozed sand and brush ringing the area in a horseshoe-shaped embankment some 7 feet high; (2) the plane was not mathematically smooth; and (3) the survey instruments used indicate less than the true ionization rate, i.e., the integrated response factor, including an operator, is lower than that obtained for Co^{60} in the calibrating direction.

It is estimated that, for average energies from 0.15 Mev to 1.2 Mev, a cleared radius of 120 feet provides from ~0.80 to ~0.70 of an infinite field (Reference 46). The Cutie Pie survey meter response, similar to the T1B between 100 kev and 1 Mev, averages about 0.85 (Reference 17). These two factors alone, then, could depress the observed/calculated ratio to ~0.64.

TABLE 3.1 TIMES OF ARRIVAL, PEAK ACTIVITY, AND CESSATION AT MAJOR STATIONS

Time of arrival (t_a) indicates the earliest reliable arrival time of fallout as determined from the incremental collector and gamma time-intensity recorder results. Time of peak activity (t_p) indicates the time of peak ionization rate (in parentheses) and the times during which the ionization rate was within 10 percent of the peak rate. I_p refers to the peak ionization rate. Time of cessation (t_c) indicates, first, the time by which 95 percent of the fallout had been deposited and, next, the extrapolated time of cessation.

Shot	Station	t_a	t_p			I_p	t_c
		TSD, hr	TSD, hr			r/hr	TSD, hr
Flathead	YAG 40 (A, B)	8.0	12	(17.0)	20	0.259	22 to 23
	YAG 39 (C)	4.5	10	(11.0)	13	0.141	13 to 15
	LST 611 (D)	6.6	9.0	(9.1)	9.2	0.098	20 to 25
	YFNB 13 (E)	0.35	1.1	(1.3)	1.5 *	21.8 *	2.0 to †
	YFNB 29 (G, H)	0.62	1.2	(1.52)	1.9	0.98	1.5 to 9.0
	How Island (F)	‡		‡		‡	‡
Navajo	YAG 40 (A, B)	6.0	11	(12.3)	13	0.129	16 to 20
	YAG 39 (C)	2.3	5.9	(6.0)	6.2	1.49	15 to 16
	LST 611 (D)	3.0	5.6	(6.1)	6.7	0.043	13 to 18
	YFNB 13 (E)	0.20	0.58	(0.63)	0.73	8.5	1.9 to 9.0 §
	YFNB 29 (G, H)	0.68	1.2	(1.33)	1.9	0.116	3.2 to 14 §
	How Island (F)	0.75		¶		¶	4.5 to 7.0 §
Zuni	YAG 40 (A, B)	3.4	6.2	(6.7)	7.7	7.6	7.4 to 13
	YAG 39 (C)	12	20	(25)	33	0.038	29 to 33
	LST 611 (D)	‡		‡		‡	‡
	YFNB 13 (E)	0.33	0.97	(1.25)	1.6 *	6 *	1.9 to 9.3
	YFNB 29 (G, H)	0.32	0.70	(0.82)	1.2	9.6	2.4 to 3.3
	How Island (F)	0.38	0.98	(1.05)	1.4	2.9	1.9 to 2.6
Tewa	YAG 40 (A, B)	4.4	6.2	(7.2)	7.6	7.43	8.5 to 16
	YAG 39 (C)	2.0	4.4	(5.0)	5.7	20.2	5.3 to 16
	LST 611 (D)	7.0	13	(13.6)	15	0.256	14 to 18
	YFNB 13 (E)	0.25	1.8	(1.9)	3.0	2.5	7.0 to 16
	YFNB 29 (G, H)	0.23	1.4	(1.7)	2.8 *	40 *	4.3 to 16
	How Island (F)	1.6	2.5	(2.9)	3.4	2.5	3.3 to 9.0

* Estimated value; gamma time-intensity recorder saturated.
† No determination possible; incremental collector failed.
‡ No fallout occurred.
§ Minimum value.
¶ Instrument failed.

IN THE ATOLL AREA

Time of arrival (t_a) indicates the arrival time of fallout as determined from the time of arrival detector results.

Station	Shot Flathead t_a	Shot Navajo t_a	Shot Zuni t_a	Shot Tewa t_a
	TSD, hr	TSD, hr	TSD, hr	TSD, hr
YFNB 13 (E)	*	*	†	*
YFNB 29 (G)	0.77	*	0.40	*
YFNB 29 (H)	0.68	*	0.40	*
How Island (F)	‡	*	0.35	*
How Island (K)	‡	*	0.40 §	*
George Island (L)	0.02 †	†	0.33	†
Charlie Island (M)	—	†	—	†
William Island (M)	‡	—	0.22	—
Raft-1 (P)	‡	‡	0.33	†
Raft-2 (R)	†	0.73	†	†
Raft-3 (S)	0.5	0.05 †	0.23	0.48
Skiff-AA	9.1 ¶	9.4	*	5.0
Skiff-BB	†	†	3.8 §	†
Skiff-CC	4.7	‡	*	4.2
Skiff-DD	‡	‡	*	‡
Skiff-EE	‡	‡	3.0 §	‡
Skiff-FF	‡	‡	†	‡
Skiff-GG	*	*	2.0 §	2.9 §
Skiff-HH	†	†	†	2.2
Skiff-KK	‡	†	*	‡
Skiff-LL	‡	‡	†	‡
Skiff-MM	*	4.3	2.9	2.0
Skiff-PP	†	1.4	*	†
Skiff-RR	4.1	†	1.7	†
Skiff-SS	10.6	—	†	—
Skiff-TT	‡	‡	†	‡
Skiff-UU	‡	—	†	—
Skiff-VV	—	—	*	—
Skiff-WW	—	—	—	†
Skiff-XX	—	—	—	1.2 §
Skiff-YY	—	—	—	†

* Skiff or instrument lost, or no instrument present.
† Instrument malfunctioned or may have malfunctioned.
‡ Activity level insufficient to trigger instrument; no fallout or only light fallout occurred.
§ Estimated value; clock reading corrected by ± an integral number of days.
¶ Instrument may have triggered at peak; low arrival rate.

TABLE 3.3 PENETRATION RATES DERIVED FROM EQUIVALENT-DEPTH DETERMINATIONS

Shot	Station	Number of Points	Time Studied From	Time Studied To	Rate	± Limits 95 pct Confidence
			TSD, hr		m/hr	m/hr
Flathead	YAG 39	10	8.3	12.8	3.0	2.5
Navajo	YAG 39	10	7.4	18.6	2.6	0.2
Navajo	YAG 40	4	10.0	13.0	4.0	2.1
Tewa	YAG 39	26	5.1	14.8	3.0	0.7
Tewa	YAG 40	5	5.2	8.1	4.0	2.9

TABLE 3.4 DEPTHS AT WHICH PENETRATION CEASED FROM EQUIVALENT-DEPTH DETERMINATIONS

Shot	Station	Number of Points	Time Studied From	Time Studied To	Depth	± Limits 95 pct Confidence	Estimated Thermocline Depth *
			TSD, hr		meters	meters	meters
Navajo	YAG 39	13	30.9	40.1	62	15	40 to 60
Tewa	YAG 39	17	15.3	20.5	49	10	40 to 60
			31.8	34.8			

* See Reference 15.

TABLE 3.5 MAXIMUM PENETRATION RATES OBSERVED

Shot	Station	Number of Points	Time Studied From	Time Studied To	Rate	± Limits 95 pct Confidence
			TSD, hr		m/hr	m/hr
Zuni	YAG 39	3	15.2	16.8	~30	—
		9	17.8	29.8	2.4	0.9
Navajo	YAG 39	5	3.1	5.2	23.0	9.8
Tewa	YAG 39	2	3.8	4.1	~300	—

TABLE 3.6 EXPONENT VALUES FOR PROBE DECAY MEASUREMENTS

The tabulated numbers are values of n in the expression: $A = A_0 (t/t_0)^n$, where A indicates the activity at a reference time, t, and A_0 the activity at the time of observation, t_0.

Shot	Exponent Values	
	Project 2.63	Project 2.62a
Zuni	0.90	1.13
Flathead	0.90	1.05
Navajo	1.39	1.39
Tewa	*	1.34

* Instrument malfunctioned.

TABLE 3.7 X-RAY DIFFRACTION ANALYSES AND SPECIFIC ACTIVITIES OF INDIVIDUAL PARTICLES, SHOT ZUNI

Serial Number	Type	Size	Activity at H + 240 hrs	Net Weight	Specific Activity	Compounds Present			Particle Description
						$CaCO_3$	CaO	$Ca(OH)_2$	
		mm	well counts/min	mg	(counts/min)/mg				
165	Sphere	2	17,500,000	6.9	2,540,000	X	X	X	Creamy-white; surface protuberances.
166	Sphere	2	36,500,000	17.3	2,110,000	X	XX*	XX	White, off-white; green-yellow; patchy.
167	Irregular	†	2,410,000	40.1	60,200	X			Rubbery; fibrous; shapeless.
168	Sphere	2	36,200,000	8.7	4,160,000	X	X	X	Pale yellow; white patches.
169	Irregular	2 × 2.5	101,140	11.9	8,500	XX			Resembles actual coral; easily fractured.
170	Irregular	2 × 6	955,340	†	†	X		X	Columnar structure.
171	Agglomerate	†	6,300,000	†	†		X	X	Broken; extremely friable.
172	Agglomerate	†	16,700,000	†	†	X	X	X	Broken; white and pale yellow-green; friable.
173	Irregular	2.5 × 5.0	2,200,000	11.4	193,000	XX		XX	Cavities and tunnels throughout.
174	Sphere	2.1	24,500,000	7.1	3,450,000	X	X	X	Off-white; slightly ellipsoidal.
175	Sphere	†	9,100,000	2.5	3,640,000		X	X	Clear cubic and yellowish irregular crystals.
176	Irregular	2 × 5	443,620	48.8	9,070	XX			Gray mass with embedded shells.
177	Agglomerate	†	2,600,000	†	†		X	X	Broken; white and pale green; very friable.
178	Irregular	8 × 8	1,900,000	388.0	4,900	X		X	Manmade, concretelike material.
179	Sphere	1.5	6,600,000	5.1	1,300,000	X	XX	XX	Yellowish mosaic surface.
180	Irregular	6 × 10	1,860,000	457.3	4,070	X		X	Same as Particle 178.
181	Irregular	2.5 × 4	27,300,000	25.8	1,060,000	X	XX	XX	Yellowish; finer-grained CaO.
182	Black sphere	1.7	70,600	9.0	7,840				$Fe_3O_4 + Fe_2O_3 \cdot H_2O$

* Examination was also made of interior of particle; XX indicates a compound detected both on exterior surface and interior.
† No data available.

TABLE 3.8 DISTRIBUTION OF PARTICLE DENSITIES, SHOT ZUNI

Total number of particles = 122. Total number of irregular particles = 7. Total number of yellow spheres = 71. Total number of white spheres = 44. Mean density of all spheres = 2.46 gm/cm^3. Mean density of yellow spheres = 2.53 gm/cm^3. Mean density of white spheres = 2.33 gm/cm^3.

Density	Percentage of Total Particles	Percentage of Yellow Spheres	Percentage of White Spheres
gm/cm^3			
2.0	2.5	1.4	4.7
2.1	6.7	2.8	11.6
2.2	7.5	2.8	16.3
2.3	22.5	14.0	35.0
2.4	9.2	9.9	9.1
2.5	10.7	8.5	13.9
2.6	15.0	22.6	4.7
2.7	19.2	29.6	4.7
2.8	5.8	8.5	2.3

TABLE 3.9 RADIOCHEMICAL PROPERTIES OF ALTERED AND UNALTERED PARTICLES, SHOT ZUNI

Quantity	Time	Altered Particles		Unaltered Particles	
		Number of Samples	Value	Number of Samples	Value
	TSD, hr				
fissions/gm ($\times 10^{14}$)	—	6	3.8 ± 3.1	9	0.090 ± 0.12
fissions/gm ($\times 10^{14}$) *	—	14	4.2 ± 2.7	24	0.033 ± 0.035
(counts/min)/10^4 fissions	71	4	0.34 ± 0.06	4	0.53 ± 0.19
(counts/min)/10^4 fissions	105	3	0.35 ± 0.08	7	1.1 ± 0.4
(counts/min)/10^4 fissions	239	1	0.054	1	0.12
(counts/min)/10^4 fissions	532	2	0.013	1	0.024
ma/10^4 fissions ($\times 10^{-17}$)	71	4	30 ± 5	4	59 ± 24
ma/10^4 fissions ($\times 10^{-17}$)	105	3	24 ± 7	7	109 ± 31
ma/10^4 fissions ($\times 10^{-17}$)	239	1	3.4	1	20
ma/10^4 fissions ($\times 10^{-17}$)	481	2	1.7	1	5.1
(counts/min)/ma ($\times 10^{14}$)	71	5	11 ± 1	4	9.3 ± 2.0
(counts/min)/ma ($\times 10^{14}$)	105	4	14 ± 3	13	8.6 ± 1.5
(counts/min)/ma ($\times 10^{14}$)	239	10	16 ± 2	6	8.2 ± 1.3

* Calculated from activity ratios on the basis of particles analyzed for total fissions.

TABLE 3.10 ACTIVITY RATIOS FOR PARTICLES FROM SHOTS ZUNI AND TEWA

Activity Ratio	Shot Zuni				Shot Tewa	
	Altered Particles		Unaltered Particles		All Particles	
	Value	Time	Value	Time	Value	Time
		TSD, hr		TSD, hr		TSD, hr
(counts/min)/ma ($\times 10^{14}$)	14. ± 3.	105	8.6 ± 1.5	105	11. ± 6.	96
	16. ± 2.	239	8.2 ± 1.3	239		
(counts/min)/10^4 fissions	0.35 ± 0.08	105	1.1 ± 0.4	105	0.38 ± 0.12	97
	0.054	239	0.12	239	0.18 ± 0.02	172
ma/10^4 fissions ($\times 10^{-17}$)	24. ± 7.	105	109. ± 31.	105	37. ± 15.	97
	3.4	239	20.	239		

TABLE 3.11 DISTRIBUTION OF ACTIVITY OF YAG 40 TEWA PARTICLES WITH SIZE AND TYPE

Size Group	Percent of Composite Total Activity	Percent of Size Group Activity		
		Irregular	Spheroidal	Agglomerated
microns				
16 to 33	<0.1	23.4	76.6	0.0
34 to 66	2.2	88.1	5.0	6.9
67 to 99	6.0	46.4	37.5	16.0
100 to 132	11.6	68.6	6.7	24.6
133 to 165	18.2	43.4	5.7	50.9
166 to 198	18.9	49.3	1.9	48.8
199 to 231	8.1	58.0	0.0	41.9
232 to 264	9.9	14.7	0.0	85.3
265 to 297	7.0	14.6	0.1	85.3
298 to 330	11.5	18.5	0.0	81.4
331 to 363	0.7	—	—	100.0
364 to 396	1.7	0.0	2.2	97.7
397 to 429	—	—	—	—
430 to 462	0.6	23.8	76.2	0.0
463 to 495	—	—	—	—
496 to 528	3.4	100.0	0.0	0.0

TABLE 3.12 PHYSICAL, CHEMICAL, AND RADIOLOGICAL PROPERTIES OF SLURRY PARTICLES

All indicated errors are standard deviations of the mean.

Time of Arrival Interval	Station	Number of Particles Measured	Average NaCl Mass	Average H_2O Mass	Average Density ± Standard Deviation	Average Diameter* ± Standard Deviation	Average Specific Activity ± Standard Deviation
TSD, hr			μg	μg	gm/cm^3	microns	$\times 10^{10}$ (counts/min)/gm†
Shot Flathead:							
1 to 3	YFNB 29	4 to 10	0.06	0.08	1.28 ± 0.1	57 ± 6	43 ± 8‡
7 to 9	YAG 39 and LST 611	50 to 52	0.42	0.62	1.29 ± 0.01	112 ± 2	282 ± 20
11 to 12	YAG 40	10	0.94	1.20	1.35 ± 0.05	129 ± 16	285 ± 160
15 to 18	YAG 40	3 to 4	0.50	0.69	1.34 ± 0.08	121 ± 6	265 ± 90
Totals		67 to 76			1.30 ± 0.01		282 ± 30§
Shot Navajo:							
1 to 3	YFNB 13	5 to 20	7.77	7.94	1.38 ± 0.04	272 ± 14	4 ± 0.6‡
3 to 5	YAG 39	9 to 14	7.62	4.49	1.50 ± 0.01	229 ± 24	16 ± 3
5 to 6	LST 611	14	1.61	1.83	1.41 ± 0.04	166 ± 6	14 ± 2
7 to 9	YAG 40	4 to 10	1.25	1.08	1.45 ± 0.04	142 ± 22	9 ± 3
9 to 10	YAG 40	5 to 23	0.44	0.60	1.31 ± 0.02	110 ± 5	11 ± 2
10 to 11	YAG 40	11 to 15	0.66	0.50	1.43 ± 0.03	111 ± 4	16 ± 4
11 to 12	YAG 40	33	0.30	0.44	1.32 ± 0.01	94 ± 4	26¶
12 to 13	YAG 40	28	0.31	0.31	1.37 ± 0.01	96 ± 2	21¶
13 to 14	YAG 40	6	0.17	0.27	1.28 ± 0.02	86 ± 7	29¶
14 to 15	YAG 40	5	0.10	0.18	1.30 ± 0.03	75 ± 2	23¶
15 to 18	YAG 40	13 to 14	0.06	0.32	1.15 ± 0.02	84 ± 4	56 ± 7
Totals		133 to 182			1.35 ± 0.01		21 ± 3§

* Diameter of spherical slurry droplet at time of arrival.

† Photon count in well counter at H + 12.

‡ Not included in calculation of total.

§ Based on summation of individual-particle specific activities.

¶ Calculated value based on total tray count, number of particles per tray, and average NaCl mass per particle; not included in calculation of total.

TABLE 3.13 COMPOUNDS IDENTIFIED IN SLURRY-PARTICLE INSOLUBLE SOLIDS

All compounds were identified by X-ray diffraction except Fe_2O_3 and $NaCa(SiO_4)$, which were identified by electron diffraction; $2CaO \cdot Fe_2O_3$ was also observed in one sample by electron diffraction. The presence of Cu in the Navajo sample was established by X-ray diffraction. I indicates definite identification and PI possible identification.

Compound	Shot Flathead	Shot Navajo
$2CaO \cdot Fe_2O_3$	I	
$CaCO_3$	I	I
Fe_2O_3	I	
Fe_3O_4	I	I
$CaSO_4 \cdot 2H_2O$	I	
NaCl	I	I
$NaCa(SiO_4)$		PI
SiO_2		PI
$MgO \cdot Fe_2O_3$		PI

TABLE 3.14 RADIOCHEMICAL PROPERTIES OF SLURRY PARTICLES, YAG 40, SHOT FLATHEAD

Analysis of the combined particles led to the following data: Description, essentially NaCl; WC, 0.872×10^6 counts/min; time of WC, 156 TSD, hrs; GIC, 88×10^{-11} ma; time of GIC, 196 TSD, hrs; fissions, 6.83×10^{10}; Ba^{140} Sr^{89}; Np^{239} product/fission ratio, 0.41; activity ratios at 196 TSD, hrs, 9.9×10^{14} (counts/min)/ma, 0.13 (counts/min)/10^4 fissions, and 13.0×10^{-17} ma/10^4 fissions.

Field Number	WC	Time of WC
	$\times 10^6$ counts/min	TSD, hrs
2680-1	0.0668	189
2682-2	0.116	190
2334-1	0.0730	190
2677-1	0.0449	193
2333-1	0.131	190
2682-1	0.0607	189
2331-1	0.249	189
2333-2	0.064	191
2334-4	0.146	190
2333-3	0.0487	190
2332-1	0.0295	190
2681-3	0.235	190
2681-1	0.141	190

TABLE 3.16 SURFACE DENSITY OF FALLOUT COMPONENTS IN TERMS OF ORIGINAL COMPOSITION

Shot	Collector	Weight, mg/ft²		
		Coral	Sea Water	Total
Flathead	YAG 40-B-19 FL	14.0 ± 1.0	195.2 ± 16.2	209.2 ± 16.2
	LST 611-D-51 FL	0.0 ± 1.0	89.2 ± 16.2	89.2 ± 16.2
	YFNB 13-E-56 FL	1.6 ± 1.0	6,155.0 ± 31.3	6,156.7 ± 31.3
	How F-67 FL	0.0 ± 2.57	32.6 ± 17.7	32.6 ± 17.9
	YFNB 29-H-81 FL	5.4 ± 1.0	564.2 ± 31.3	569.5 ± 31.3
Navajo	YAG 40-B-19 NA	4.3 ± 1.0	646.8 ± 31.3	651.1 ± 31.3
	YAG 39-C-36 NA	3.2 ± 1.0	1,416.4 ± 31.3	1,418.6 ± 31.3
	LST 611-D-51 NA	13.0 ± 1.0	1,299.5 ± 31.3	1,312.5 ± 31.3
	YFNB 13-E-54 NA	51.6 ± 1.0	5,129.8 ± 31.3	5,181.5 ± 31.3
	How F-67 NA	12.0 ± 2.6	561.3 ± 35.4	573.3 ± 35.4
	YFNB 29-H-81 NA	24.0 ± 1.0	0.0 ± 31.3	24.0 ± 31.3
Zuni	YAG 40-B-17 ZU	1,810.1 ± 1.0	116.8 ± 16.2	1,927.0 ± 16.2
	YAG 40-B-19 ZU	522.6 ± 1.0	166.1 ± 31.3	688.7 ± 31.3
	YAG 39-C-23 ZU	17.8 ± 1.0	88.6 ± 16.2	106.4 ± 16.2
	YAG 39-C-36 ZU	19.2 ± 1.0	55.0 ± 31.3	74.2 ± 31.3
	YFNB 13-E-56 ZU	1,574.8 ± 1.0	1,121.6 ± 16.2	2,696.4 ± 16.2
	YFNB 13-E-58 ZU	797.9 ± 1.0	583.9 ± 16.2	1,381.8 ± 16.2
	How F-63 ZU	989.5 ± 2.6	86.7 ± 0.3	1,076.2 ± 2.6
	How F-67 ZU	592.3 ± 2.6	221.8 ± 17.7	814.2 ± 17.9
	YFNB 29-H-79 ZU	2,912.9 ± 1.0	561.0 ± 16.2	3,473.8 ± 16.2
	YFNB 29-H-81 ZU	2,788.4 ± 1.0	1,274.2 ± 16.2	4,062.6 ± 16.2
Tewa	YAG 40-B-19 TE	661.7 ± 1.0	273.6 ± 16.2	935.3 ± 16.2
	YAG 39-C-36 TE	1,726.8 ± 1.0	517.5 ± 16.2	2,244.4 ± 16.2
	LST 611-D-51 TE	62.9 ± 1.0	0.0 ± 31.3	62.9 ± 31.3
	YFNB 13-E-56 TE	54.1 ± 1.0	199.0 ± 16.2	253.2 ± 16.2
	How F-67 TE	15.0 ± 2.4	13.6 ± 0.2	28.6 ± 2.4
	YFNB 29-H-81 TE	4,533.1 ± 1.0	0.0 ± 31.3	4,533.1 ± 31.3

Page 66 Deleted.
Pages 68 thru 75 Deleted

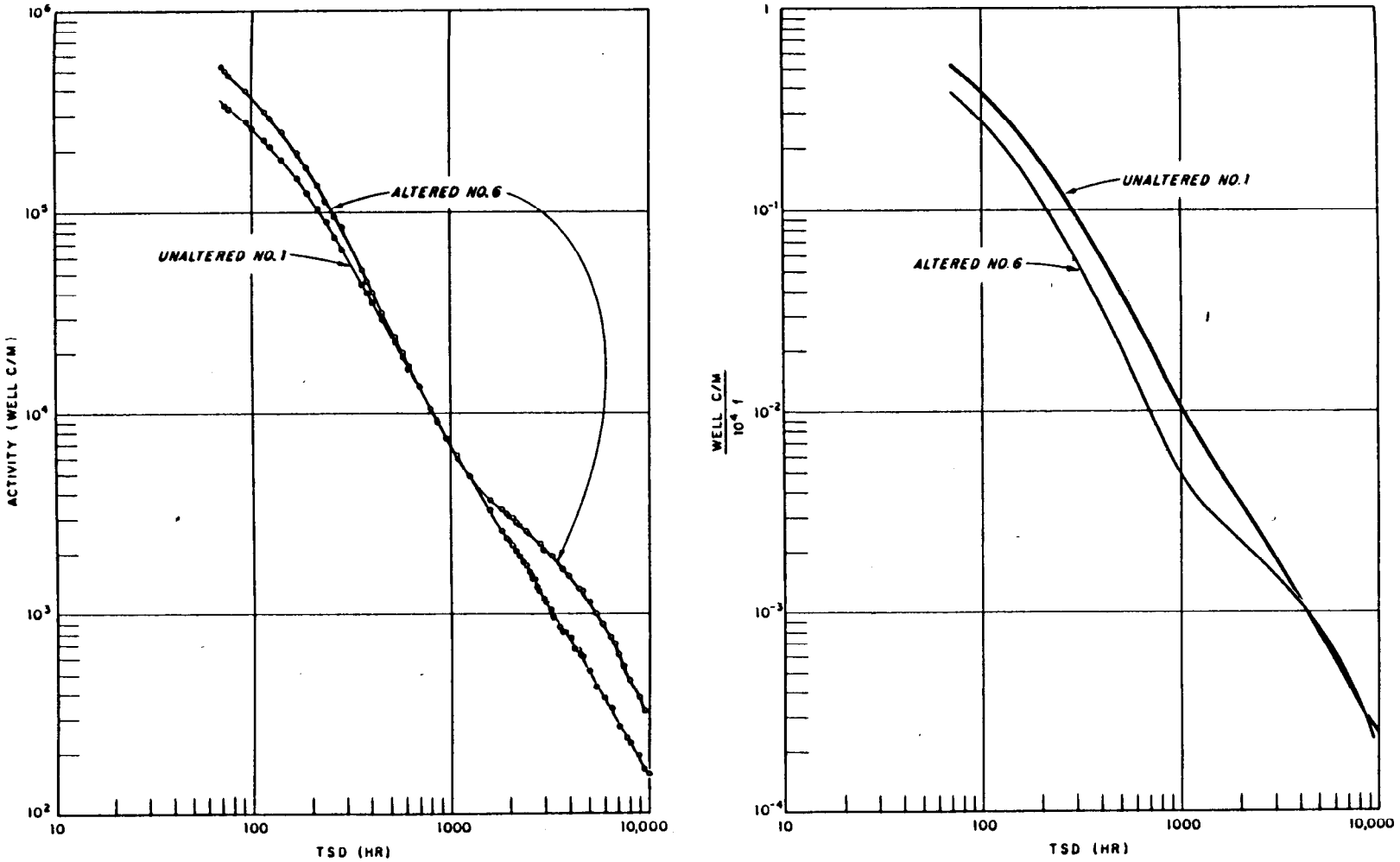

Figure 3.26 Gamma decay of altered and unaltered particles, Shot Zuni.

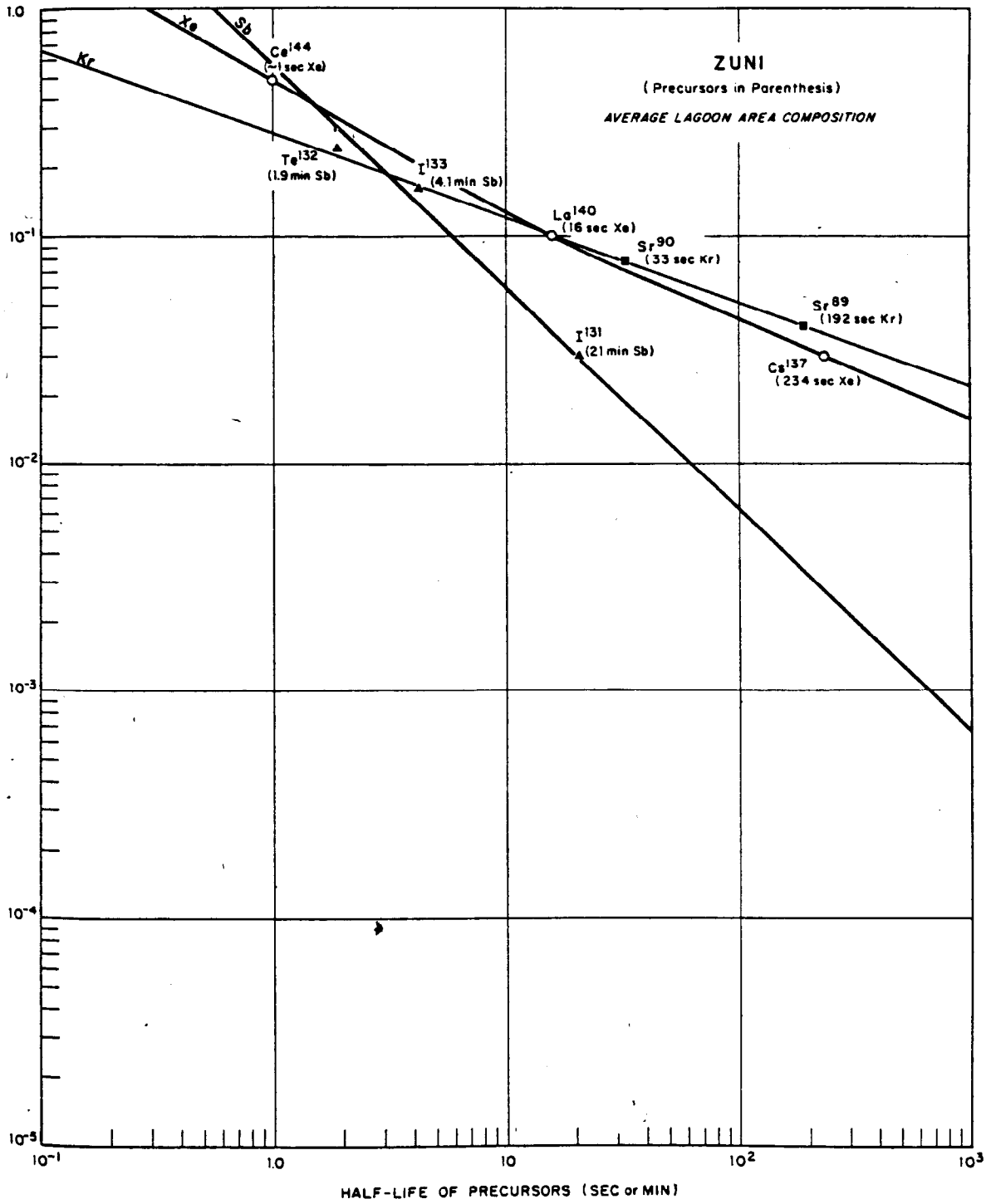

Figure 3.32 Radionuclide fractionation of xenon, krypton, and antimony products, Shot Zuni.

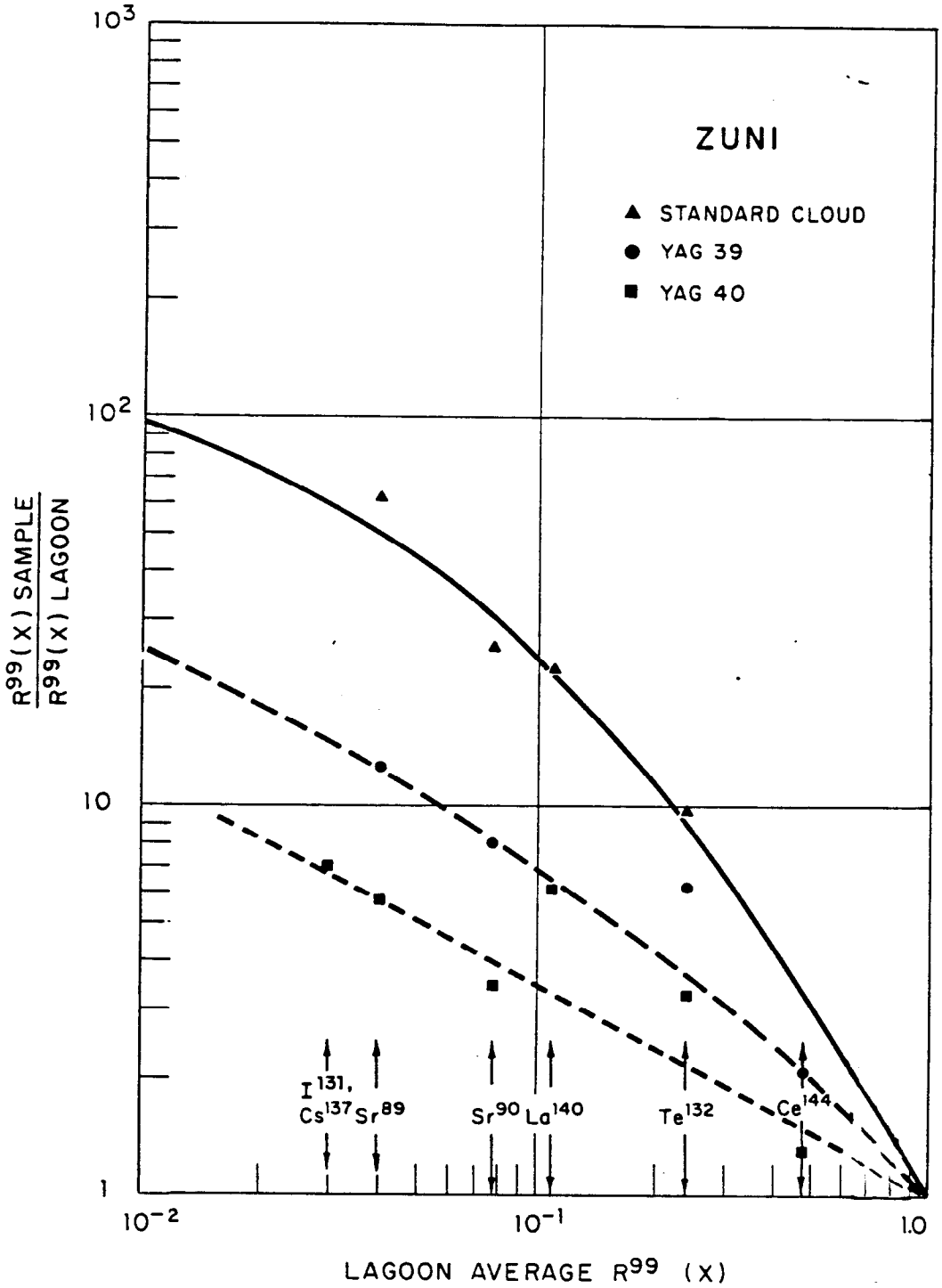

Figure 3.33 R-value relationships for several compositions, Shot Zuni.

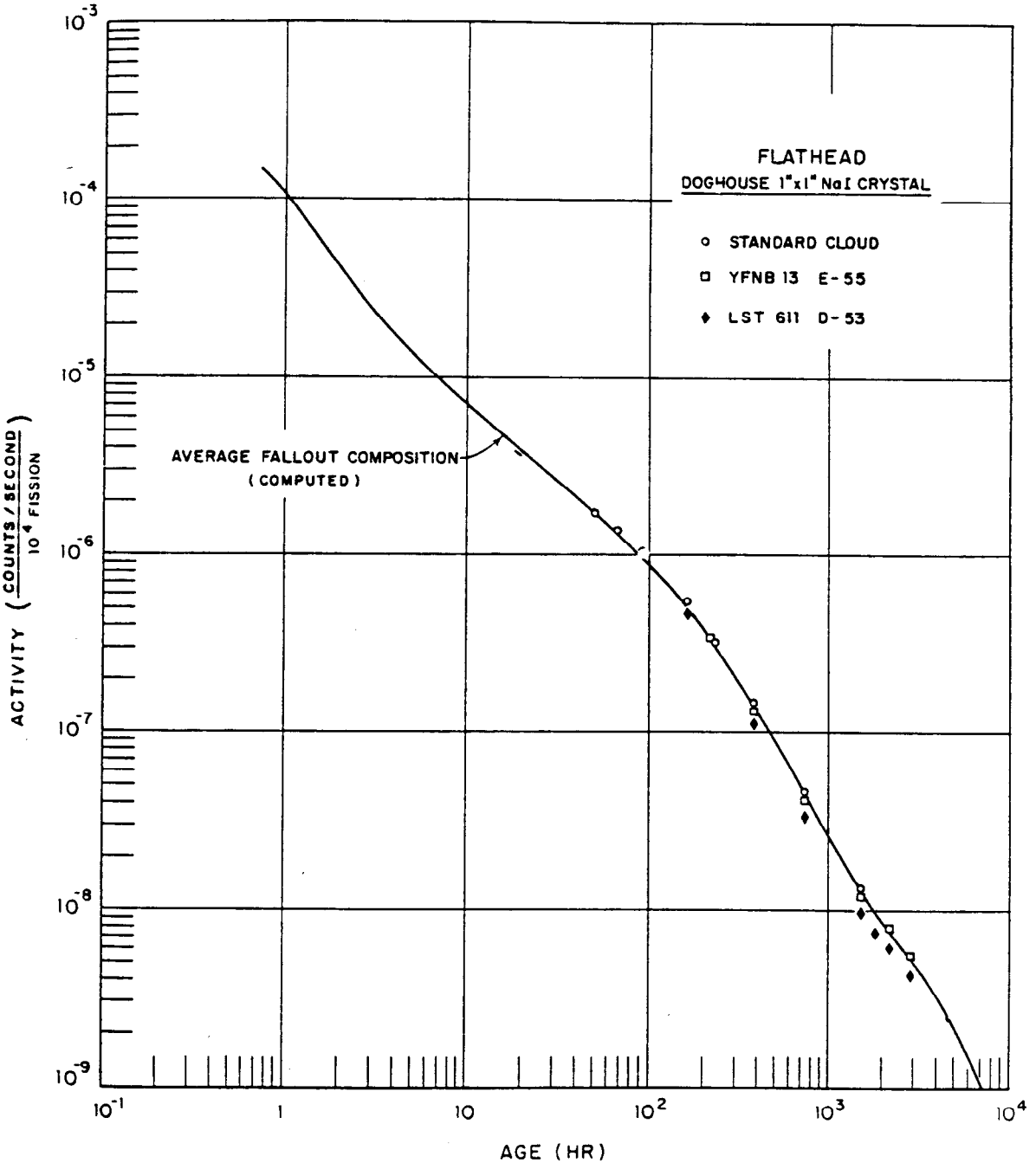

Figure 3.34 Photon-decay rate by doghouse counter, Shot Flathead.

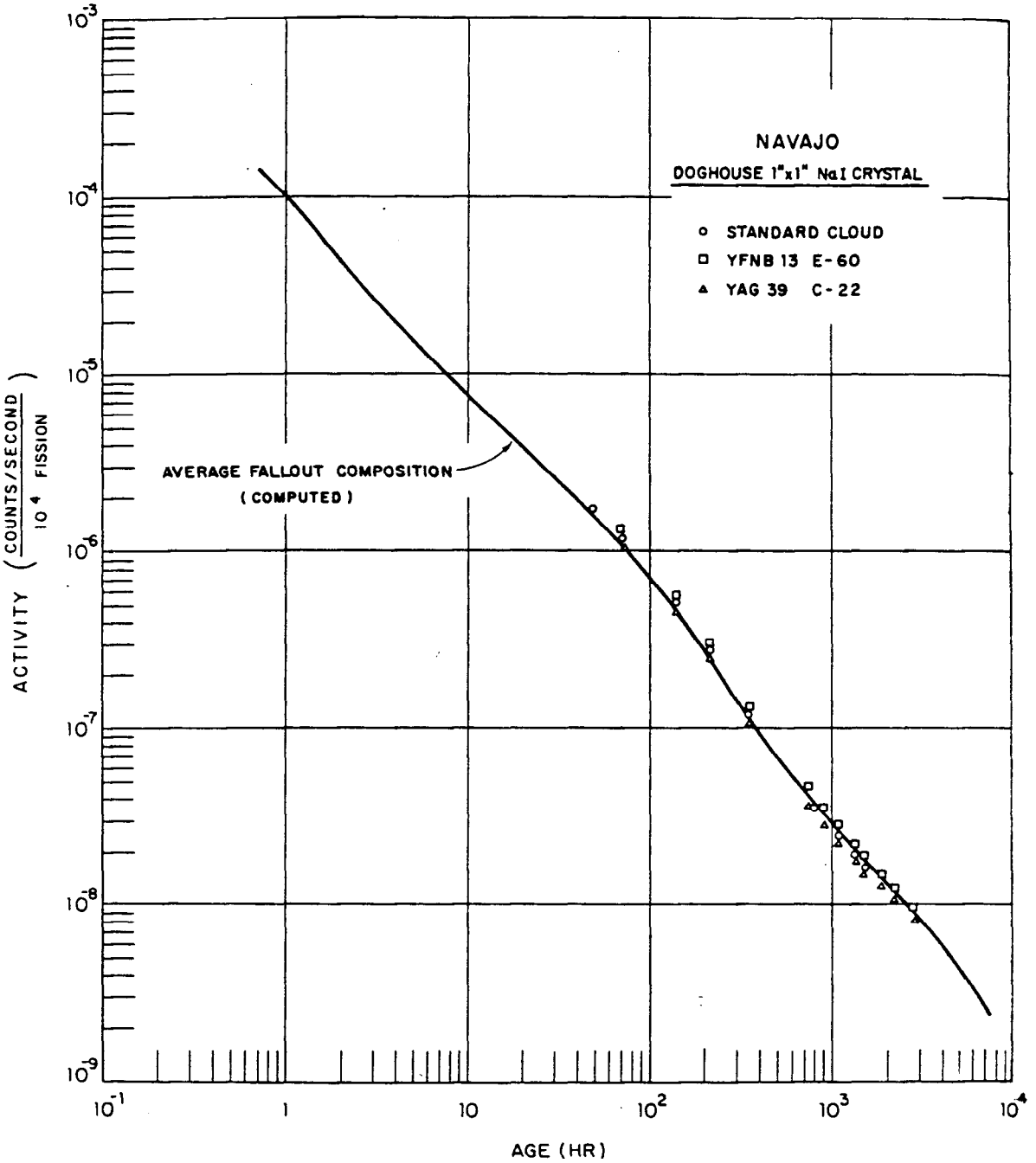

Figure 3.35 Photon-decay rate by doghouse counter, Shot Navajo.

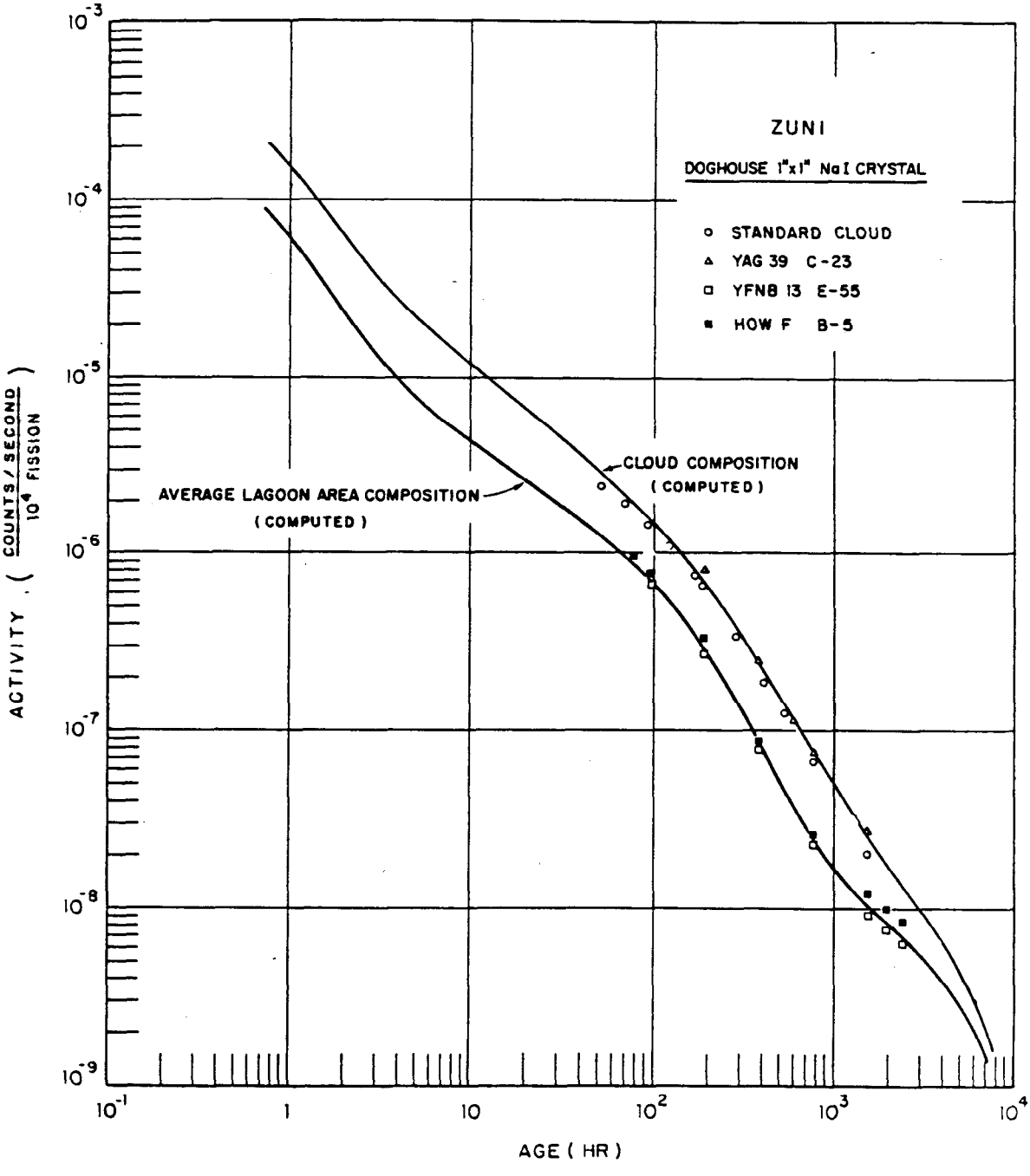

Figure 3.36 Photon-decay rate by doghouse counter, Shot Zuni.

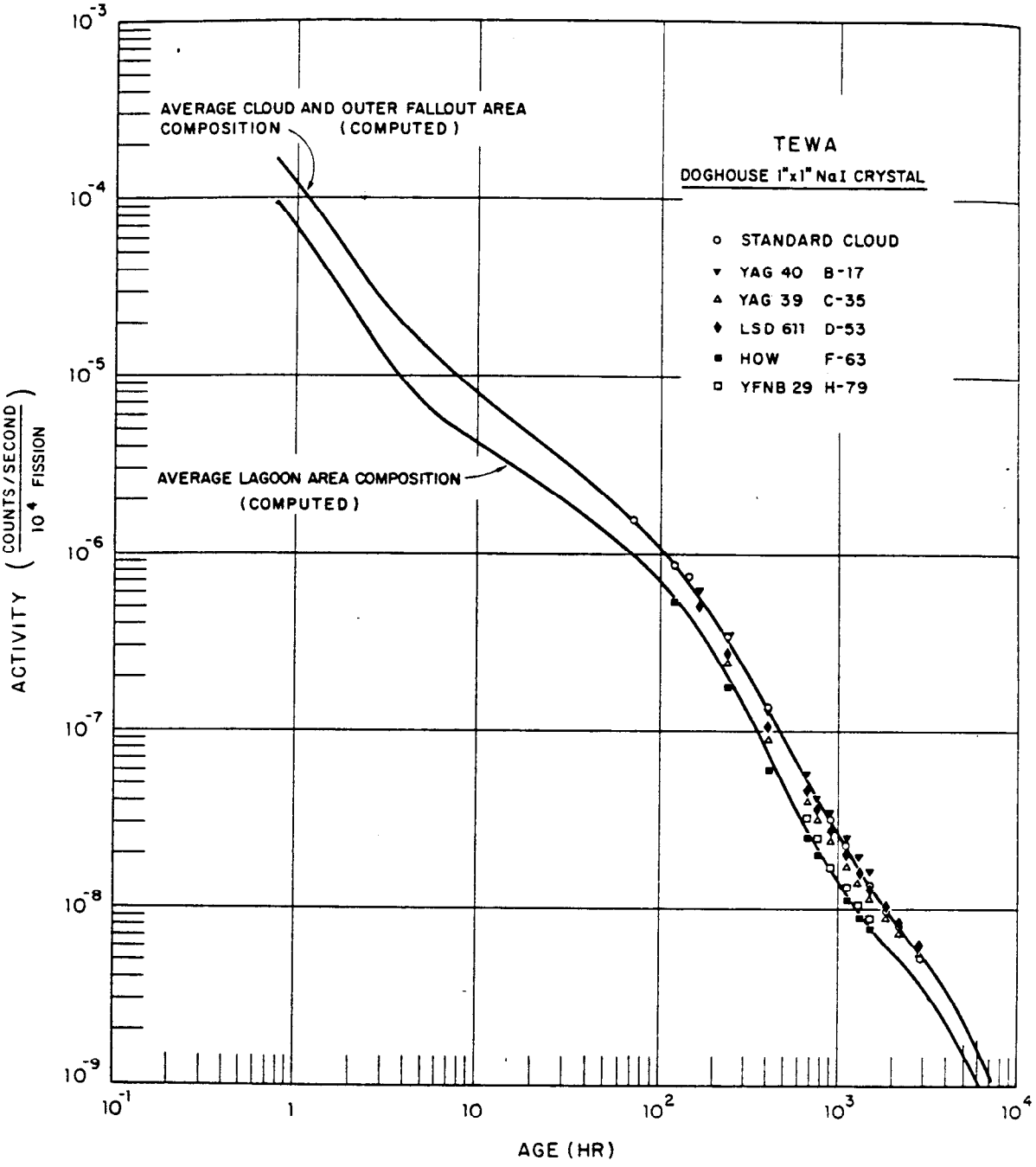

Figure 3.37 Photon-decay rate by doghouse counter, Shot Tewa.

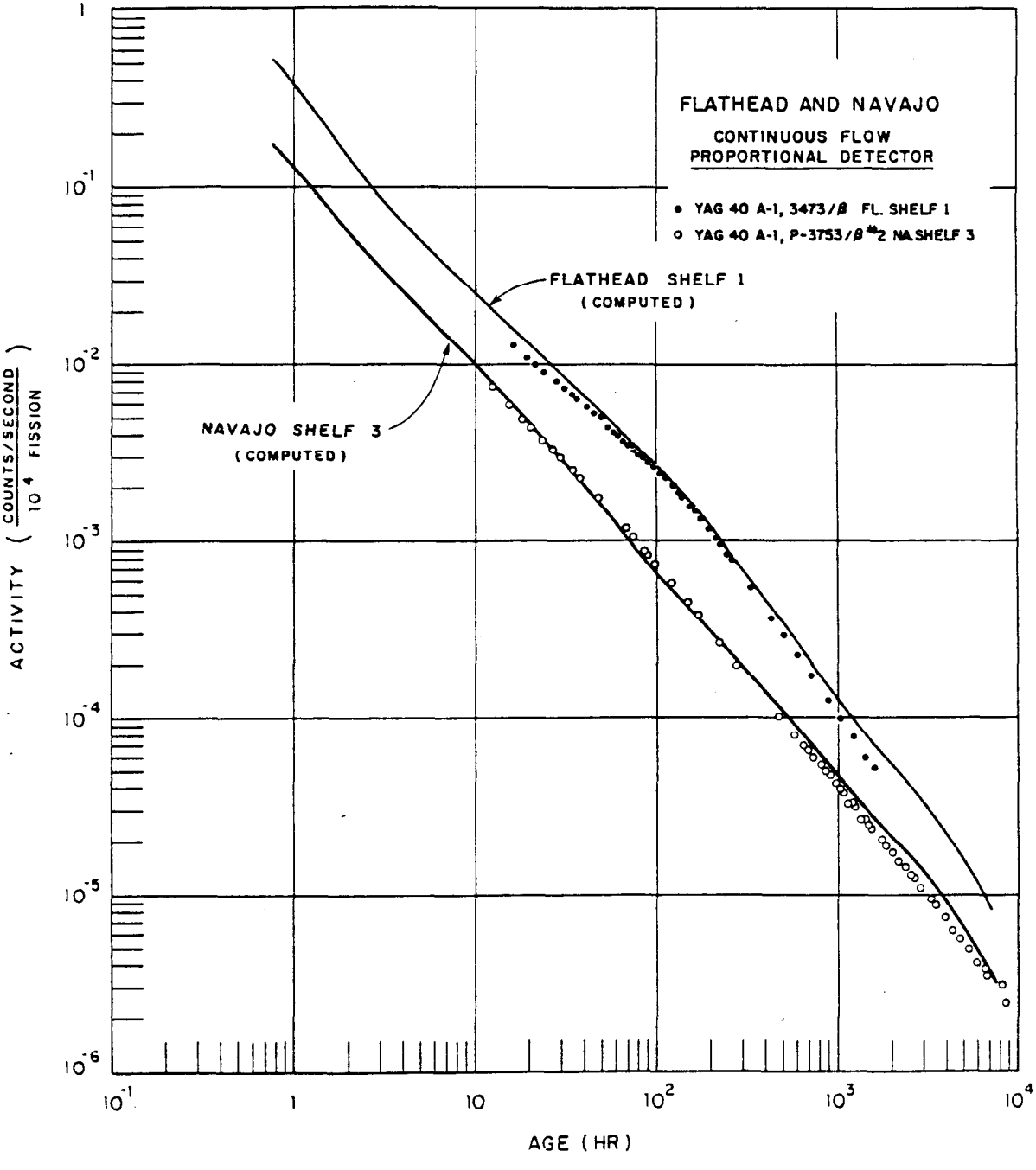

Figure 3.38 Beta-decay rates, Shots Flathead and Navajo.

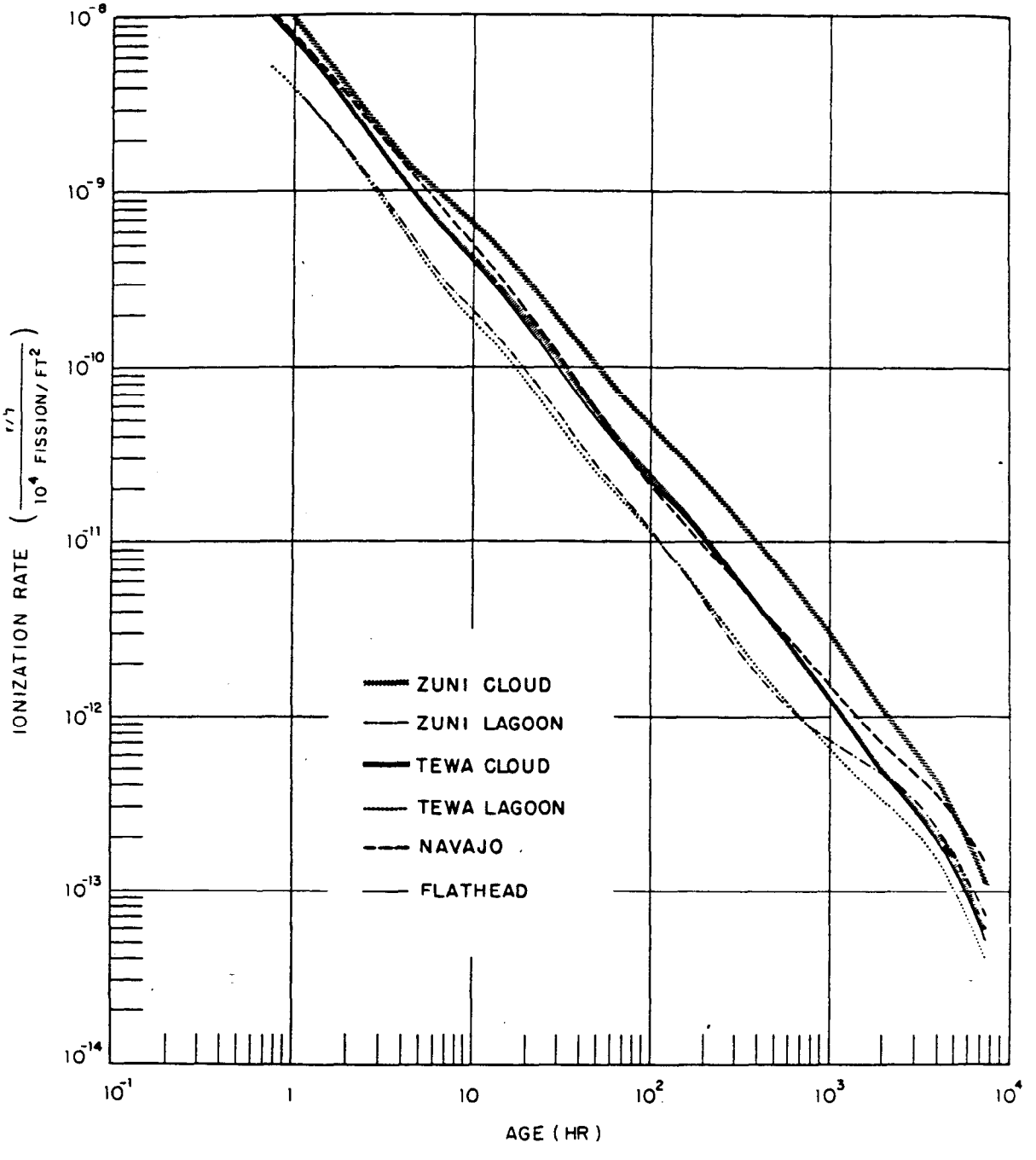

Figure 3.39 Computed ionization-decay rates, Shots Flathead, Navajo, Zuni, and Tewa.

TABLE 4.3 COMPARISON OF PREDICTED AND OBSERVED TIMES OF ARRIVAL AND MAXIMUM PARTICLE-SIZE VARIATION WITH TIME

Shot *	Station	Time of Arrival		Maximum Particle Size (microns) at					
				Time of Arrival		Time of Peak Activity †		Time of Cessation †	
		Predicted	Observed †	Predicted	Observed ‡	Predicted	Observed ‡	Predicted	Observed ‡
		TSD, hr							
Flathead	YFNB 13	§	0.35	—	—	—	—	—	—
	How I	§	§	—	—	—	—	—	—
	YAG 39	3	4.5	200	—	¶	—	¶	—
	YAG 40	9	8.0	125	—	70	120	<70	—
	LST 611	6	6.6	120	112	¶	—	¶	—
Navajo	YFNB 13	<0.5	0.20	>1,000	—	>1,000	—	—	—
	How I	1.5	0.75	500	—	500	—	¶	—
	YAG 39	2	2.3	500	—	180	—	~100	—
	YAG 40	4	6.0	200	—	130	96	~75	84
	LST 611	3	3.0	300	—	180	166	—	—
Zuni	YFNB 13	<1	0.33	500	1,400	500	695	500	545
	How I	<1.5	0.38	>500	—	>500	365	>500	—
	YAG 40	~6	3.4	§	325	150	300	125	245
	YAG 39	9	12	100	—	¶	—	¶	—
	LST 611	§	§	—	—	—	—	—	—
Tewa	YFNB 13	<0.5	0.25	2,000	285	350	—	¶	—
	YFNB 29	<1	0.23	800	1,100	500	1,000	¶	—
	How I	1	1.6	1,000	205	250	285	¶	—
	YAG 39	2	2.0	500	—	180	395	¶	—
	YAG 40	3.5	4.4	200	—	100	285	90	255
	LST 611	7	7.0	150	285	80	205	—	—

* The following cloud dimensions were used in the calculations:

	Shot Flathead	Shot Navajo	Shot Zuni	Shot Tewa
Top, × 1,000 ft	65	85	80	90
Base, × 1,000 ft	35	50	50	50
Diameter, naut mi	6	40	40	60

† Table 3.1.

‡ Section 3.2.4 and Tables B.3 and B.5.

§ No fallout, or no fallout at reference time.

¶ Fallout completed by reference time.

TABLE 4.5 COMPARISON OF HOW ISLAND COLLECTIONS

Shot	Standard Platform	Buried Trays	AOC_2	Platform/Buried Trays
	weighted mean fissions/ft^2	weighted mean fissions/ft^2	fissions/ft^2	
Zuni	$2.07 \pm 0.47 \times 10^{14}$	$2.08 \pm 0.22 \times 10^{14}$	1.87×10^{14}	0.995 ± 0.249
Flathead	$6.14 \pm 2.72 \times 10^{10}$ *	†	2.16×10^{10}	—
Navajo	$1.49 \pm 0.17 \times 10^{12}$	$1.24 \pm 0.51 \times 10^{12}$	2.67×10^{11}	1.202 ± 0.512
Tewa	$2.61 \pm 0.49 \times 10^{13}$	$2.30 \pm 0.35 \times 10^{13}$	1.53×10^{13}	1.135 ± 0.274

* Mean of six total collectors.

† No activity resolvable from Zuni background.

TABLE 4.6 SURFACE DENSITY OF ACTIVITY DEPOSITED ON THE OCEAN

Shot	Station	Ocean, Probe Analysis		Decay Tank, YAG 39		OCC, Ship Platform	
		Method I	Method II	Method I	Method III	Weighted Mean	Maximum Extrapolation *
		fissions/ft^2		fissions/ft^2		fissions/ft^2	
Zuni	YAG 39	9×10^{12} †	—	8.3×10^{12}	—	$2.74 \pm 1.70 \times 10^{12}$	5.02×10^{12}
	YAG 40	1×10^{14} ‡	—	—	—	$3.67 \pm 0.95 \times 10^{14}$	—
Flathead	YAG 39	1.1×10^{13}	—	7.0×10^{12}	$6.96 \pm 2.89 \times 10^{12}$	$4.36 \pm 2.32 \times 10^{12}$	—
	YAG 40	3×10^{13}	—	—	—	$1.55 \pm 1.27 \times 10^{13}$	3.15×10^{13}
Navajo	YAG 39	1.6×10^{14}	—	5.2×10^{13}	$3.40 \pm 0.72 \times 10^{13}$	$1.54 \pm 0.41 \times 10^{13}$	—
	Horizon	—	$5.98 \pm 1.02 \times 10^{13}$ §	—	—	—	—
	YAG 40	4.4×10^{13}	—	—	—	$6.05 \pm 1.26 \times 10^{12}$	—
Tewa	YAG 39	2.2×10^{15} †	—	3.6×10^{15}	$2.75 \pm 0.88 \times 10^{15}$	$1.11 \pm 0.76 \times 10^{15}$	2.08×10^{15}
	Horizon	—	$3.00 \pm 0.77 \times 10^{15}$ ¶	—	—	—	—
	YAG 40	1.1×10^{15} †	—	—	—	$4.70 \pm 3.20 \times 10^{14}$	8.85×10^{14}

* For cases of essentially single-wind deposition.

† Not corrected for material possibly lost by settling below stirred layer.

‡ Considerable motion of ship during fallout period.

§ Average of profiles taken at Horizon stations 4, 4A, 5, 7, and 8 from 18.6 to 34.3 hours (Table B.33).

¶ Average of profiles taken at Horizon stations 2-5, 5A, 6, and 12 from 21.3 to 81.2 hours (Table B.33).

TABLE 4.9 GAMMA DOSAGE BY ESL FILM DOSIMETER AND INTEGRATED TIR MEASUREMENTS

Station	Shot Zuni			Shot Flathead			Shot Navajo			Shot Tewa		
	Film Dose	TIR Dose	Exposure Time	Film Dose	TIR Dose	Exposure Time	Film Dose	TIR Dose	Exposure Time	Film Dose	TIR Dose	Exposure Time
	r	r	to H+hr	r	r	to H+hr	r	r	to H+hr	r	r	to H+hr
YAG 40-B	30	19.8	28.2	2.5	1.7	33.6	1.77	0.8	32.8	41.6	31.0	32.6
YAG 39-C	0.2	0.2	34.6	0.05	0.5	26.1	10	4.6	50.3	68	67.0	51.3
LST 611-D	<0.05	0.0	62.0	1.7	1.3	51.6	0.81	0.3	26.6	3.62	3.4	31.7
YFNB 13-E	44	17.8 *	26.7	400	74.6 *	26.7	68.5	13.7	58.3	20.3	8.7	7.8
YFNB 29-G	20	23.6	6.9	7.5	3.7	5.7	1.64	0.2	6.5	310	158.0 *	51.1
YFNB 29-H	43	41.7	27.7	12	3.9	25.9	1.65	0.7	5.5	320	284.0 *	75.6
How F	19	6.7	11.1	0.22	0.0	6.3	1.82	†	6.7	4.5	0.8	8.3
How K	51	—	30.2	3.1	—	6.3	3.37	—	10.7	6.7	—	8.4
George L	260	—	32.7	230	—	31.7	150	—	32.5	†	—	†
Charlie M	—	—	—	—	—	—	107	—	32.7	†	—	†
William M	110	—	31.6	5.2	—	30.9	—	—	—	—	—	—
Raft 1	25	—	30.8	1.5	—	29.4	1.32	—	27.3	3.35	—	31.7
Raft 2	40	—	29.8	24	—	28.6	4.62	—	28.1	45.5	—	32.3
Raft 3	34	—	28.6	19	—	27.8	16.1	—	28.8	204	—	33
Skiff AA	17	—	52.1	25	—	24.2	13.2	—	59.9	45.5	—	63.25
Skiff BB	33	—	56.9	59	—	28.3	†	—	†	141	—	37.9
Skiff CC	20	—	72.9	9.4	—	30.6	5.2	—	53.2	42.5	—	36.6
Skiff DD	17	—	74.6	†	—	†	2.56	—	50.3	1.28	—	33.4
Skiff EE	2.3	—	171.9	0.6	—	48.4	1.45	—	48.8	9.87	—	31.7
Skiff FF	‡	—	‡	1.1	—	55.1	0.56	—	29.3	0.3	—	26.5
Skiff GG	10	—	59.3	‡	—	‡	—	—	—	295	—	60.1
Skiff HH	16	—	60.8	20	—	32.7	29.5	—	52.3	61	—	39.8
Skiff KK	6.8	—	75.7	2.0	—	51.4	6.3	—	33.0	0.62	—	34.7
Skiff LL	†	—	†	1.0	—	53.4	2.05	—	31.0	1.40	—	29.8
Skiff MM	1.8	—	50.1	‡	—	‡	†	—	†	410	—	61.5
Skiff PP	—	—	—	16	—	34.8	77	—	35.4	60	—	58.3
Skiff RR	2.4	—	77.1	2.0	—	60.8	11.7	—	33.8	0.6	—	41.9
Skiff SS	1.1	—	155.3	3.6	—	58.0	—	—	—	—	—	—
Skiff TT	1.2	—	168.7	1.2	—	56.4	1.09	—	27.8	0.3	—	28.0
Skiff UU	†	—	†	0.45	—	59.3	—	—	—	—	—	—
Skiff VV	†	—	†	—	—	—	—	—	—	—	—	—
Skiff WW	—	—	—	—	—	—	—	—	—	154	—	56.7
Skiff XX	—	—	—	—	—	—	—	—	—	2.05	—	54.6
Skiff YY	—	—	—	—	—	—	—	—	—	1.41	—	52.6

* Estimated value, TIR saturated. † Instrument malfunctioned or lost. ‡ Not instrumented.

Page 130 Deleted

TABLE 4.10 PERCENT OF FILM DOSIMETER READING RECORDED BY TIR

Station	Shot Zuni	Shot Flathead	Shot Navajo	Shot Tewa
	pct	pct	pct	pct
YAG 40-B	66	68	45	75
YAG 39-C	100	~100	46	97
LST 611-D	*	76	37	94
YFNB 13-E	41 †	19 †	20	43
YFNB 29-G	~100 ‡	49	12	51 †
YFNB 29-H	97	32	42	89 †
How F	35 ‡	*	§	18

* No fallout occurred.
† TIR saturated.
‡ Dosimeter location varied from other shots.
§ Instrument malfunctioned.

TABLE 4.11 COMPARISON OF THEORETICAL DOGHOUSE ACTIVITY OF STANDARD-CLOUD SAMPLES BY GAMMA SPECTROMETRY AND RADIOCHEMISTRY

Time of Spectral Run	Observed Dog-house Activity	Computed Activity and Errors			
		Spectrometer	Error	Radiochemical	Error
H+hr	counts/min	counts/min	pct	counts/min	pct
Shot Zuni Standard Cloud, 9.84×10^{12} fissions					
53	142,500	95,300	−33.1	163,541	+14.8
117	70,000	47,450	−32.2	74,981	+7.11
242	26,700	20,640	−22.7	29,107	+9.01
454	9,500	7,516	−20.9	10,745	+13.1
790	3,700	3,790	+2.43	4,546	+22.9
1,295	1,550	1,973	+27.3	1,984	+28.0
Shot Flathead Standard Cloud, 2.79×10^{13} fissions					
96.5	171,000	142,090	−16.9	154,008	−9.93
195	72,000	51,490	−28.5	66,960	−7.00
262	45,000	29,850	−33.7	43,022	−4.39
334	30,500	22,760	−25.4	29,128	−4.49
435	19,300	14,920	−22.7	19,084	−1.11
718	8,200	6,778	−17.3	7,985	−2.62
1,031	4,400	3,341	−22.5	4,152	−5.63
1,558	2,130	2,243	+5.31	2,076	−2.53
Shot Navajo Standard Cloud, 3.46×10^{12} fissions					
51.5	34,000	27,470	−19.2	31,350	−7.79
69	25,500	20,724	−18.7	22,630	−11.3
141	11,000	9,432	−14.2	9,757	−11.3
191	7,000	7,411	+5.87	6,290	−10.1
315	3,050	2,834	−7.08	2,927	−4.03
645	980	958	−2.24	1,038	+5.92
Shot Tewa Standard Cloud, 4.71×10^{13} fissions					
71.5	442,000	244,930	−44.6	429,600	−2.81
93.5	337,000	194,170	−42.4	325,000	−3.56
117	262,000	157,890	−39.7	255,800	−2.37
165	169,000	134,910	−20.2	161,000	−4.73
240	97,000	74,780	−22.9	91,000	−6.19
334	54,000	38,770	−28.2	52,280	−3.19
429	34,500	25,200	−27.0	33,200	−3.77
579	20,200	14,770	−26.9	19,640	−2.77
766	12,400	10,860	−12.4	12,150	−2.02
1,269	5,200	5,660	+8.85	4,974	−4.35
1,511	3,850	4,550	+18.2	3,759	−2.36

TABLE 4.12 COMPARISON OF ACTIVITIES PER UNIT AREA COLLECTED BY THE HIGH VOLUME FILTER AND OTHER SAMPLING INSTRUMENTS

Shot	Designation and Exposure Period, H+hr					Fissions/ft^2 (Mo^{99})		
	HVF		IC		OCC and AOC_1	HVF (area = 0.06696 ft^2)	IC (area = 0.05584 ft^2)	OCC and AOC_1 (area = 2.60 ft^2)
Zuni	YAG 40-B-9	3.4 to 4.8				10.14×10^{13}		
	YAG 40-B-10	5.3				23.48		
	YAG 40-B-11	5.8				23.73		
	YAG 40-B-12	6.3				21.79		
	YAG 40-B-13	6.8				6.42		
	YAG 40-B-14	7.3				6.93		
	YAG 40-B-15	7.8				0.39		
	YAG 40-B-8	16.4				3.97		
	HVF to	16.4	YAG 40-B-7	to 15.6	To 16.3 and 28.2 *	9.68×10^{14}	6.06×10^{14}	$3.71 \pm 0.88 \times 10^{14}$
Flathead	YAG 40-B-8	to 26.4	YAG 40-B-7	to 19.9	To 26.4	2.03×10^{12}	3.87×10^{12}	$16.3 \pm 13.4 \times 10^{12}$
	YAG 39-C-25	to 26.1	YAG 39-C-20	to 18.2	To 23.8	1.57×10^{12} †	4.85×10^{12}	$4.37 \pm 2.37 \times 10^{12}$
Navajo	YAG 40-B-8	to 19.1	YAG 40-B-7	to 15.5	To 8.7 and 19.7 *	3.72×10^{12}	3.70×10^{12}	$6.08 \pm 1.26 \times 10^{12}$
	YAG 39-C-25	to cessation	YAG 39-C-20	to 16.1	To 15.9 and 24.1 *	5.50×10^{12}	11.9×10^{12}	$14.6 \pm 3.5 \times 10^{12}$

* Short-exposure trays as active as long.

† DMT spilled on recovery.

TABLE 4.13 NORMALIZED IONIZATION RATE (SC), CONTAMINATION INDEX, AND YIELD RATIO

A number in parentheses indicates the number of zeros between the decimal point and first significant figure.

Shot	Age	r/hr / fissions/ft^2
Hypothetical, 100 pct fission, unfractionated fission products, no induced activities	1.12 hrs	(12)6254
	1.45 days	(14)6734
	9.82 days	(15)6748
	30.9 days	(15)1816
	97.3 days	(16)3713
	301 days	(17)5097
Zuni, lagoon-area composition	1.12 hrs	(12)3356
	1.45 days	(14)4134
	9.82 days	(15)3197
	30.9 days	(16)9165
	97.3 days	(16)4097
	301 days	(17)7607
Zuni, cloud composition	1.12 hrs	(12)7093
	1.45 days	(13)1407
	9.82 days	(14)1766
	30.9 days	(15)4430
	97.3 days	(16)8755
	301 days	(16)1121
Flathead, average composition	1.12 hrs	(12)5591
	1.45 days	(14)6994
	9.82 days	(15)7924
	30.9 days	(15)1893
	97.3 days	(16)3832
	301 days	(17)5230
Navajo, average composition	1.12 hrs	(12)6864
	1.45 days	(14)9481
	9.82 days	(15)7816
	30.9 days	(15)2160
	97.3 days	(16)5933
	301 days	(16)1477
Tewa, lagoon-area composition	1.12 hrs	(12)3321
	1.45 days	(14)3564
	9.82 days	(15)3456
	30.9 days	(16)9158
	97.3 days	(16)2843
	301 days	(17)4208
Tewa, cloud and outer fallout composition	1.12 hrs	(12)6446
	1.45 days	(14)8913
	9.82 days	(15)8670
	30.9 days	(15)1971
	97.3 days	(16)4019
	301 days	(17)6009

* Ratio of (r/hr)/(Mt(total)/ft^2) at t for device to (r/hr)/(Mt(total)/ft^2) at t for hypothetical device.

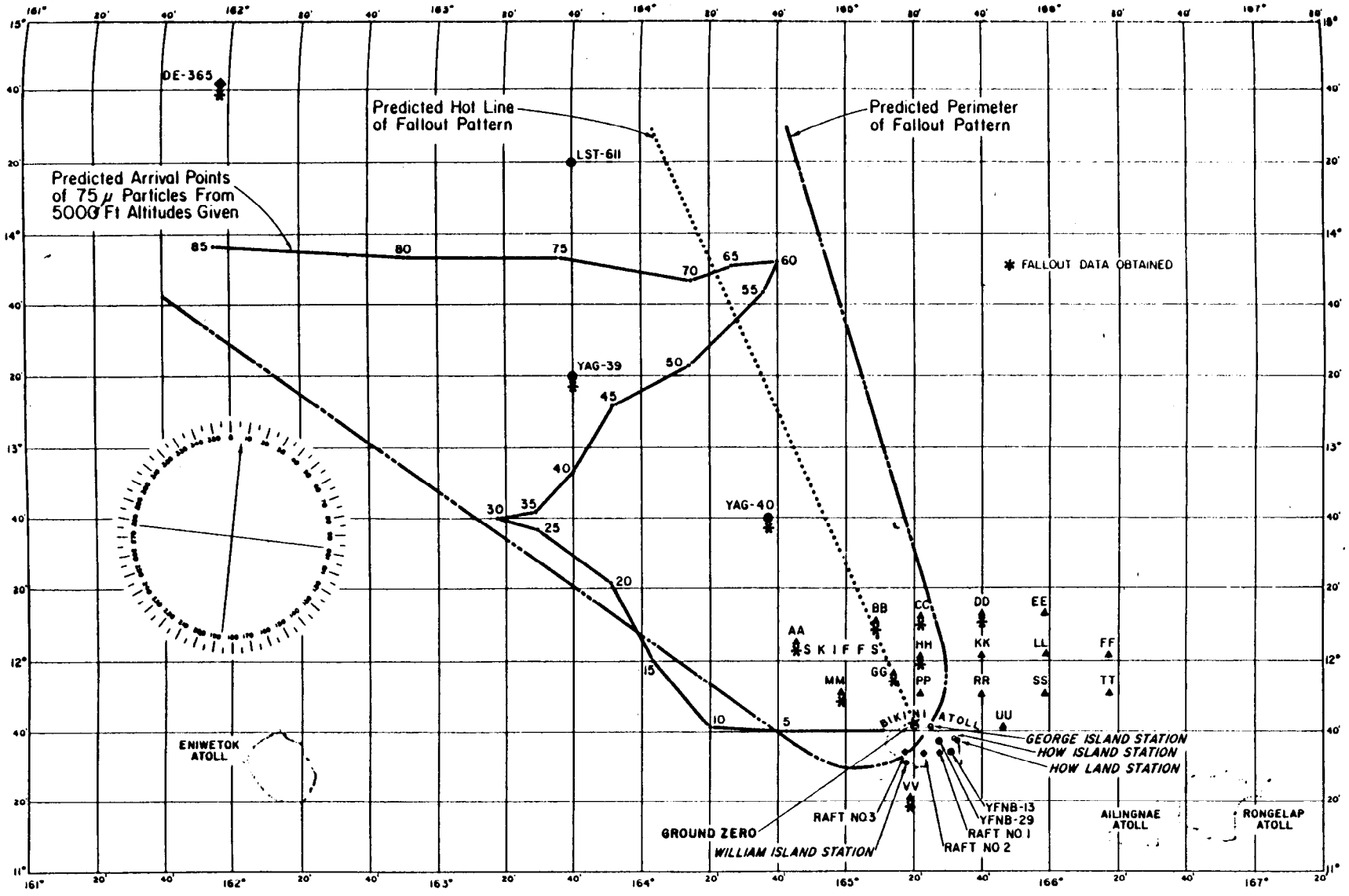

Figure 4.1 · Approximate station locations and predicted fallout pattern, Shot Cherokee.

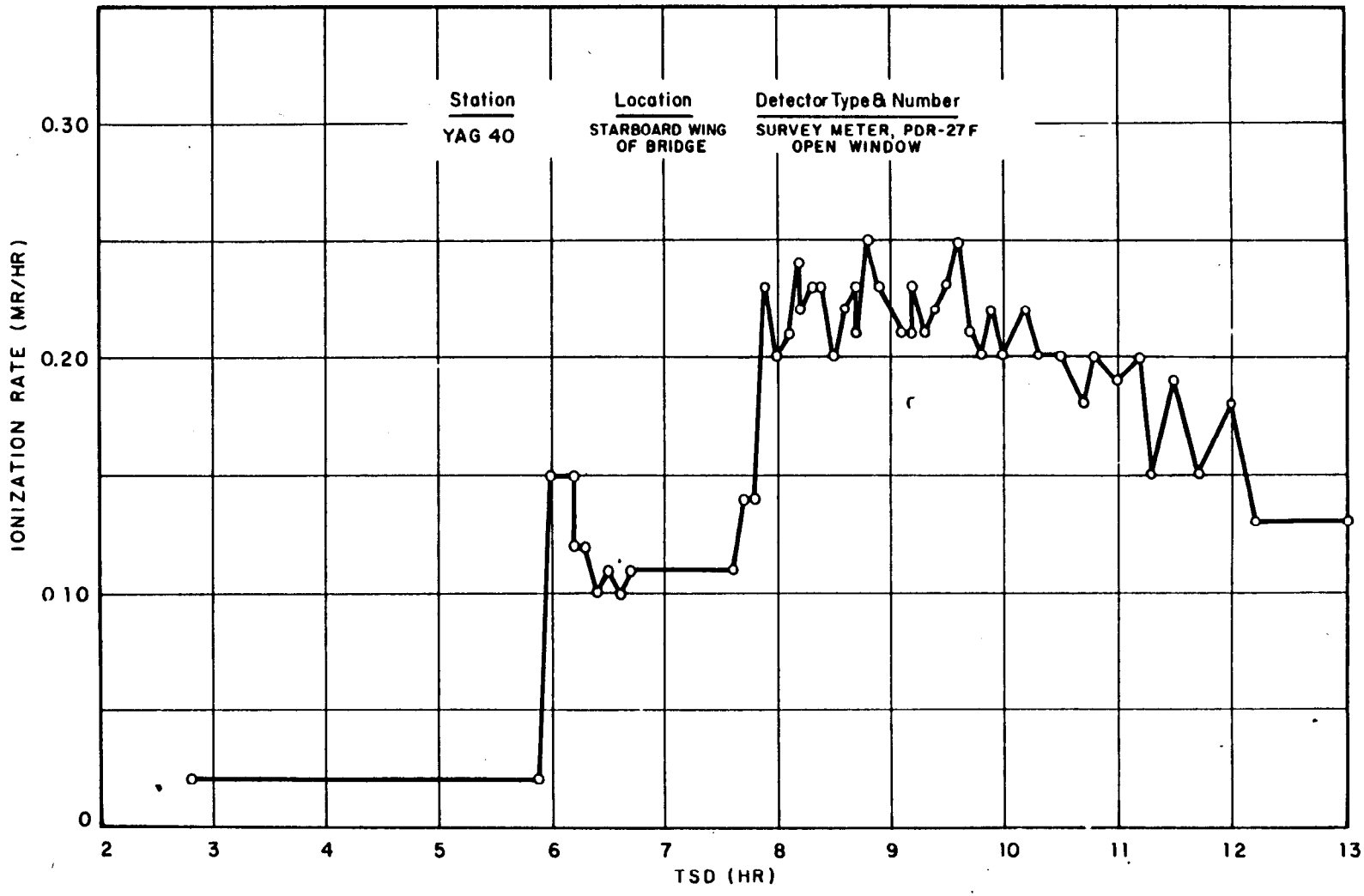

Figure 4.2 Survey-meter measurement of rate of arrival on YAG 40, *Shot Cherokee*.

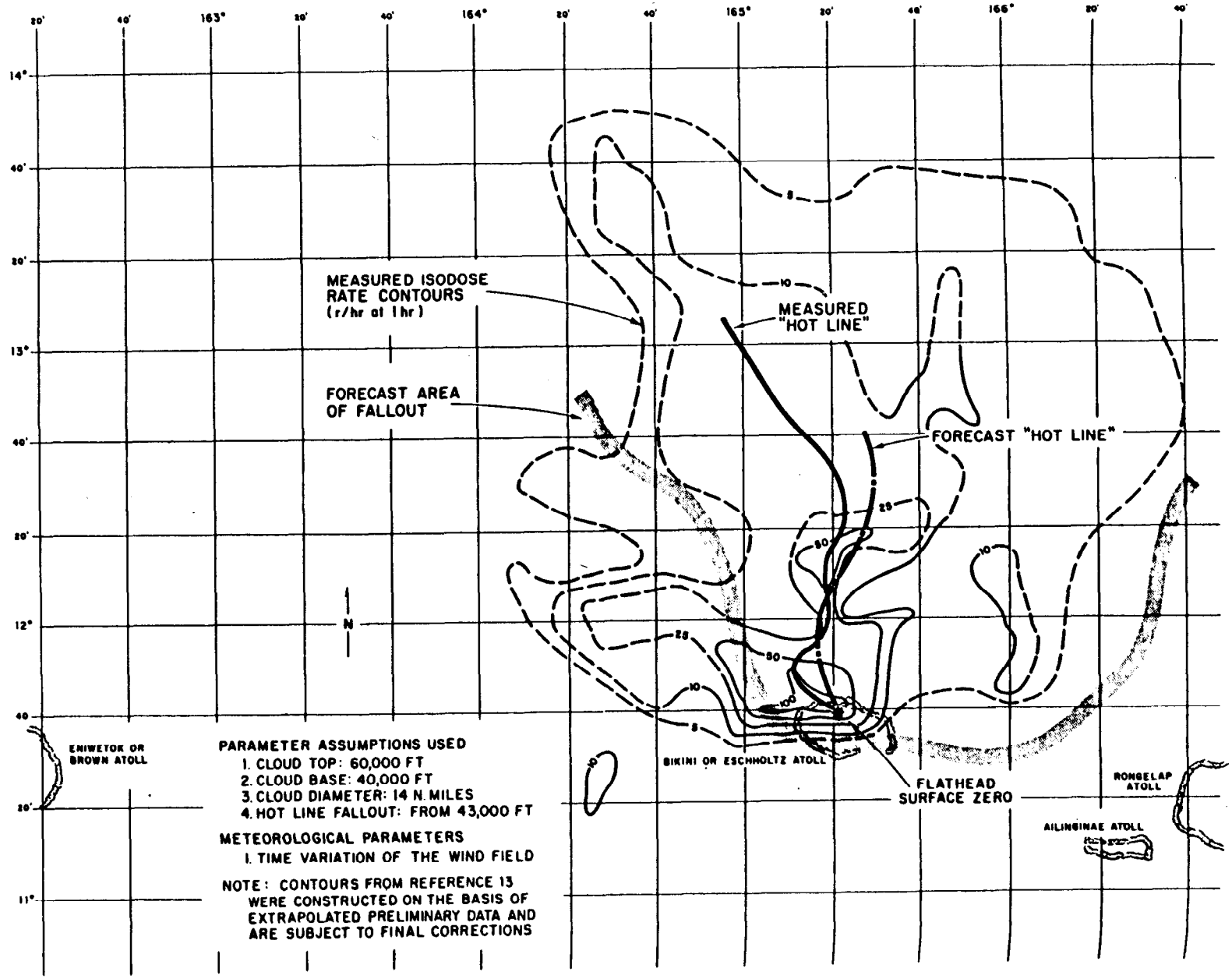

Figure 4.6 Predicted and observed fallout pattern, *Shot Flathead.*

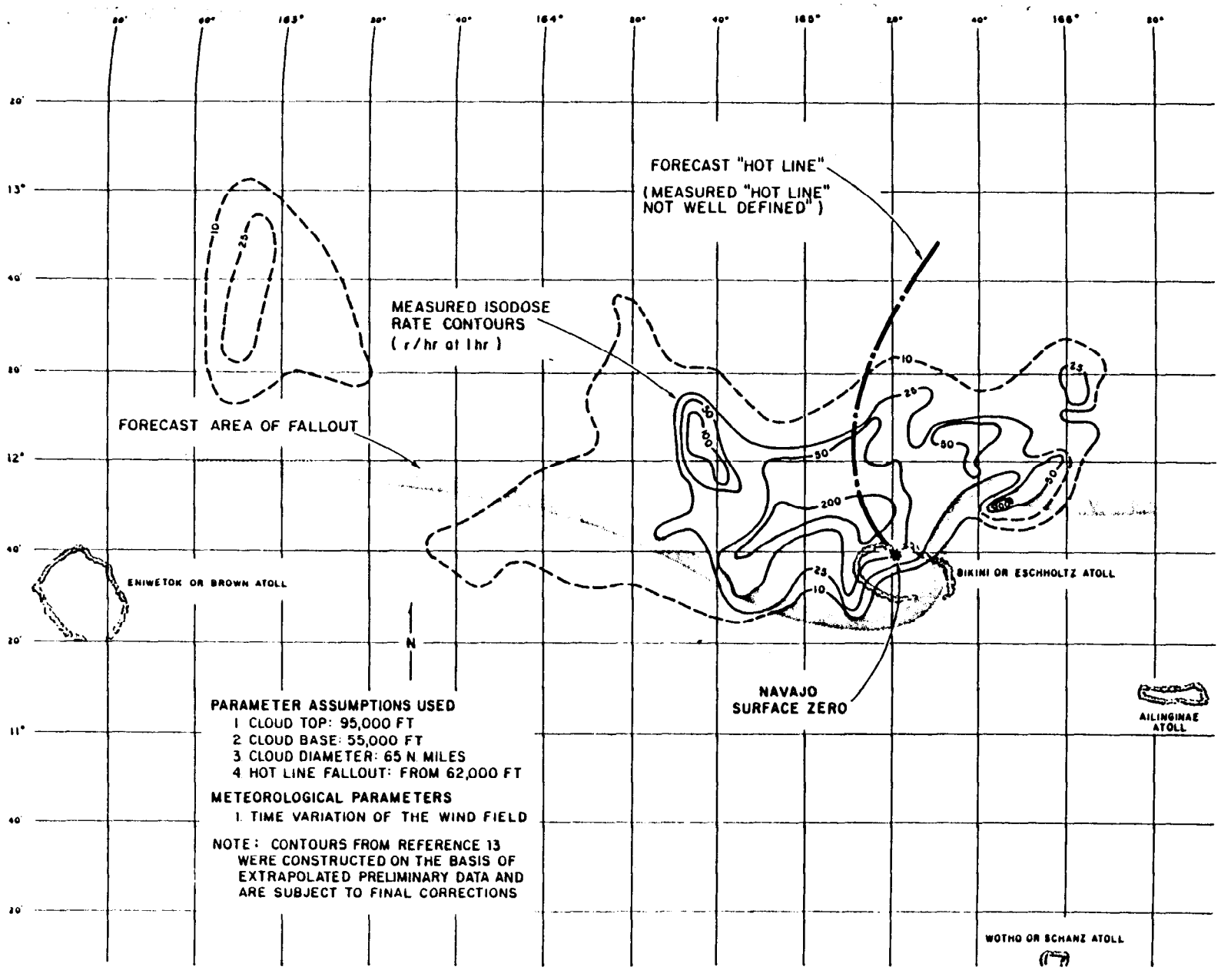

Figure 4.7 Predicted and observed fallout pattern, Shot Navajo.

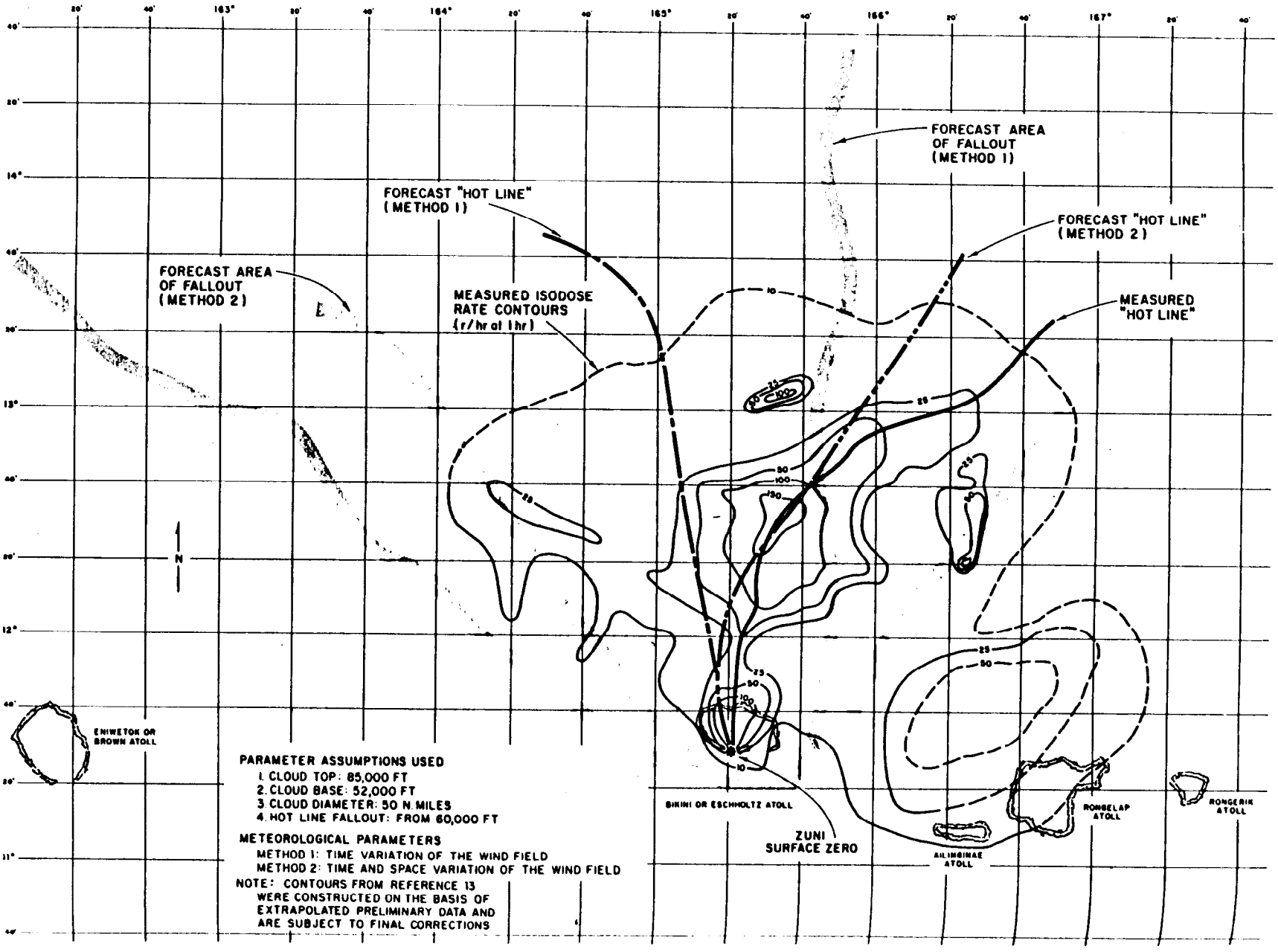

Figure 4.8 Predicted and observed fallout pattern, Shot Zuni.

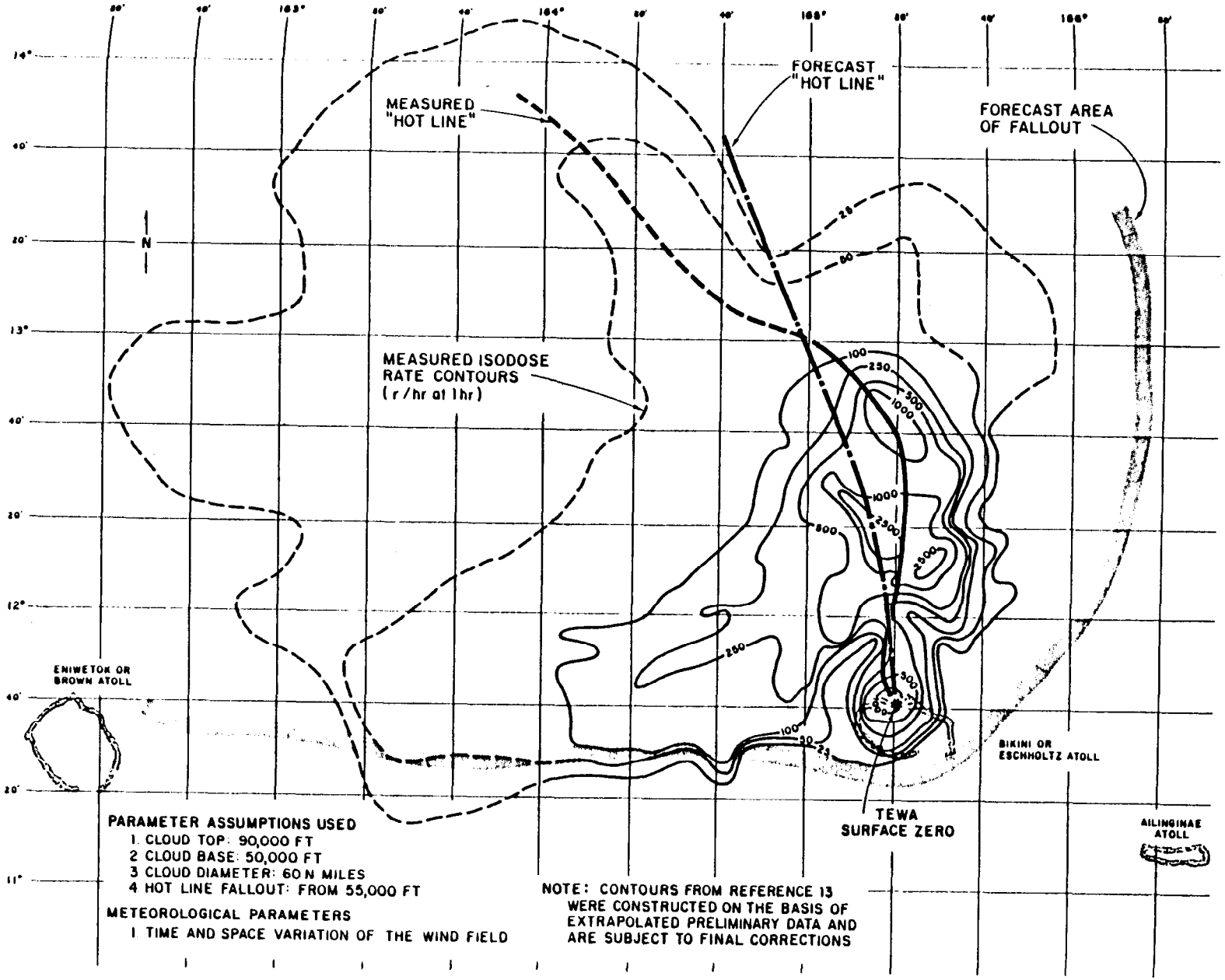

Figure 4.9 Predicted and observed fallout pattern, Shot Tewa.

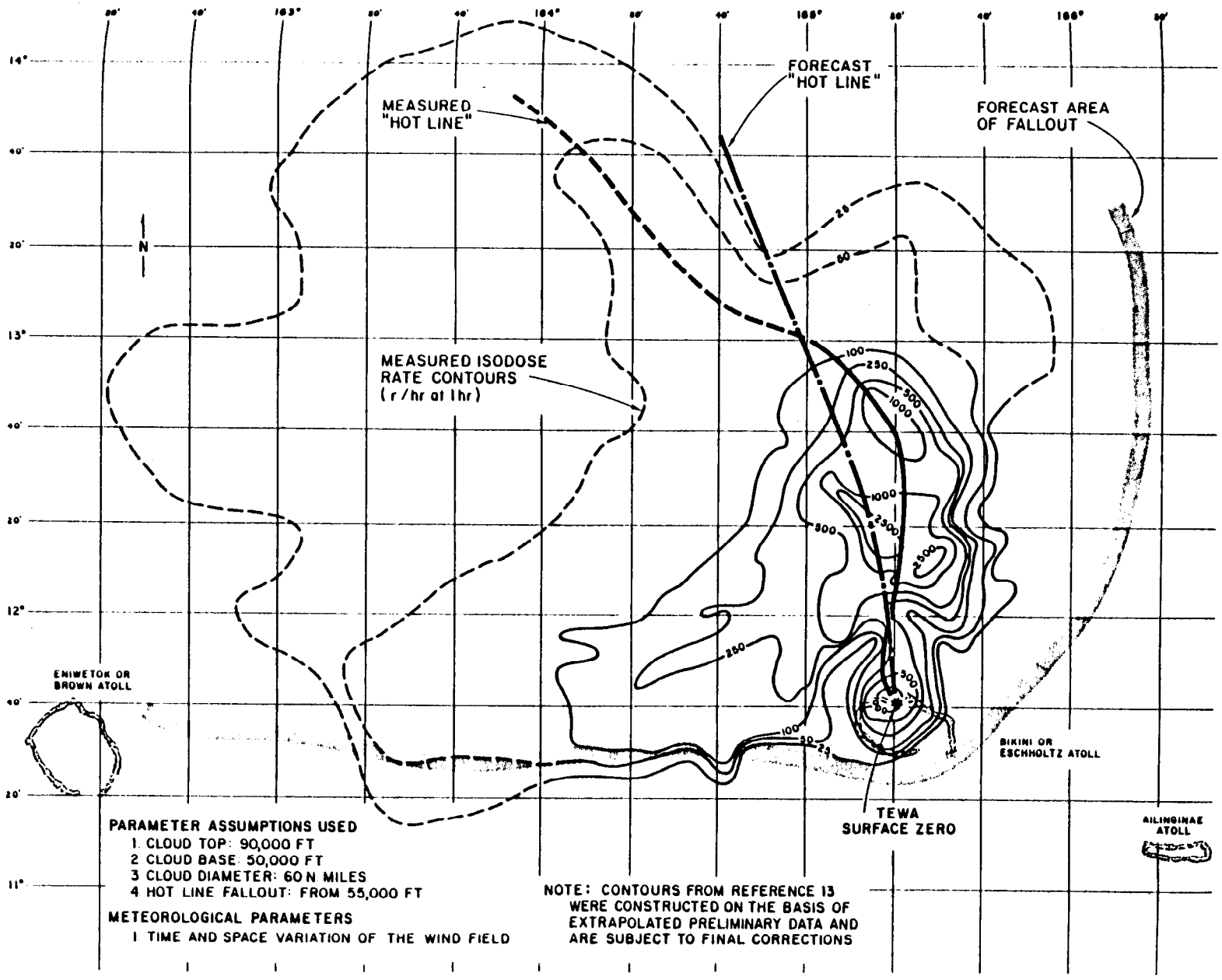

Figure 4.9 Predicted and observed fallout pattern, Shot Tewa.

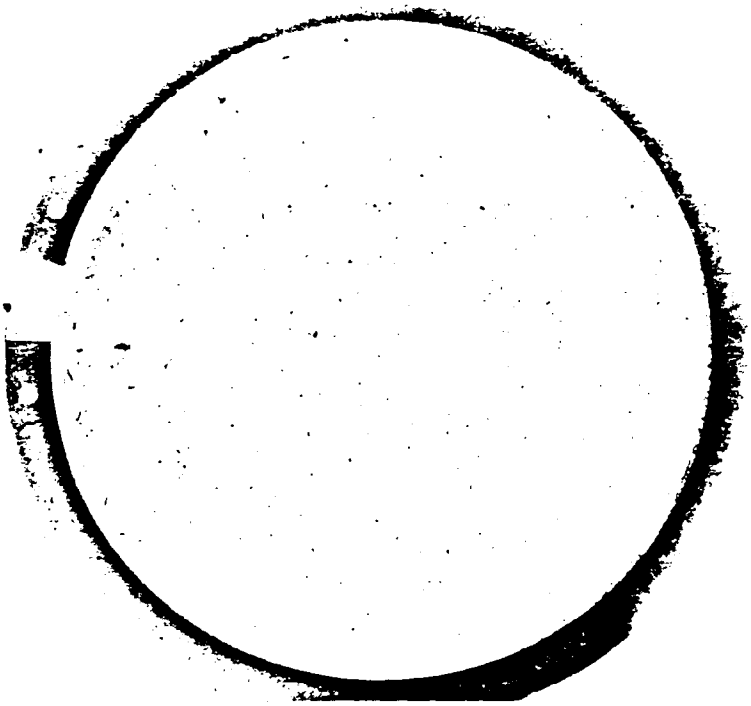

A HEAVY
COLLECTION
FAR OUT
15 MINUTE EXPOSURE

TRAY NO. 411

YAG 40, B-7
ZUNI

A HEAVY
COLLECTION
CLOSE IN
15 MINUTE EXPOSURE

TRAY NO. 1204

YFNB 13, E-57
ZUNI

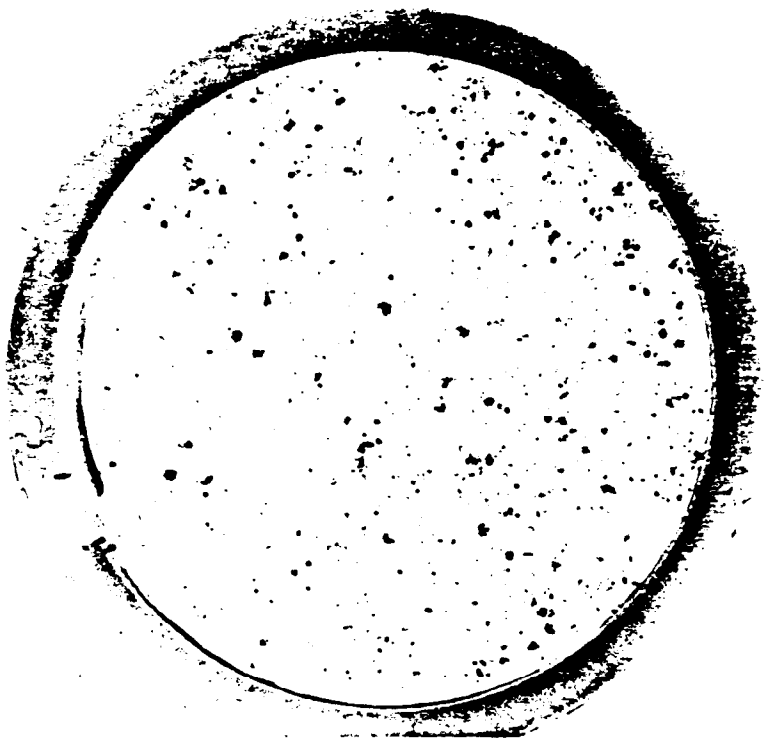

Figure 4.10 Close and distant particle collections, Shot Zuni.

REFERENCES

1. C. E. Adams, F. R. Holden, and N. R. Wallace; "Fall-Out Phenomenology"; Annex 6.4, Operation Greenhouse, WT-4, August 1951; U. S. Naval Radiological Defense Laboratory, San Francisco 24, California; Confidential.

2. I. G. Poppoff and others; "Fall-Out Particle Studies"; Project 2.5a-2, Operation Jangle, WT-395 (in WT-371), April 1952; U. S. Naval Radiological Defense Laboratory, San Francisco 24, California; Secret Restricted Data.

3. R. K. Laurino and I. G. Poppoff; "Contamination Patterns at Operation Jangle"; USNRDL-399, 30 April 1953; U. S. Naval Radiological Defense Laboratory, San Francisco 24, California; Unclassified.

4. W. B. Heidt, Jr. and others; "Nature, Intensity, and Distribution of Fall-Out from Mike Shot"; Project 5.4a, Operation Ivy, WT-615, April 1953; U. S. Naval Radiological Defense Laboratory, San Francisco 24, California; Unclassified.

5. R. L. Stetson and others; "Distribution and Intensity of Fallout"; Project 2.5a, Operation Castle, WT-915, January 1956; U. S. Naval Radiological Defense Laboratory, San Francisco 24, California; Secret Restricted Data.

6. Headquarters, Joint Task Force Seven, letter; Subject: "Radiological Surveys of Several Marshall Island Atolls," 18 March 1954.

7. T. R. Folsom and L. B. Werner; "Distribution of Radioactive Fallout by Survey and Analyses of Sea Water"; Project 2.7, Operation Castle, WT-935, April 1959; Scripps Institution of Oceanography, La Jolla, California, and U. S. Naval Radiological Defense Laboratory, San Francisco 24, California; Secret Restricted Data.

8. H. D. LeVine and R. T. Graveson; "Radioactive Debris from Operation Castle Aerial Survey of Open Sea Following Yankee-Nectar"; NYO-4618.

9. M. B. Hawkins; "Determination of Radiological Hazard to Personnel"; Project 2.4, Operation Wigwam, WT-1012, May 1957; U. S. Naval Radiological Defense Laboratory, San Francisco 24, California; Official Use Only.

10. R. L. Stetson and others; "Distribution and Intensity of Fallout from the Underground Shot"; Project 2.5.2, Operation Teapot, WT-1154, March 1958; U. S. Naval Radiological Defense Laboratory, San Francisco 24, California; Unclassified.

11. D. C. Borg and others; "Radioactive Fall-Out Hazards from Surface Bursts of Very High Yield Nuclear Weapons"; AFSWP-507, May 1954; Headquarters, Armed Forces Special Weapons Project, Washington 13, D. C.; Secret Restricted Data.

12. "Fall-Out Symposium"; AFSWP-895, January 1955; Armed Forces Special Weapons Project, Washington 25, D. C.; Secret Restricted Data.

13. V. A. J. VanLint and others; "Fallout Studies During Operation Redwing"; Program 2, Operation Redwing, ITR-1354, October 1956; Field Command, Armed Forces Special Weapons Project, Sandia Base, Albuquerque, New Mexico; Secret Restricted Data.

14. R. T. Graveson; "Fallout Location and Delineation by Aerial Surveys"; Project 2.64, Operation Redwing, ITR-1318, February 1957; U. S. AEC Health and Safety Laboratory, New York, New York; Secret Restricted Data.

15. F. D. Jennings and others; "Fallout Studies by Oceanographic Methods"; Project 2.62a, Operation Redwing, ITR-1316, November 1956; University of California, Scripps Institution of Oceanography, La Jolla, California; Secret Restricted Data.

16. M. Morgenthau and others; "Land Fallout Studies"; Project 2.65, Operation Redwing, ITR-1319, December 1956; Radiological Division, Chemical Warfare Laboratories, Army Chemical Center, Maryland; Secret Restricted Data.

17. C. F. Miller and P. Loeb; "The Ionization Rate and Photon Pulse Rate Decay of Fission Products from Slow Neutron Fission of U^{235}"; USNRDL-TR-247, August 1958; U. S. Naval Radiological Defense Laboratory, San Francisco 24, California; Unclassified.

18. P. D. LaRiviere; "The Relationship of Time of Peak Activity from Fallout to Time of Arrival"; USNRDL-TR-137, February 1957; U. S. Naval Radiological Defense Laboratory, San Francisco 24, California; Unclassified.

19. J. W. Hendricks; "Fallout Particle Size Measurements from Operation Redwing"; USNRDL-TR-264, July 1958; U. S. Naval Radiological Defense Laboratory, San Francisco 24, California; Confidential.

20. S. Baum; "Behavior of Fallout Activity in the Ocean"; NRDL Technical Report (in publication); U. S. Naval Radiological Defense Laboratory, San Francisco 24, California; Secret.

21. C. E. Adams; "The Nature of Individual Radioactive Particles. II. Fallout Particles from M-Shot, Operation Ivy"; USNRDL-408, 1 July 1953; U. S. Naval Radiological Defense Laboratory, San Francisco 24, California; Confidential.

22. C. E. Adams; "The Nature of Individual Radioactive Particles. IV. Fallout Particles from the First Shot, Operation Castle"; USNRDL-TR-26, 17 January 1955; U. S. Naval Radiological Defense Laboratory, San Francisco 24, California; Confidential.

23. C. E. Adams; "The Nature of Individual Radioactive Particles. V. Fallout Particles from Shots Zuni and Tewa, Operation Redwing"; USNRDL-TR-133, 1 February 1957; U. S. Naval Radiological Defense Laboratory, San Francisco 24, California; Confidential.

24. C. E. Adams and J. D. O'Connor; "The Nature of Individual Radioactive Particles. VI. Fallout Particles from a Tower Shot, Operation Redwing"; USNRDL-TR-208, December 1957; U. S. Naval Radiological Defense Laboratory, San Francisco 24, California; Unclassified.

25. W. Williamson, Jr.; "Investigation and Correlation of Some Physical Parameters of Fallout Material"; USNRDL-TR-152, 28 March 1957; U. S. Naval Radiological Defense Laboratory, San Francisco 24, California; Unclassified.

26. J. Mackin and others; "Radiochemical Analysis of Individual Radioactive Fallout Particles from a Land Surface Detonation"; USNRDL-TR-386, September 1958; U. S. Naval Radiological Defense Laboratory, San Francisco 24, California; Unclassified.

27. C. D. Coryell and N. Sugarman; "Radiochemical Studies: The Fission Products"; Book 3; McGraw-Hill, 1951.

28. "Radiochemical Procedures in Use at the University of California Radiation Laboratory, Livermore"; UCRL-4377, 10 August 1954; University of California Radiation Laboratory, Livermore, California.

29. L. D. McIsaac; "Determination of Np^{239}, "Total Fissions," Mo^{99}, and Ce^{141} in Fission Product Mixtures by Gamma-Ray Scintillation Spectrometry"; USNRDL-TR-72, 5 January 1956; U. S. Naval Radiological Defense Laboratory, San Francisco 24, California; Unclassified.

30. H. K. Chan; "Activity-Size Relationship of Fallout Particles from Two Shots, Operation Redwing"; USNRDL-TR-314, February 1959; U. S. Naval Radiological Defense Laboratory, San Francisco 24, California; Unclassified.

31. N. H. Farlow and W. R. Scheil; "Physical, Chemical, and Radiological Properties of Slurry Particulate Fallout Collected During Operation Redwing"; USNRDL-TR-170, 5 May 1957; U. S. Naval Radiological Defense Laboratory, San Francisco 24, California; Unclassified.

32. W. R. Schell; "Physical Identification of Micron-Sized, Insoluble Fallout Particles Collected During Operation Redwing"; USNRDL-TR-364, 24 September 1959; U. S. Naval Radiological Defense Laboratory, San Francisco 24, California; Unclassified.

33. N. H. Farlow; "Quantitative Analysis of Chloride Ion in 10^{-6} to 10^{-12} Gram Particles"; Analytical Chemistry; 29: 883, 1957.

34. L. R. Bunney and N. E. Ballou; "Bomb-Fraction Measurement Techniques"; USNRDL-TR-176, September 1957; U. S. Naval Radiological Defense Laboratory, San Francisco 24, California; Secret Restricted Data.

35. M. Honma; "Flame Photometric Determination of Na, K, Ca, Mg, and Sr in Seawater"; USNRDL-TR-62, September 1955; U. S. Naval Radiological Defense Laboratory, San Francisco 24, California; Unclassified.

36. M. Honma; "Flame Photometric Determination of Na, K, Ca, Mg, and Sr in Coral"; Unpublished data; U. S. Naval Radiological Defense Laboratory, San Francisco 24, California.

37. F. D. Snell and C. T. Snell; "Colorimetric Methods of Analysis"; Vol. II Third Edition; D. Van Nostrand Co., New York; 1949.

38. A. P. Smith and F. S. Grimaldi; "The Fluorimetric Determination of Uranium in Nonsaline and Saline Waters, Collected Papers on Methods of Analysis for Uranium and Thorium"; Geological Survey Bulletin 1006; U. S. Government Printing Office, Washington, D. C.; 1954.

39. A. E. Greendale and M. Honma; "Glove Box and Associated Equipment for the Removal of Radioactive Fallout from Hexcell Collectors"; USNRDL-TR-157, May 1957; U. S. Naval Radiological Defense Laboratory, San Francisco 24, California; Unclassified.

40. M. Honma and A. E. Greendale; "Correction for Hexcell Background in Fallout Samples"; Unpublished data; U. S. Naval Radiological Defense Laboratory, San Francisco 24, California.

41. R. C. Bolles and N. E. Ballou; "Calculated Activities and Abundances of U^{235} Fission Products"; USNRDL-456, August 1956; U. S. Naval Radiological Defense Laboratory, San Francisco 24, California; Unclassified.

42. C. F. Miller; "Response Curves for USNRDL 4-Pi Ionization Chamber"; USNRDL-TR-155, May 1957; U. S. Naval Radiological Defense Laboratory, San Francisco 24, California; Unclassified.

43. P. D. LaRiviere; "Response of Two Low-Geometry Scintillation Counters to Fission and Other Products"; USNRDL-TR-303, February 1959; U. S. Naval Radiological Defense Laboratory, San Francisco 24, California; Unclassified.

44. C. F. Miller; "Proposed Decay Schemes for Some Fission-Product and Other Radionuclides"; USNRDL-TR-160, 17 May 1957; U. S. Naval Radiological Defense Laboratory, San Francisco 24, California; Unclassified.

45. C. F. Miller; "Analysis of Fallout Data. Part III; The Correlation of Some Castle Fallout Data from Shots 1, 2, and 3"; USNRDL-TR-222, May 1958; U. S. Naval Radiological Defense Laboratory, San Francisco 24, California; Secret Restricted Data.

46. V. A. J. VanLint; "Gamma Rays from Plane and Volume Source Distributions"; Program 2, Operation Redwing, ITR-1345, September 1956; Weapons Effects Tests, Field Command, Armed Forces Special Weapons Project, Sandia Base, Albuquerque, New Mexico; Confidential Restricted Data.

47. "The Effects of Nuclear Weapons"; U. S. Atomic Energy Commission, Washington, D. C., June 1957; Unclassified.

48. L. E. Glendenin; "Determination of Strontium and Barium Activities in Fission"; NNES IV, 9, Paper 236, 1951.

49. D. N. Hume; "Determination of Zirconium Activity by the Barium Fluozirconate Method"; NNES IV, 9, Paper 245, 1951.

50. E. M. Scadden; "Improved Molybdenum Separation Procedure"; Nucleonics 15, 102, 1957.

51. L. E. Glendenin; "Improved Determination of Tellurium Activity in Fission"; NNES IV, 9, Paper 274, 1951.

52. E. Mizzan; "Phosphotungstate Precipitation Method of Analysis of Radioactive Cesium in Solutions of Long-Lived Fission Products"; AECL Report PDB-128, July 1954.

53. L. E. Glendenin and others; "Radiochemical Determination of Cerium in Fission"; Anal. Chem. 27, 59, 1955.

54. L. Wish and M. Rowell; "Sequential Analysis of Tracer Amounts of Np, U, and Pu in Fission-Product Mixtures by Anion Exchange"; USNRDL-TR-117, 11 October 1956; U. S. Naval Radiological Defense Laboratory, San Francisco 24, California; Unclassified.

55. "Salted Weapons (C)"; AFSWP SWPDV-11-942.6, May 1957; Secret Restricted Data.

56. J. O. Blomeke; "Nuclear Properties of U^{235} Fission Products"; ORNL-1783, November 1955; Oak Ridge National Laboratory, Oak Ridge, Tennessee; Unclassified.

57. W. E. Thompson; "Spectrometric Analysis of Gamma Radiation from Fallout from Operation Redwing"; USNRDL-TR-146, 29 April 1957: U. S. Naval Radiological Defense Laboratory, San Francisco 24, California; Confidential Restricted Data.

58. "The Effects of Atomic Weapons"; U. S. Atomic Energy Commission, Washington, D. C., Revised September 1950; Unclassified.

59. K. Way and E. P. Wigner; "The Rate of Decay of Fission Products"; MDDC 1194, August 1947; Unclassified; also Phys. Rev. 73, 1318, 1948.

60. H. F. Hunter and N. E. Ballou; "Simultaneous Slow Neutron Fission of U^{235} Atoms. Individual Total Rates of Decay of the Fission Products"; USNRDL ADC-65, April 1949; U. S. Naval Radiological Defense Laboratory, San Francisco 24, California; Unclassified.

61. C. F. Miller; "Gamma Decay of Fission Products from the Slow-Neutron Fission of U^{235}"; USNRDL-TR-187, 11 July 1957; U. S. Naval Radiological Defense Laboratory, San Francisco 24, California; Unclassified.

62. "Radiological Recovery of Fixed Military Installations"; Navy, Bureau of Yards and Docks, NavDocks TPPL-13; Army Chemical Corps TM 3-225, interim revision, April 1958; Unclassified.

63. E. R. Tompkins and L. B. Werner; "Chemical, Physical, and Radiochemical Characteristics of the Contaminant"; Project 2.6a, Operation Castle, WT-917, September 1955; U. S. Naval Radiological Defense Laboratory, San Francisco 24, California; Secret Restricted Data.

64. H. V. Sverdrup, M. W. Johnson, and R. H. Fleming; "The Oceans, Their Physics, Chemistry, and General Biology"; Prentice-Hall, New York, 1942.

65. K. O. Emery, J. L. Tracey, Jr., and H. S. Ladd; "Geology of Bikini and Nearby Atolls. Bikini and Nearby Atolls: Part 1, Geology"; Geological Survey Professional Paper 260-A, U. S. Government Printing Office, Washington, D. C., 1954.

66. S. C. Foti; "Construction and Calibration of a Low Geometry Scintillation Counter"; Un-

published data, U. S. Naval Radiological Defense Laboratory, San Francisco 24, California.

67. E. A. Schuert; "A Fallout Forecasting Technique with Results Obtained at the Eniwetok Proving Ground"; USNRDL-TR-139, 3 April 1957; U. S. Naval Radiological Defense Laboratory, San Francisco 24, California; Unclassified.

68. E. A. Schuert; "A Fallout Plotting Device"; USNRDL-TR-127, February 1957; U. S. Naval Radiological Defense Laboratory, San Francisco 24, California; Unclassified.

69. L. Fussell, Jr.; "Cloud Photography"; Project 9.1a, Operation Redwing, ITR-1343, March 1957; Edgerton, Germeshausen and Grier, Inc., Boston, Massachusetts; Secret Formerly Restricted Data.

70. Meteorological Report on Operation Redwing; Part I, "Meteorological Data," Volumes 1, 2, and 11 and Part II, "Meteorological Analyses," Volumes 1, 2, and 3; Joint Task Force 7; JTFMC TP-1, 1956; Unclassified.

71. D. F. Rex; "Vertical Atmospheric Motions in the Equatorial Central Pacific"; Joint Task Force 7 Meteorological Center, Pearl Harbor, T. H.; Unclassified.

72. J. C. Kurtyka; "Precipitation Measurements Study"; State of Illinois Water Survey Division, Report of Investigation No. 20, 1953.

73. L. E. Egeberg and T. H. Shirasawa; "Standard Platform Sampling Bias Studies, Part I, Preliminary Studies of Airflow"; USNRDL-TM-70, 25 February 1957; U. S. Naval Radiological Defense Laboratory, San Francisco 24, California; Unclassified.

74. H. K. Chan; "Analysis of Standard Platform Wind Bias to Fallout Collection at Operation Redwing"; USNRDL-TR-363, September 1959; U. S. Naval Radiological Defense Laboratory, San Francisco 24, California; Unclassified.

75. W. W. Perkins and G. Pence; "Standard Platform Sampling Bias Studies, Part II, Rainfall Bias Studies"; USNRDL Technical Memorandum (in publication); U. S. Naval Radiological Defense Laboratory, San Francisco 24, California; Unclassified.

76. P. Brown and others; "Gamma Exposure versus Distance"; Project 2.1, Operation Redwing, WT-1310, 20 February 1960; U. S. Army Signal Engineering Laboratories, Fort Monmouth, New Jersey; Secret Restricted Data.

Appendix A
INSTRUMENTATION

A.1 COLLECTOR IDENTIFICATION

Collector designations are shown in Figure A.1.

A.2 DETECTOR DATA

A.2.1 End-Window Counter.

Crystal dimensions and type: 1½-inch diameter × ½ inch thick, NaI(Tl), Harshaw

Photomultiplier tube type: 6292 DuMont

Scaler types: Model 162 Nuclear Instrument Corporation, and Model 182 Nuclear-Chicago (in tandem)

Pb shield dimensions: 8½-inch outside diameter × 20 inches high × 1½ inches thick; additional 2-inch thickness in Site Elmer laboratory

Counting chamber dimensions: 5½-inch diameter × 4 inches high

Al absorber thickness: ¼ inch

Shelf distances from bottom of absorber:

Shelf	Distance cm
1	1.0
2	2.6
3	4.2
4	5.8
5	7.4

Ratios to Shelf 5 (most commonly used) for centered Cs^{137} point source:

Shelf	Ratio
1	5.87
2	3.02
3	1.88
4	1.31
5	1.00

Minimum count rate requiring coincidence loss correction: 1.0×10^6 counts/min

Counting procedure: ordinarily 3- to 1-minute intervals for each sample

A.2.2 Beta Counter.

Gas proportions: 90 percent A, 10 percent CO_2

Pb shield dimensions: 8½-inch outside diameter × 12 inches high × 1½ inches thick; additional 2-inch thickness in Site Elmer laboratory

Counting chamber dimensions: 5½-inch diameter × 4 inches high

Al window thickness: 0.92 mg/cm²

Shelf geometries from bottom of window:

Shelf	Distance cm	Physical Geometry Correction
1	0.85	0.2628
2	1.50	0.1559
3	2.15	0.0958
4	3.75	0.0363
5	5.35	0.0177

Minimum count rate requiring coincidence loss correction: 3.0×10^5 counts/min

A.2.3 4-π Ionization Chamber (Analytical and Standards Branch). (Two newer chambers of modified design were also used. The response of these to 100 μg of Ra ≃ 700×10^{-9} ma at 600 psi; therefore, all readings were normalized to the latter value. Use of precision resistors (1 percent) eliminated scale correction factors.)

Gas type and pressure: A ~ 600 psi

Shield dimensions: Pb ~ 19-inch outside diameter × 22 inches high × 4 inches thick; additional 1-foot thickness of sandbags in Site Elmer laboratory

Counting chamber dimensions: 11-inch diameter × 14 inches high

Thimble dimensions: 1¾-inch inside diameter × 12 inches deep

Useful range: ~ 217×10^{-11} ma (background) to 200×10^{-8} ma

Correction factors to equivalent 10^9 scale:

Scale ~ ohms	Factor
10^{11}	0.936
10^{10}	0.963
10^9	1.000
10^8	1.000

Response versus sample (Ra) position:

Distance from Bottom of Tube in	Relative Response pct
0 to 3	100
3.5 to 5.5	99 to 92

Response to 100 μg Ra: 5.58×10^{-9} ma at ~ 600 psi

Efficiency factors relative to Co^{60} for various nuclides:

Nuclide	Factor
Ce^{141}	0.186
Hg^{203}	0.282
Au^{198}	0.355
Cs^{137}	0.623
Sc^{46}	0.884
Co^{60}	1.000
K^{42}	1.205
Na^{24}	1.312

A.2.4 Well Counter.

Nuclear-Chicago Model DS-3

Crystal dimensions and type: 1¾-inch diameter × 2 inches thick, NaI(T1)

Well dimensions: ¾-inch diameter × 1½ inches deep

Photomultiplier tube type: 6292 DuMont

Scaler type: Model MPC-1 Berkeley, or Nuclear Instrument Corporation 162 with Nuclear-Chicago 182 in tandem

Pb shield thickness: 1½ inches, with ¾-inch diameter hole above crystal well; additional 2-inch thickness in YAG 40 laboratory

Counting rate versus sample volume in test tube (15 × 125 mm):

Sample Volume	Relative Count Rate
ml	pct
0.01	100
1.81	99.2
3.9 (~ well depth)	90.6

Efficiency for several nuclides:

Nuclide	Efficiency counts/dis
Au^{198}	0.42
Co^{60}	0.43
I^{131}	0.51

Minimum count rate requiring coincidence loss correction: 1.0×10^6 counts/min

Counting procedure: minimum of 10^4 counts to maintain a statistical error of ~1.0 percent

A.2.5 20-Channel Analyzer.

Crystal dimensions and type: 2-inch diameter × 2 inches thick, NaI(T1)

Glow transfer tube types: GC-10B and GC-10D

Fast register type: Sodeco

Voltage gain (with delay line pulse shaping): 1,000

Attenuation (with ladder attenuator): 63 decibels in 1-decibel steps

Pb shield thickness: ~2 inches

Counting chamber dimensions: 8-inch diameter × 3½ inches high

Shelf distances from bottom of detector:

Shelf	Distances cm
1	2.07
2	4.76
3	5.25
4	6.84

Tray distance from bottom of detector when outside of ½-inch diameter collimator: 13.95 cm

Calibration standards: Ba^{133}, Ce^{141}, Hg^{203}, Na^{22}, and Cs^{137}

Calibration procedure: one per day and one following each adjustment of amplifier or detector voltage

Counting procedure: equal counting times for each series on a given sample

A.2.6 Doghouse Counter (Reference 43)

Crystal dimensions and type: 1-inch diameter × 1 inch thick, NaI(T1), Harshaw aluminum absorber ¼-inch thick

Photomultiplier tube type: 6292 DuMont

Scaler type: Model 162 Nuclear Instrument Corporation, and Model 182 Nuclear-Chicago (in tandem)

Pb shield dimensions (detector): 10-inch diameter × 20 inches high × 1½ inches thick

Pb shield thickness (counting chamber): 2 inches

Counting chamber dimensions: 20 × 24 × 34 inches high

Size of hole in roof of counting chamber for detector: 7-inch diameter

Distance from bottom of sample tray to bottom of crystal: 36 inches

Sample tray dimensions: 18 × 21 × 2 inches deep

Counting efficiency for several point-source nuclides, centered in bottom of tray with ¼-inch aluminum cover in place:

Nuclide	counts/dis × 10^{-4}
Na^{22}	1.70
Na^{24}	0.936
K^{42}	0.151
Sc^{46}	1.16
Co^{60}	1.02
Nb^{95}	0.506
Cs^{137}-Ba^{137m}	0.548
Ce^{141}	0.622
Au^{198}	0.711
Hg^{203}	0.842

Relative counter photon efficiency, computed for total aluminum thickness = ½ inch (3.43 gm/cm²):

Energy Mev	Efficiency pct
0.01	0
0.02	0.0034
0.03	3.24
0.05	33.3
0.07	48.7
0.10	57.8
0.15	63.7

0.20	61.5
0.30	54.0
0.50	43.3
0.70	37.5
1.00	33.4
1.50	29.5
2.00	27.1
3.00	25.3
4.00	24.4

Minimum count rate requiring coincidence loss correction: 1.0×10^6 counts/min

Counting procedure: ordinarily 3- to 1-minute intervals for each sample; trays decontaminated and counted with ¼-inch aluminum cover in place

A.2.7 Dip Counter.

Crystal dimensions and type: 1½-inch diameter × 1 inch thick, NaI(Tl)

Photomultiplier tube type: 6292 DuMont

Scaler type: Same as doghouse counter

Shield thickness and counting chamber dimensions: Same as doghouse counter

Sample volume: 2,000 ml (constant geometry)

Counting efficiency for several nuclides: (Private communication from J. O'Connor, NRDL)

Nuclide	counts/dis × 10^{-2}
Ce^{141}	1.20
Hg^{203}	1.72
Au^{198}	1.28
Cs^{137}	0.916
Nb^{95}	0.870
Sc^{46}	1.76
Co^{60}	1.56
Na^{24}	1.29

Minimum count rate requiring coincidence loss correction: 2×10^6 counts/min

Counting procedure: 2,000-ml samples at constant geometry; counting intervals selected to maintain a statistical error < 1.0 percent

A.2.8 Single-Channel Analyzer (Nuclear Radiation Branch) (Reference 57)

Crystal dimensions and type: 4-inch diameter × 4 inches thick, NaI(Tl)

Photomultiplier tube type: 6364 DuMont

Pulse-height analyzer type: Model 510-SC Atomic Instruments

Pb shield thickness: 2½ inches

Collimator dimensions: ½-inch diameter × 6 inches long

Sample container type and size: glass vial, ½-inch diameter × 2½ inches long

Distance from bottom of sample to collimator opening: 2 inches

Calibration standards: Na^{22}, and Hg^{203}

A.2.9 Gamma Time-Intensity Recorder. The energy and directional response characteristics of the standard TIR detector, consisting of four ion chambers (A, Am, Bm, and Cm) with a protective dome, were determined at NRDL. (Measurements and calculations were carried out by G. Hitchcock, T. Shirasawa, and R. Caputi.)

A special jig permitted both horizontal and vertical rotation about the center of the chamber under study. Directional response was measured and recorded continuously for 360 degrees in planes at 30-degree increments through the longitudinal axis of the Cm chamber. Relative response data was obtained by effectively exposing the chamber to a constant ionization rate at six different energies—four X-ray energies: 35 kev, 70 kev, 120 kev and 180 kev; and two source energies: Cs^{137} (0.663 Mev) and Co^{60} (1.2 Mev).

The results for three mutually perpendicular planar responses have been illustrated graphically to show: (1) shadowing interference by other chambers in the horizontal plane (Figure A.2), (2) maximum shadowing interference by other chambers in the vertical plane (Figure A.3), and (3) minimum shadowing interference by other chambers in the vertical plane (Figure A.4).

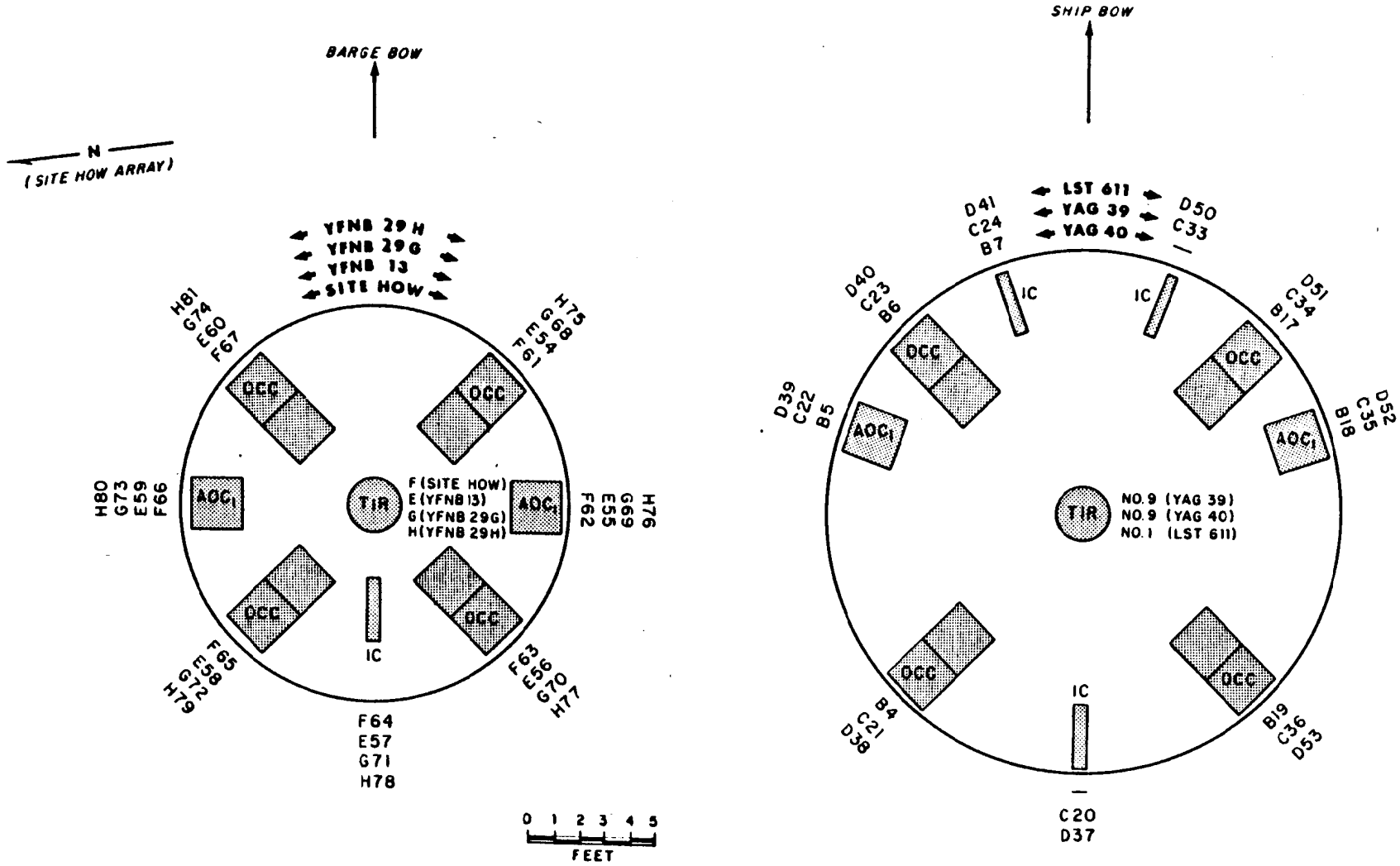

Figure A.1 Collector designations.

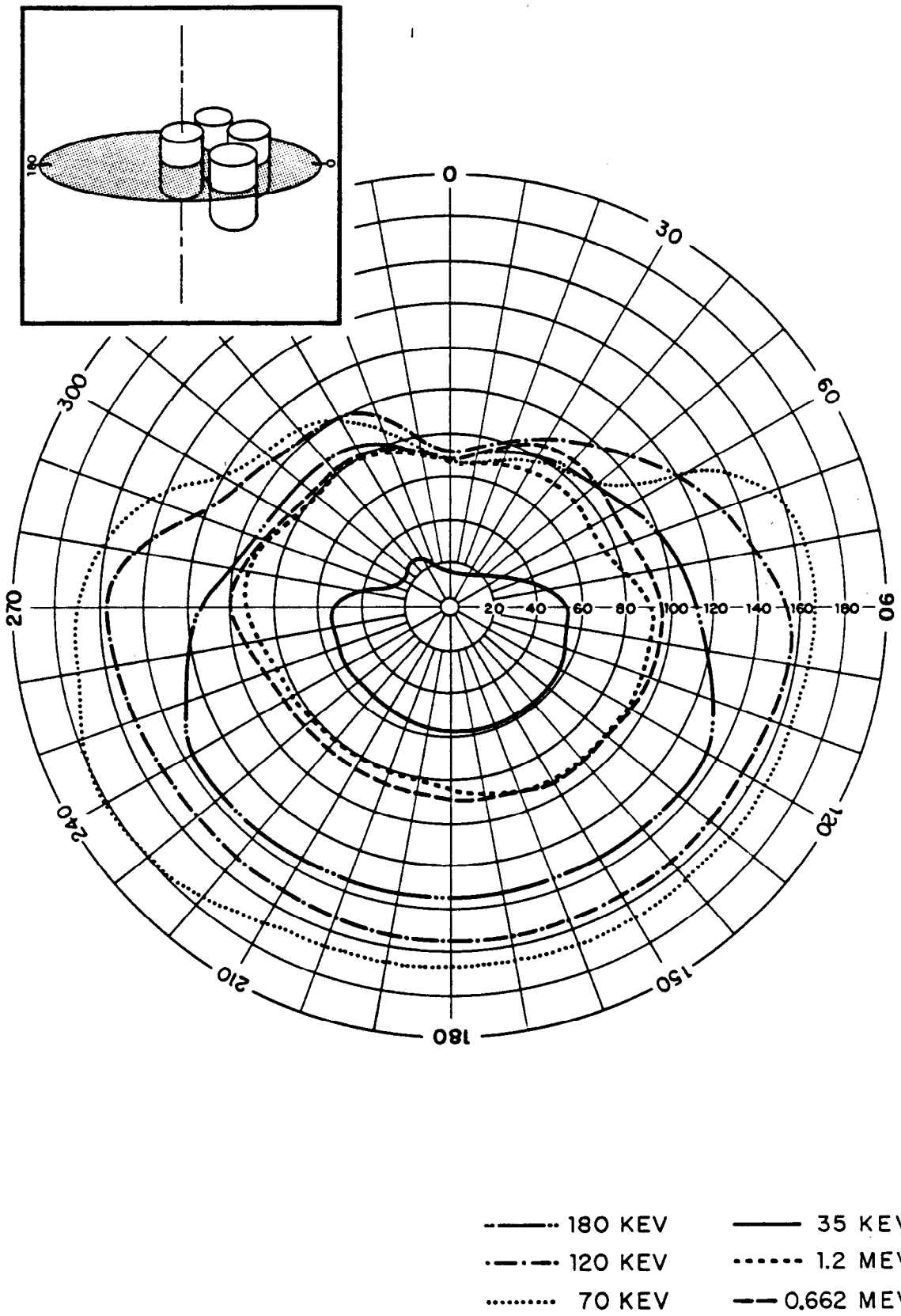

Figure A.2 Shadowing interference in horizontal plane for TIR.

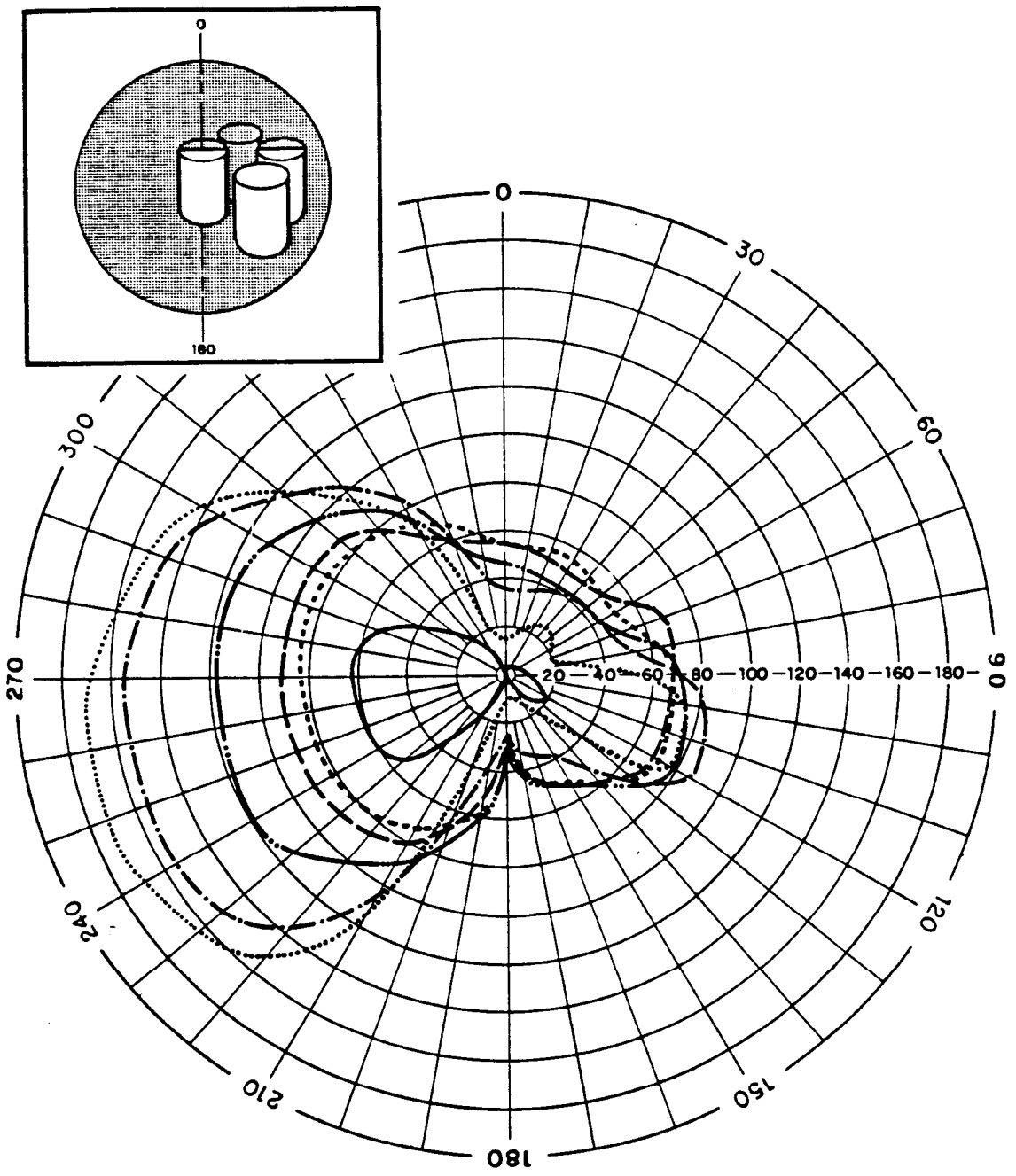

Figure A.3 Maximum shadowing interference in vertical plane for TIR.

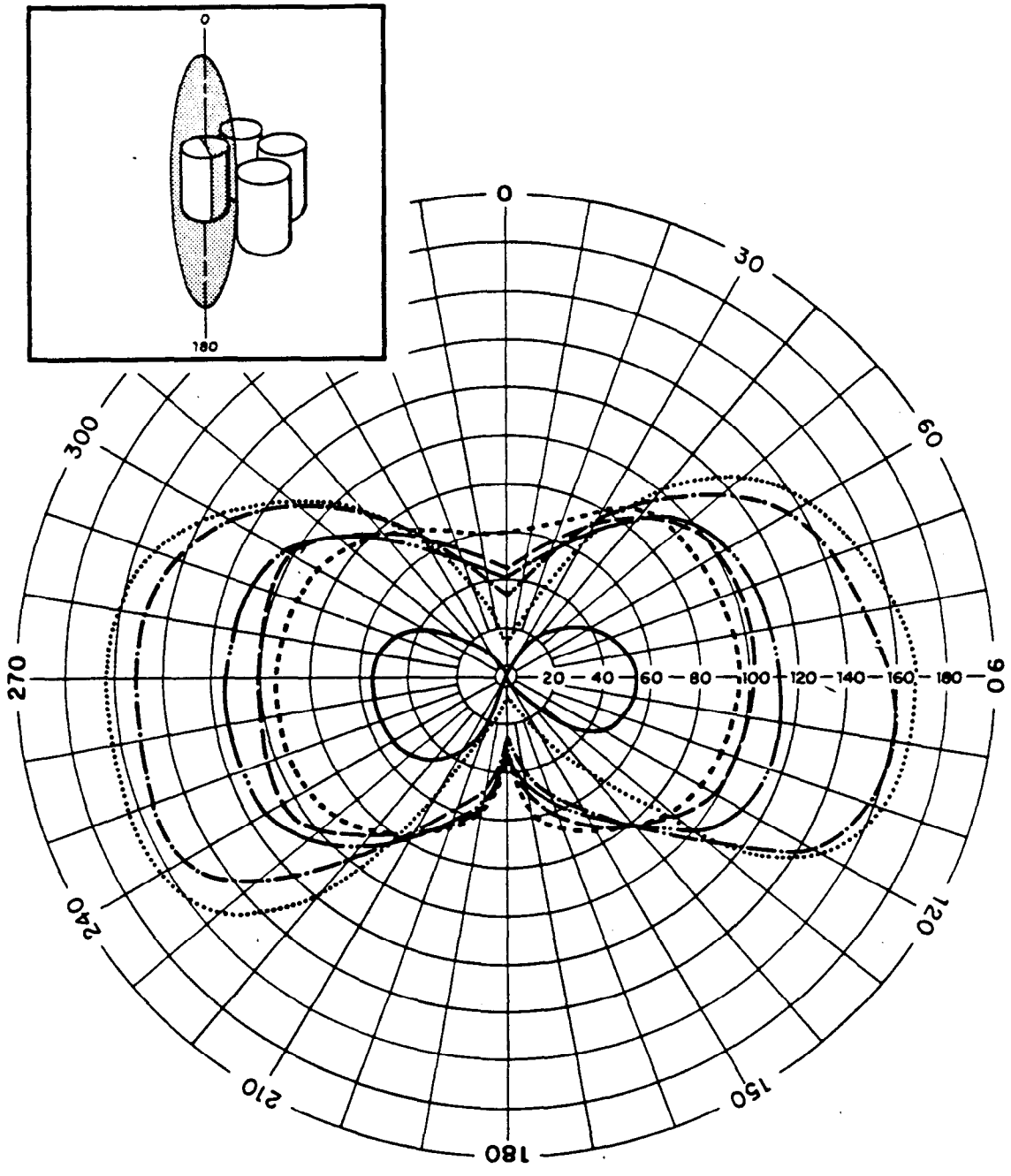

Figure A.4 Minimum shadowing interference in vertical plane for TIR.

Appendix B
MEASUREMENTS

B.1 BUILDUP DATA

TABLE B.1 OBSERVED IONIZATION RATE, BY TIME-INTENSITY RECORDER

Station and Shot	
YAG 40-B, No. 9 ZU	
H + hr	mr/hr
3.37	2.28
3.57	16.8
3.73	44.2
4.07	129
4.37	470
5.07	1,480
6.07	3,340
7.07	1,660
8.07	1,360
9.07	1,240
11.1	966
14.1	754
18.1	588
22.1	478
26.1	404
30.1	340
42.1	233
54.1	181
66.1	129
78.1	105

YAG 40, No. 13 (Deck) ZU	
H + hr	r/hr
3.53	0.0165
3.63	0.0318
3.70	0.0386
3.77	0.0722
3.85	0.0847
3.97	0.128
4.05	0.165
4.17	0.249
4.32	0.480
4.57	0.957
4.77	1.31
4.95	1.92
5.08	2.37
5.25	3.25
5.40	4.06
5.57	4.58
5.73	5.67
5.90	5.76
6.07	6.20
6.32	6.75
6.57	7.57
6.82	7.57
7.07	7.29
7.32	7.20
7.57	6.94
7.82	6.66
8.07	6.30
8.32	6.20
8.57	6.02
8.82	5.76
9.07	5.67

Station and Shot	
YAG 40, No. 13 (Deck) ZU	
H + hr	r/hr
9.32	5.49
9.57	5.31
9.82	5.13
10.1	5.13
10.6	4.68
11.1	4.41
11.6	4.14
12.1	3.97
12.6	3.97
13.1	3.70
13.6	3.61
14.1	3.34
14.6	3.43
15.1	3.25
15.6	3.07
16.1	3.07
16.6	2.98
17.1	2.90
17.6	2.81
18.1	2.72
19.1	2.62
20.1	2.45
21.1	2.36
22.1	2.28
24.1	2.10
26.1	1.92
28.1	1.75
30.1	1.66
34.1	1.49
38.1	1.31
42.1	1.17
46.1	1.11
50.1	0.940
54.1	0.844
58.1	0.740
62.1	0.679
66.1	0.635
72.1	0.583
78.1	0.539
80.1	0.495

YAG 39-C, No. 9 ZU	
H + hr	mr/hr
12.7	0.559
13.1	0.706
13.6	0.765
14.1	0.926
15.1	1.47
16.1	2.96
17.1	4.29
18.1	6.54
19.1	8.36
20.1	9.42
21.1	10.2
22.1	10.2
23.1	10.8

Station and Shot	
YAG 39-C, No. 9 ZU	
H + hr	mr/hr
24.1	11.1
25.1	11.4
27.1	11.8
29.1	11.3
30.1	11.3
32.1	10.5
34.1	10.2
36.1	8.96
38.1	8.51
40.1	8.21
42.1	7.74
46.1	6.54
50.1	6.25
54.1	5.64
58.1	5.19
62.1	4.89
66.1	4.60
70.1	4.29
74.1	4.14
78 1	4.00
80.5	3.85

YAG 39, No. 13 (Deck) ZU	
H + hr	mr/hr
13.0	3.24
14.0	4.86
15.0	6.66
16.0	13.1
17.0	17.2
18.0	25.4
19.0	31.8
20.0	34.2
21.0	34.9
24.0	37.4
25.0	37.6
29.0	36.3
30.0	36.2
31.0	34.6
32.2	33.5
42.0	26.3
48.0	21.8
49.0	20.8
50.0	19.9
52.0	19.8
66.0	15.8
68.0	15.4
69.0	14.9
70.0	14.6
72.0	14.2

Station and Shot	
YFNB 13-E, ZU	
H + min	r/hr
20	0.0016
21	0.007
22	0.009
23	0.016
24	0.068
27	0.31
28	0.55
29	0.72
55	2.89
180	1.83
195	1.69
210	1.5
300	0.96
420	0.66
600	0.43
1,015	0.22
1,495	0.16
1,975	0.078
3,415	0.041

How F, ZU	
H + min	r/hr
23	0.0055
24	0.0086
26	0.013
27	0.051
28	0.092
28+	0.37
30	0.47
32	0.66
33	0.68
34	0.73
41	0.87
46	1.09
49	1.61
54	2.13
59	2.57
62	2.87
64	2.87
68	2.74
70	2.57
74	2.74
80	2.61
87	2.57
97	2.48
106	2.48
112	2.39
120	2.17
130	2.00
151	1.70
200	1.17
400	0.54

TABLE B.1 CONTINUED

YFNB 29-G ZU

H+min	r/hr
10	0.0005
20	0.03
26	0.26
27	0.54
28	0.83
29	0.99
31	1.32
33	3.10
35	4.0
36	4.94
43	9.21
49	9.64
94	7.05
124	5.64
139	4.7
184	3.06
274	2.12
424	1.36
484	0.99
544	0.80
574	0.78
649	0.70
799	0.55
1,624	0.31
2,524	0.19
3,424	0.15

YAG 40-B, No. 9 FL

H + hr	mr/hr
6.00	0.050
8.00	0.550
9.00	5.10
10.0	17.4
11.0	48.0
12.0	71.1
15.0	71.1
16.0	81.5
17.0	81.5
18.0	81.5
19.0	71.1
20.0	71.1
21.0	69.7
22.0	59.4
23.0	58.2
25.0	53.0
30.0	39.0
35.0	35.2
40.0	30.0
45.0	27.6
50.0	16.2
55.0	14.9
58.0	13.7
63.0	12.4
70.0	11.1
75.0	10.4
79.0	9.20

YAG 40, No. 13 (Deck) FL

H+hr	mr/hr
6.00	0
8.00	1.93
8.57	8.18
9.00	17.4
9.57	38.0
10.0	61.9
11.0	142
12.0	225
13.0	248
14.0	237
15.0	237
16.0	248
17.0	259
18.0	248
19.0	237
20.0	231
21.0	225
22.0	214
23.0	197
24.0	180
30.0	145
35.0	125
40.0	109
45.0	88.4
50.0	56.8
55.0	52.3
58.0	46.6
63.0	44.4
70.0	39.9
75.0	37.6
79.0	22.1

YAG 39-C, No. 9 FL

H + hr	mr/hr
4.12	0.061
4.37	0.417
4.53	0.646
4.78	1.01
4.95	1.88
5.10	3.30
5.38	6.19
5.68	8.23
6.05	10.7
6.27	12.3
6.52	15.4
6.72	19.4
7.02	21.9
7.28	21.9
7.50	23.7
7.75	26.1
8.02	28.6
8.28	29.9
8.57	29.9
8.77	32.3
9.19	32.9
9.60	31.7

YAG 39-C, No. 9 FL

H + hr	mr/hr
10.1	32.3
10.5	35.5
11.0	33.4
11.6	37.2
12.1	36.0
12.6	34.6
13.1	33.4
13.6	32.3
14.1	31.0
15.1	29.2
16.0	27.3
17.0	26.1
18.0	24.9
19.0	23.7
20.0	22.5
21.0	21.3
22.0	19.4
23.0	19.4
24.0	17.7
26.0	16.3
28.0	14.6
30.0	13.4
32.0	12.4
34.0	11.6
36.0	11.0
38.0	10.4
40.0	9.80
45.0	8.71
50.0	6.55
55.0	5.77
60.0	5.04
64.9	4.68
70.1	4.33
75.0	4.15
80.0	3.50

YAG 39, No. 13 (Deck) FL

H + hr	mr/hr
4.62	3.34
5.23	21.8
5.57	42.9
6.57	45.6
7.07	78.4
7.57	87.8
8.57	121
9.00	121
10.0	121
11.0	141
12.0	131
13.0	121
15.0	102
18.0	83.0
22.0	69.0
26.0	55.0
30.0	46.5
36.0	39.2

YAG 39, No. 13 (Deck) FL

H+hr	mr/hr
42.0	33.7
47.0	28.2
48.0	21.8
54.0	15.4
66.0	10.8
75.0	9.27
76.0	6.30
80.0	6.04

LST 611-D, No. 1 FL

H + hr	mr/hr
6.57	0.14
7.32	0.67
7.57	2.2
7.90	15.3
8.40	32
8.73	57
8.90	76
9.07	99
9.23	88
9.40	83
9.57	80
10.1	78
10.9	71
12.1	65
13.1	60
14.1	55
15.6	48
17.6	44
19.6	38
21.6	35
23.6	32

YFNB 13-E FL

H + min	r/hr
21	0.0016
24	0.0054
26	0.0048
30	0.030
32	0.56
35	2.26
37	6.82
77	21.8
137	11.5
257	5.5
377	2.5
437	1.9
497	1.6
557	1.5
617	1.2
617	1.4

TABLE B.1 CONTINUED

Station and Shot		Station and Shot		Station and Shot		Station and Shot	
YFNB 29 H FL		YAG 40-B, No. 9 NA		YAG 40, No. 13 (Deck) NA		YAG 40, No. 13 (Deck) NA	
H + min	r/hr	H + hr	mr/hr	H + hr	mr/hr	H + hr	mr/hr
35	0.004	11.0	45.7	7.18	6.64	50.2	9.15
36	0.0046	11.3	49.3	7.30	10.0	52.1	7.84
38	0.011	11.6	51.2	7.47	11.4	54.0	7.62
40	0.018	11.9	52.7	7.63	12.4	56.0	4.79
42	0.042	12.1	52.7	7.80	13.7	57.9	4.46
44	0.075	12.3	55.3	7.95	14.3	60.1	4.35
45	0.10	12.5	55.3	8.10	13.1	64.0	4.08
51	0.27	12.7	57.8	8.33	13.0	68.1	3.81
53	0.38	12.9	55.3	8.48	13.5	72.0	3.48
54	0.49	14.0	55.3	8.62	16.0	74.9	3.32
56	0.57	15.0	55.3	8.75	18.6		
58	0.63	16.0	55.3	8.85	27.4	YAG 39-C, No. 9 NA	
77	0.96	17.0	55.3	9.02	38.2	H + hr	mr/hr
91	0.98	17.6	51.4	9.27	51.4	1.97	0.161
100	0.94	18.0	50.2	9.47	56.5	2.22	4.00
175	0.55	19.0	48.8	9.67	63.9	2.38	14.4
250	0.33	20.0	46.3	9.98	74.5	2.47	21.4
470	0.14	21.0	25.9	10.3	80.2	2.55	33.5
630	0.077	22.0	21.0	10.6	92.0	2.65	48.2
850	0.055	23.0	18.4	11.0	103	3.00	68.3
1,100	0.043	24.0	17.7	11.3	120	3.30	88.2
1,500	0.024	25.0	16.6	11.6	122	3.50	95.7
1,800	0.0198	26.0	16.2	12.0	125	3.70	144
		27.0	14.3	12.2	129	3.87	207
YAG 40-B, No. 9 NA		28.0	13.9	12.3	126	4.18	372
H + hr	mr/hr	29.0	13.1	12.5	129	4.42	431
5.07	0.146	30.0	12.5	12.7	120	4.62	481
6.02	0.120	32.0	11.8	13.0	116	4.85	485
6.23	0.175	34.0	10.8	13.5	113	5.17	498
6.38	0.260	36.0	10.3	14.0	113	5.33	525
6.62	0.370	38.0	9.80	15.0	105	5.48	507
6.87	0.590	40.0	9.20	15.9	103	5.67	516
6.98	0.800	42.0	9.40	16.9	101	5.85	516
7.09	1.44	44.0	9.10	18.0	91.4	6.02	512
7.14	1.30	46.0	8.20	18.9	87.0	6.37	481
7.18	1.88	48.0	7.70	20.0	82.5	6.57	471
7.26	2.31	51.0	7.40	20.2	70.1	6.77	445
7.36	3.61	54.0	6.05	20.4	36.2	7.18	422
7.52	3.55	55.0	6.55	21.0	27.4	7.40	400
7.73	4.30	56.0	6.30	22.0	24.1	7.63	386
7.93	4.80	58.0	6.18	23.0	21.3	8.10	361
8.10	5.55	59.0	5.55	24.0	21.9	8.37	347
8.45	7.05	60.0	5.49	25.0	20.8	8.62	329
8.69	9.30	62.0	5.30	26.0	19.7	9.18	304
8.90	13.1	65.0	4.93	27.0	17.0	9.48	289
9.12	19.0	69.0	4.68	28.0	16.4	9.78	267
9.27	22.2	75.0	4.18	29.0	15.4	10.2	259
9.42	24.1			30.0	14.9	10.5	246
9.55	26.0	YAG 40, No. 13 (Deck) NA		32.0	14.3	10.9	232
9.70	28.3	H + hr	mr/hr	34.0	13.4	11.3	222
9.90	31.0	4.83	0.200	36.0	12.9	11.6	207
10.1	33.6	5.57	0.556	38.0	12.0	12.1	203
10.3	34.8	6.12	0.808	40.0	11.7	12.6	193
10.5	38.7	6.65	1.80	42.0	11.1	13.0	184
10.8	42.5	6.97	3.15	44.0	10.6	14.1	168
				46.0	10.2		
				48.0	9.58		

TABLE B.1 CONTINUED

Station and Shot		Station and Shot		Station and Shot		Station and Shot	
YAG 39-C, No. 9 NA		YAG 39, No. 13 (Deck) NA		LST 611-D, No. 1 NA		How F NA	
H+hr	mr/hr	H + hr	mr/hr	H + hr	r/hr	H + min	r/hr
15.2	149	6.57	1,130	2.2	0.00042	6	0.0010
16.0	80.0	6.82	900	2.4	0.00045	33	0.0011
17.0	60.7	7.00	773	2.7	0.00051	45	0.0019
18.0	58.1	7.32	728	2.9	0.00087	48	0.0056
19.0	56.9	7.57	671	3.1	0.0015	53	0.048
20.0	53.1	7.82	624	3.2	0.0029	54	0.069
21.0	45.8	8.32	603	3.4	0.0044	55	0.083
22.0	36.1	8.82	557	3.7	0.0085	59	0.11
23.0	34.7	9.32	502	3.8	0.013	66	0.145
24.0	32.4	9.82	468	4.0	0.015	76	0.137
26.0	29.9	10.3	434	4.1	0.017	93	0.13
27.0	25.0	10.8	412	4.4	0.010	100	0.135
28.0	22.6	11.6	378	4.6	0.008	110	0.14
30.0	22.0	12.0	344	4.7	0.011	120	0.148
32.0	21.4	12.6	332	4.80	0.0109	125	0.146
34.0	19.6	13.0	305	4.9	0.012	134	0.148
36.0	18.4	13.6	288	4.97	0.012	140	0.150
38.0	17.8	14.1	277	5.07	0.016	Malfunction	
40.0	17.2	14.6	266	5.6	0.042		
42.0	16.0	15.0	243	6.1	0.043	YFNB 29-H, NA	
44.0	15.3	15.6	221	7.1	0.034	H + min	r/hr
46.0	14.6	15.7	132	10.1	0.020	11	0.0011
48.0	13.9	16.0	110	14.1	0.012	40	0.0012
50.0	13.2	16.6	108	16.1	0.0081	45	0.0026
55.0	11.7	17.0	106	18.1	0.0067	47	0.0091
59.0	10.6	18.0	98.7	24.1	0.0044	50	0.033
60.0	11.7	19.0	92.1	27.0	0.0039	51	0.062
64.0	10.1	20.0	88.9			52	0.075
70.1	9.15	21.0	76.7	YFNB 13-E NA		53	0.079
73.9	8.43	22.0	69.1	H + min	r/hr	54	0.083
		23.0	65.8	10	0.0047	60	0.084
YAG 39, No. 13 (Deck) NA		24.0	63.8	18	0.037	72	0.10
H + hr	mr/hr	25.0	61.3	27	0.60	80	0.116
1.82	0.78	26.0	59.1	29	4.04	104	0.108
2.30	11.0	27.0	53.6	38	8.5	180	0.087
2.37	18.7	28.0	51.4	46	7.0	205	0.080
2.43	36.1	30.0	48.1	58	4.6	255	0.066
2.50	73.3	32.0	44.8	72	3.4	330	0.047
2.68	110	34.0	42.8	91	2.75	400	0.035
2.78	101	36.0	41.0	118	2.3	420	0.030
3.00	143	38.0	39.3	121	2.1	480	0.026
3.12	177	40.0	37.5	136	1.8	610	0.018
3.40	221	42.0	35.8	219	1.0	780	0.013
3.65	310	44.0	34.5	301	0.67	920	0.011
3.90	558	47.0	31.8	406	0.41	1,000	0.0078
4.12	900	50.0	29.1	631	0.20	1,005	0.0054
4.32	1,240	53.0	25.4	1,006	0.08	1,150	0.0050
4.57	1,070	56.0	23.6	1,066	0.059	1,250	0.0040
4.82	900	59.0	23.6	1,306	0.042	1,300	0.0034
5.00	900	64.0	21.8	1,546	0.036	1,600	0.0028
5.32	1,010	66.0	20.8	1,666	0.033	1,900	0.0023
5.57	1,130	74.0	18.1	1,786	0.031	2,400	0.0020
5.82	1,130			1,906	0.046	2,700	0.0014
6.00	1,490			2,026	0.056		
6.32	1,240			2,146	0.056		
				2,266	0.041		
				2,626	0.032		
				3,106	0.02		
				3,466	0.015		

TABLE B.1 CONTINUED

Station and Shot		Station and Shot		Station and Shot		Station and Shot	
YAG 40-B, No. 9 TE		YAG 40-B, No. 9 TE		YAG 40, No. 13 (Deck) TE		YAG 39-C, No. 9 TE	
H + hr	r/hr	H + hr	r/hr	H + hr	r/hr	H + hr	r/hr
4.35	0.0017	44.2	0.262	24.0	2.74	3.32	1.70
4.60	0.0057	46.2	0.207	25.0	2.64	3.37	1.88
4.73	0.0134	48.2	0.193	26.0	2.52	3.42	2.05
4.95	0.127	50.2	0.191	26.6	2.08	3.45	2.05
5.20	0.598	52.2	0.179	27.0	1.47	3.50	2.33
5.43	1.08	54.2	0.173	28.0	1.42	3.53	2.51
5.58	1.33	56.2	0.167	29.0	1.42	3.57	2.51
5.88	1.76	58.2	0.159	30.0	1.36	3.62	2.69
6.10	1.86	60.2	0.152	31.0	1.35	3.63	2.69
6.38	1.90	62.2	0.139	32.0	1.30	3.67	3.05
6.62	1.98	64.2	0.133	33.0	1.25	3.70	3.14
6.85	2.13	66.2	0.129	34.0	1.22	3.73	3.14
7.10	2.23	68.2	0.127	35.0	1.19	3.85	3.59
7.28	2.24	70.2	0.126	36.0	1.14	3.93	4.96
7.70	2.21	72.2	0.118	37.0	1.08	3.95	5.43
8.23	2.03	75.2	0.113	38.0	0.730	4.00	5.89
8.75	1.94			39.0	0.660	4.03	6.34
9.25	2.09	YAG 40, No. 13 (Deck) TE		40.0	0.588	4.10	6.72
9.75	1.89	H + hr	r/hr	41.0	0.572	4.13	7.28
10.3	1.85	4.48	0.0040	42.0	0.566	4.15	7.55
10.8	1.79	4.62	0.0097	43.0	0.512	4.20	7.55
11.2	1.80	4.75	0.0252	44.0	0.478	4.22	8.20
11.7	1.56	4.90	0.111	45.0	0.470	4.25	8.67
12.2	1.60	4.97	0.233	46.0	0.260	4.28	8.20
12.8	1.57	5.07	0.793	48.0	0.243	4.30	8.67
13.2	1.48	5.15	1.20	50.0	0.215	4.31	9.15
13.8	1.40	5.32	2.41	52.0	0.203	4.32	8.67
14.2	1.35	5.48	3.52	54.0	0.172	4.35	9.15
14.7	1.32	5.73	5.08	55.0	0.181	4.42	10.1
15.2	1.25	6.00	6.31	57.0	0.172	4.47	11.0
15.8	1.21	6.23	6.76	59.0	0.154	4.52	11.0
16.2	1.15	6.73	7.22	61.0	0.154	4.58	11.5
16.7	1.13	7.00	7.22	63.0	0.152	4.62	11.0
17.2	1.09	7.23	7.43	65.0	0.140	4.73	9.15
17.8	1.05	7.73	6.65	68.0	0.132	5.07	8.20
18.2	1.01	8.00	6.19	72.0	0.123	5.15	8.20
19.2	0.992	8.23	5.97	75.0	0.115	5.23	7.55
20.2	0.927	8.57	5.97			6.15	5.43
21.2	0.881	9.00	6.54	YAG 39-C, No. 9 TE		7.15	4.52
22.2	0.832	9.23	6.65	H + hr	r/hr	8.15	4.06
23.2	0.784	10.0	6.65	2.00	0.0017	9.15	3.59
24.2	0.770	11.0	6.65	2.20	0.0175	10.2	2.96
25.2	0.702	11.6	6.65	2.23	0.0308	11.2	2.70
26.2	0.670	12.0	6.54	2.28	0.0467	12.2	2.33
27.3	0.608	13.0	5.64	2.30	0.0591	13.2	2.15
28.2	0.596	14.0	5.42	2.33	0.0714	14.2	1.88
29.3	0.576	15.0	4.29	2.35	0.0837	15.2	1.70
30.2	0.568	16.0	3.97	2.37	0.109	16.2	1.52
31.2	0.554	17.0	3.84	2.70	0.514	17.2	1.30
32.2	0.527	18.0	3.52	2.85	0.728	18.1	1.13
33.4	0.439	19.0	3.29	2.97	0.906	19.2	1.07
34.1	0.432	20.0	3.18	3.05	1.08	20.2	0.995
35.3	0.415	21.0	3.08	3.13	1.29	21.1	0.942
36.1	0.403	22.0	2.96	3.20	1.41	22.1	0.888
38.4	0.339	23.0	2.86	3.27	1.60	24.2	0.763
40.4	0.307					26.2	0.594
42.2	0.292					28.2	0.505

TABLE B.1 CONTINUED

YAG 39 C, No. 9 TE	
H+hr	r/hr
30.1	0.465
32.2	0.461
34.2	0.412
36.2	0.381
38.3	0.376
40.1	0.310
42.2	0.292
44.0	0.290
48.0	0.243
50.1	0.238
53.2	0.215
56.2	0.192
60.1	0.171
63.9	0.158
66.2	0.151
70.5	0.139
72.4	0.136
74.4	0.131
76.4	0.123
78.6	0.113
79.4	0.113

YAG 39, No. 13 (Deck) TE	
H + hr	r/hr
1.30	0.0002
2.10	0.0082
2.23	0.0479
2.32	0.138
2.35	0.172
2.38	0.263
2.57	0.691
2.73	1.55
3.00	2.81
3.23	4.41
3.32	5.31
3.57	8.02
4.00	13.6
4.07	14.5
4.32	18.4
4.57	19.3
5.00	20.2
5.57	18.7
6.00	16.9
6.57	15.5
7.00	14.5
7.57	13.4
8.57	12.7
9.00	11.7
9.57	10.8
10.0	9.83
10.6	8.96
11.0	8.96
12.0	8.49
13.0	7.12
14.0	6.19
15.0	5.84
16.0	5.84
17.0	5.13
18.0	4.85

YAG 39, No. 13 (Deck) TE	
H+hr	r/hr
20.0	3.88
21.0	3.61
22.0	3.52
23.0	3.52
24.0	3.07
25.0	2.98
26.0	2.90
27.0	2.36
28.0	2.28
29.1	2.19
30.1	2.10
31.0	2.10
32.1	1.92
33.1	1.84
34.0	1.75
35.0	1.49
36.0	1.44
37.1	1.36
38.1	1.37
39.0	1.09
40.0	1.04
41.0	1.00
42.0	0.972
42.9	0.955
45.0	0.894
47.2	0.886
49.0	0.825
51.0	0.799
53.0	0.772
55.0	0.711
57.0	0.659
59.0	0.642
61.0	0.616
63.1	0.564
64.9	0.555
66.0	0.529
67.0	0.516
69.0	0.499
71.0	0.485
73.0	0.459
75.0	0.451
77.0	0.424
79.0	0.376
80.2	0.374

LST 611-D, No. 1 TE	
H + hr	r/hr
7.18	0.002
7.23	0.0033
7.73	0.024
8.23	0.019
8.65	0.027
8.95	0.048
9.28	0.082
9.51	0.10
9.78	0.12
10.0	0.12
10.28	0.13
10.48	0.17

LST 611-D, No. 1 TE	
H+hr	r/hr
10.73	0.24
10.98	0.18
11.23	0.182
11.73	0.187
12.23	0.198
12.35	0.205
12.98	0.224
13.56	0.256
14.23	0.247
14.85	0.236
15.48	0.215
21.11	0.146
24.23	0.112
31.73	0.085
34.48	0.066
38.48	0.054
40.48	0.051

YFNB 13-E TE	
H+min	r/hr
18	0.0056
26	0.013
30	0.021
32	0.022
35	0.020
36	0.025
37	0.019
40	0.018
43	0.020
46	0.022
50	0.030
61	0.090
71	0.20
81	0.52
91	1.11
101	1.87
111	2.13
114	2.34
116	2.5
118	2.34
123	2.21
177	2.25
204	1.9
309	1.0
429	0.7
909	0.30
1,269	0.15
1,500	0.12
2,109	0.076
3,069	0.042
3,309	0.016
3,549	0.009
3,789	0.0085
4,029	0.0081
4,509	0.0072

How F TE	
H+min	r/hr
101	0.0069
107	0.016
109	0.024
112	0.032
113	0.036
115	0.041
116	0.044
117	0.051
118	0.060
119	0.064
128	0.101
142	0.15
149	0.19
152	0.20
173	0.22
195	0.21
221	0.19
251	0.173
341	0.11
401	0.092
599	0.061
749	0.051
899	0.042
1,289	0.029
1,589	0.024
1,889	0.021

YFNB 29-H TE	
H+min	r/hr
1	0.00056
3	0.00046
14	0.0016
16	0.015
20	0.047
22	0.30
24	0.60
25	0.80
26	0.90
28	2.0
34	3.8
38	7.4
44	10.0
49	13.2
490	9.9
670	7.1
730	6.9
850	6.3
920	5.9
970	5.3
1,300	3.5
2,000	1.9
3,000	1.14
3,200	0.72

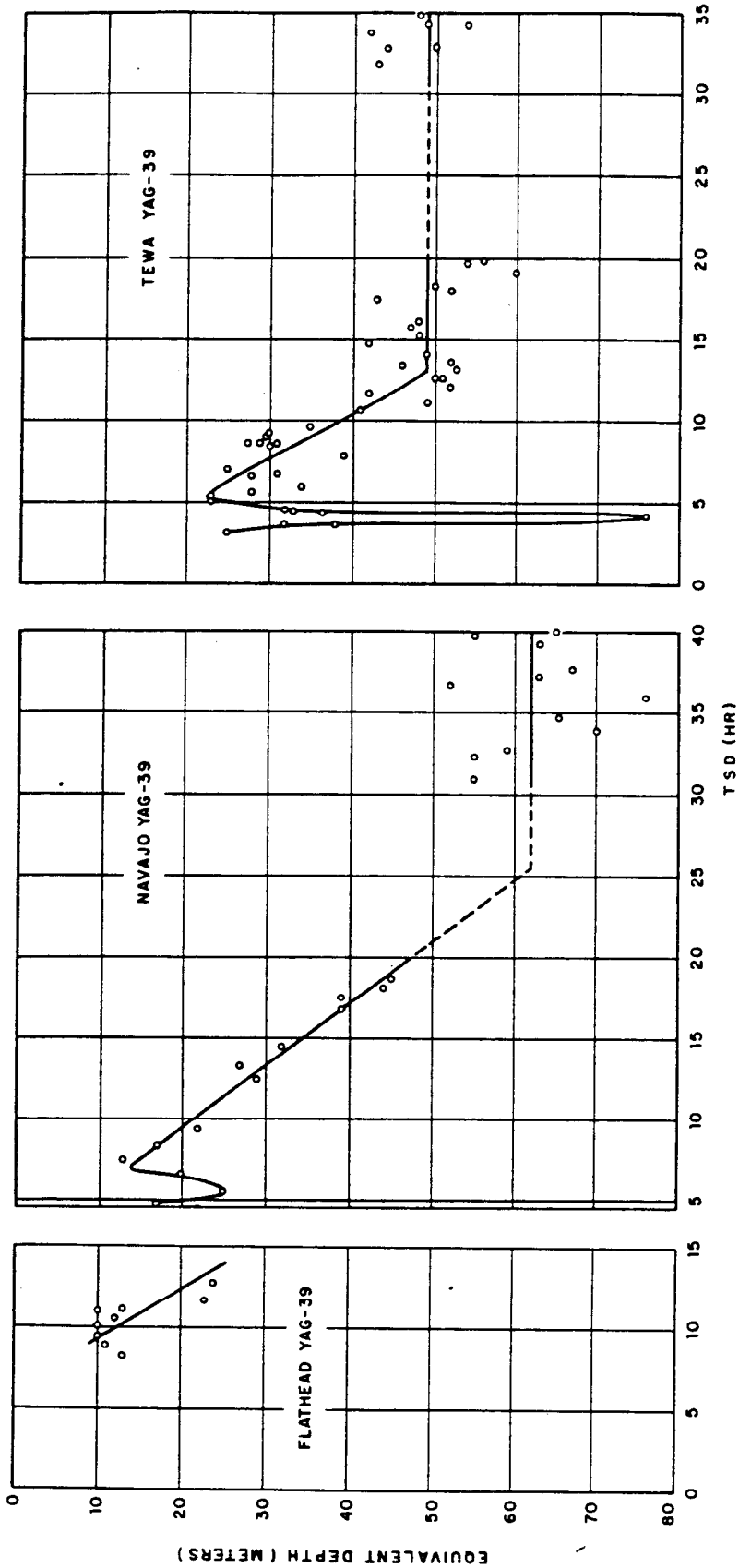

Figure B.1 Ocean-penetration rates, Shots Flathead, Navajo, and Tewa.

TABLE B.8 WEIGHT, ACTIVITY, AND FISSION VALUES FOR SIZED FRACTIONS FROM WHIM SAMPLE YFNB 29 ZU

Size Range	Weight		CIC Assay *			Fissions	
	Grams	Percent of Total	Value at H + 262 hr	Percent of Total	Specific Activity	Total	Per Gram
microns			10^{-5} ma		10^{-5} ma/gm	10^{14}	10^{14}
1,000	37.70	41.8	1.08	15.8	0.0286	21.	0.56
500 to 1,000	41.91	46.4	3.14	46.0	0.0749	60.	1.4
250 to 500	4.97	5.5	1.35	19.8	0.272	26.	5.2
100 to 250	3.51	3.9	0.734	10.7	0.209	14.	4.0
50 to 100	0.80	0.9	0.155	2.3	0.194	3.0	3.8
50	1.38	1.5	0.371	5.4	0.269	7.1	5.1
Total	90.27		6.83		0.0757	131.	1.5

* Response to 100 μg of Ra = 588 × 10^{-8} ma

PAGE 208 DELETED

TABLE B.11 TOTAL ACTIVITY AND MASS OF SLURRY FALLOUT

Collecting Station	Shot Flathead			Shot Navajo		
	Total Activity * (counts/min)/ft^2 × 10^8	Total Mass NaCl μg/ft^2	Total Number Droplets number/ft^2	Total Activity * (counts/min)/ft^2 × 10^8	Total Mass NaCl μg/ft^2	Total Number Droplets number/ft^2
YFNB 13-E-57	†	—	—	51.0	125,000	16,000
YFNB 29-H-78	45.9	10,700	178,000	3.6	9,000	1,150
YAG 39-C-20	8.4	300	714	21.2	13,200	1,740
YAG 39-C-24	1.6	57	135	†	—	—
LST 611-D-37	19.6	690	1,640	†	—	—
LST 611-D-50	2.6	92	219	†	—	—
YAG 40-A-1	13.1	460	489	9.2	4,400	15,000
YAG 40-A-2	11.5	410	436	†	—	—
YAG 40-B-7	6.5	230	460	†	—	—

* Photon count in well counter at H + 12 hours.

† Values unavailable due to instrument malfunction or incomplete sampling run.

TABLE B.19 AIR-IONIZATION RATES OF INDUCED PRODUCTS FOR 10^4 FISSIONS/FT^3, PRODUCT/FISSION RATIO OF UNITY (SC)

Product half life is given directly below the nuclide symbol. Values are in r/hr and the number in parentheses indicates the number of zeros between the decimal point and the first significant figure.

Age		Na^{24}	Cr^{51}	Mn^{54}	Mn^{56}	Fe^{59}	Co^{57}	Co^{58}	Co^{60}	Cu^{64}	Sb^{122}
	hr	15h	27.2d	304d	2.58h	45.2d	270d	72d	5.27y	12.8h	2.75d
45.8 minutes	0.763	(8)250	(12)539	(11)118	(8)547	(10)119	(12)218	(11)598	(12)575	(9)174	(10)740
1.12 hours	1.12	(8)246	(12)539	(11)118	(8)496	(10)119	(12)218	(11)598	(12)575	(9)171	(10)737
1.64	1.64	(8)240	(12)539	(11)118	(8)432	(10)118	(12)218	(11)598	(12)575	(9)166	(10)735
2.40	2.40	(8)232	(12)538	(11)118	(8)352	(10)118	(12)218	(11)598	(12)575	(9)160	(10)727
3.52	3.52	(8)220	(12)538	(11)118	(8)261	(10)118	(12)218	(11)597	(12)575	(9)150	(10)719
5.16	5.16	(8)204	(12)537	(11)118	(8)167	(10)118	(12)218	(11)597	(12)575	(9)137	(10)707
7.56	7.56	(8)182	(12)535	(11)118	(9)878	(10)118	(12)218	(11)597	(12)575	(9)121	(10)689
11.1	11.1	(8)155	(12)533	(11)118	(9)341	(10)118	(12)218	(11)596	(12)575	(10)997	(10)666
16.2	16.2	(8)123	(12)531	(11)118	(10)865	(10)117	(12)218	(11)594	(12)575	(10)756	(10)630
23.8	23.8	(9)887	(12)526	(11)118	(10)112	(10)117	(12)218	(11)592	(12)575	(10)502	(10)581
1.45 days	34.8	(9)524	(12)520	(11)118	(12)583	(10)116	(12)217	(11)590	(12)575	(10)277	(10)517
2.13	51.1	(9)244	(12)511	(11)118	(14)751	(10)115	(12)217	(11)586	(12)575	(10)115	(10)438
3.12	74.9	(10)823	(12)498	(11)118	(16)126	(10)113	(12)217	(11)580	(12)575	(11)319	(10)340
4.57	109.7	(10)166	(12)480	(11)117		(10)111	(12)216	(11)572	(12)574	(12)488	(10)236
6.70	160.8	(11)156	(12)455	(11)117		(10)107	(12)215	(11)561	(12)574	(13)309	(10)138
9.82	235.7	(13)478	(12)420	(11)116		(10)102	(12)213	(11)545	(12)573	(15)554	(11)630
14.4	345.6	(15)321	(12)374	(11)115		(11)951	(12)210	(11)521	(12)572	(17)138	(11)198
21.1	506.4		(12)315	(11)113		(11)858	(12)207	(11)488	(12)571		(12)366
30.9	741.6		(12)246	(11)110		(11)738	(12)202	(11)444	(12)569		(13)310
45.3	1,087		(12)170	(11)107		(11)592	(12)194	(11)387	(12)566		(15)837
66.4	1,594		(13)994	(11)102		(11)428	(12)184	(11)315	(12)562		(17)399
97.3	2,335		(13)452	(12)949		(11)267	(12)170	(11)235	(12)556		
143	3,432		(13)141	(12)855		(11)132	(12)151	(11)151	(12)547		
208	4,992		(14)272	(12)738		(12)488	(12)128	(12)808	(12)534		
301	7,224		(15)252	(12)596		(12)117	(12)101	(12)330	(12)516		

TABLE B.19 CONTINUED

Age		Sb^{124}	Ta^{180}	Ta^{182}	Au^{198}	Pb^{203}	U^{237}	U^{239}	Np^{239}	Np^{240}
	hr	60d	8.15h	114d	2.7d	52h	6.75d	23.5m	56h	7.3m
45.8 minutes	0.763	(10)133	(10)703	(11)513	(10)711	(10)501	(10)126	(9)507	(10)258	(9)290
1.12 hours	1.12	(10)133	(10)684	(11)513	(10)709	(10)500	(10)125	(9)270	(10)300	(9)287
1.64	1.64	(10)133	(10)652	(11)513	(10)704	(10)496	(10)125	(9)107	(10)326	(9)281
2.40	2.40	(10)133	(10)614	(11)513	(10)699	(10)490	(10)125	(10)280	(10)338	(9)270
3.52	3.52	(10)133	(10)557	(11)513	(10)689	(10)484	(10)124	(11)386	(10)337	(9)256
5.16	5.16	(10)132	(10)484	(11)513	(10)677	(10)474	(10)123	(12)212	(10)332	(9)236
7.56	7.56	(10)132	(10)394	(11)513	(10)660	(10)459	(10)122	(14)301	(10)321	(9)210
11.1	11.1	(10)132	(10)292	(11)512	(10)636	(10)437	(10)120	(17)577	(10)308	(9)176
16.2	16.2	(10)132	(10)190	(11)511	(10)603	(10)408	(10)118		(10)289	(9)137
23.8	23.8	(10)131	(11)992	(11)510	(10)554	(10)370	(10)113		(10)263	(10)944
1.45 days	34.8	(10)131	(11)388	(11)509	(10)494	(10)319	(10)108		(10)230	(10)550
2.13	51.1	(10)130	(12)973	(11)507	(10)415	(10)256	(10)101		(10)188	(10)248
3.12	74.9	(10)128	(12)129	(11)504	(10)321	(10)186	(11)914		(10)140	(11)767
4.57	109.7	(10)126	(14)668	(11)499	(10)221	(10)118	(11)789		(11)909	(11)139
6.70	160.8	(10)123	(16)872	(11)493	(10)128	(11)595	(11)634		(11)482	(12)113
9.82	235.7	(10)119	(18)149	(11)484	(11)576	(11)219	(11)458		(11)191	(14)290
14.4	345.6	(10)112		(11)470	(11)178	(12)507	(11)287		(12)491	(16)126
21.1	506.4	(10)104		(11)452	(12)318	(13)594	(11)143		(13)670	
30.9	741.6	(11)929		(11)426	(13)258	(14)259	(12)529		(14)364	
45.3	1,087	(11)786		(11)390	(15)643	(16)256	(12)121		(16)509	
66.4	1,594	(11)616		(11)343	(17)277	(19)304	(13)137		(19)954	
97.3	2,335	(11)431		(11)284	(21)995		(15)578			
143	3,432	(11)254		(11)215			(17)520			
208	4,992	(11)120		(11)145			(20)742			
301	7,224	(12)410		(12)825						

TABLE B.21 GAMMA-RAY PROPERTIES OF CLOUD AND FALLOUT SAMPLES BASED ON GAMMA-RAY SPECTROMETRY (NRB)

Cloud samples are particulate collections in small pieces of filter paper. All fallout samples are aliquots of OCC sample solutions except those indicated as solid, which are aliquoted undissolved, by weight.

Sample Designation	Age	Number of Fissions	Average Energy $\bar{E}$	mr/hr at 3 ft, (SC), for N_f fissions/ft²			Total Photons per sec	Photons/sec 10^6 fission
				By Line E	By $\bar{E}$	Error Using $\bar{E}$		
	hr	N_f	kev			pct	$\times 10^6$	
Shot Cherokee								
Standard cloud sample								
1	53	8.82×10^{12}	294	20.64	21.15	2.47	11.62	1.317
2	74		299	17.18	17.66	2.79	9.65	1.094
3	98		310	11.94	12.15	1.76	6.53	0.740
4	166		337	7.88	8.36	6.09	4.04	0.458
5	191		379	6.36	6.87	8.02	2.91	0.330
6	215		391	5.82	6.24	7.22	2.59	0.294
7	242		417	5.00	5.40	8.00	2.10	0.238
8	262.5		446	4.44	4.81	8.33	1.75	0.198
9	335		490	3.46	3.81	10.12	1.26	0.143
10	405.5		509	2.85	3.10	8.77	0.99	0.112
11	597.5		626	1.82	1.98	8.79	0.52	0.059
Shot Zuni								
Standand cloud sample								
1	53	9.84×10^{12}	477	62.47	67.36	7.83	22.98	2.335
2	69		413	49.92	52.89	5.95	20.82	2.116
3	93		422	37.90	39.64	4.59	15.28	1.553
4	117		433	28.45	30.12	5.87	11.31	1.149
5	192		437	16.71	17.78	6.40	6.62	0.673
6	242		485	13.05	14.03	7.51	4.71	0.479
7	454		589	6.28	6.84	8.92	1.90	0.193
8	790		624	3.29	3.52	6.99	0.93	0.095
9	1,295		559	1.56	1.65	6.45	0.48	0.049
How F-61								
1	240	1.00×10^{13}	210	1.72	1.73	0.58	1.34	0.134
2	460		247	0.64	0.65	1.56	0.43	0.043
YAG 40-B-19								
2	266	3.71×10^{14}	419	181.18	193.33	6.71	74.98	0.202
3	362	(solid)	480	110.18	119.14	8.13	40.4	0.109
4	459		508	105.62	113.95	7.89	36.29	0.098
5	790		606	51.07	54.87	7.44	14.83	0.040
6	983		731	53.46	56.63	5.93	12.87	0.035
6'	987		706	49.24	51.89	5.38	12.21	0.033
7	1,298		710	38.09	40.91	7.40	9.58	0.026
8	1,728.5		706	28.41	30.05	5.77	7.07	0.019
9	2,568.5		711	18.85	19.60	3.98	4.60	0.012
10	2,810		731	14.50	16.02	10.48	3.65	0.010
How F-67								
1	359	7.29×10^{13}	318	10.66	11.38	6.75	5.82	0.080
2	460.5	(solid)	385	8.31	8.73	5.05	3.69	0.051
3	981		610	4.38	4.53	3.42	1.20	0.016
4	1,606		646	3.54	3.64	2.82	0.93	0.013
YAG 40-B-6								
1	383	5.08×10^{13}	444.76	12.92	13.79	6.73	5.05	0.10
2	458		457.16	9.43	10.07	6.79	3.58	0.070
3	982		656.58	4.49	4.76	6.01	1.2	0.024
4	1,605		695.12	3.47	3.60	3.75	0.86	0.017

pgs 235 thru 236 Deleted

TABLE B. 21 CONTINUED

Sample Designation	Age	Number of Fissions	Average Energy $\bar{E}$	mr/hr at 3 ft, (SC), for N_f fissions/ft^2			Total Photons per sec	Photons/sec / 10^6 fissions
				By Line E	By $\bar{E}$	Error Using $\bar{E}$		
	hr	N_f	kev			pct	$\times 10^6$	
Shot Flathead								
Standard cloud sample								
2	96.5	2.79×10^{13}	335.88	61.12	62.88	2.88	30.49	1.093
3	195	↓	402.04	27.94	29.18	4.44	11.82	0.424
4	262		489.13	18.94	20.36	7.50	6.44	0.231
5	334		535.96	16.31	17.73	8.39	5.39	0.193
6	435		573.61	11.06	12.01	8.59	3.43	0.123
7	718		661.49	6.08	6.56	7.89	1.64	0.059
8	1,031		708.63	3.16	3.42	8.23	0.80	0.029
9	1,558		678.61	2.08	2.21	6.25	0.54	0.019
YAG 39-C-36								
1	119.5	1.06×10^{13} *	306.28	14.77	15.20	2.91	8.08	0.762
2	598	(solid)	532.08	1.99	2.17	9.05	0.65	0.061
YFNB 13-E-56								
1	337	4.44×10^{12}	515.74	13.38	14.52	8.52	4.58	0.103
2	722	(solid)	659.93	5.96	6.38	7.05	1.60	0.036
3	1,032	↓	681.15	3.71	3.95	6.47	0.96	0.022
4	1,538		699.09	1.77	1.85	4.52	0.44	0.010
YFNB 13-E-54								
1	357	3.81×10^{13}	389.11	12.41	13.52	8.94	5.66	0.149
2	720	↓	549.26	5.08	5.51	8.46	1.64	0.043
3	1,034.5		672.88	3.55	3.73	5.07	0.92	0.024
4	1,538.5		662.90	1.94	2.00	3.09	0.50	0.013
Shot Navajo								
Standard cloud sample								
1	51.5	3.46×10^{12}	567.68	20.50	22.97	12.05	6.62	1.913
2	69	↓	483.11	13.32	14.65	9.98	4.94	1.428
3	141		396.37	5.00	5.31	6.70	2.18	0.630
4	191		482.27	4.84	5.18	7.02	1.75	0.506
5	315		604.29	2.13	2.32	8.92	0.63	0.182
6	645.5		585.68	0.72	0.78	8.33	0.22	0.064
YFNB 13-E-54								
1	197	2.40×10^{13}	496.15	9.34	9.96	6.63	3.27	0.136
3	311	(solid)	658.79	8.15	8.74	7.24	2.19	0.091
4	360	↓	710.86	8.36	8.92	6.70	2.09	0.087
5	551		818.31	5.69	6.01	5.62	1.24	0.052
YAG 39-C-36								
1	216	—	436.11	1.92	2.05	6.77	0.76	—
2	260	—	549.03	0.99	1.04	5.05	0.31	—
YFNB 13-E-66								
1	237.5	6.50×10^{12}	518.87	4.40	4.75	7.95	1.49	0.229
2	359	↓	676.86	2.98	3.21	7.72	0.78	0.120
3	551		688.41	1.58	1.70	7.59	0.41	0.063
YAG 39-C-21	309.5	3.90×10^{12}	604.65	1.96	2.10	7.14	0.57	0.146

TABLE B. 21 CONTINUED

Sample Designation	Age	Number of Fissions	Average Energy $\bar{E}$	mr/hr at 3 ft, (SC), for N_f fissions/ft^2			Total Photons per sec	Photons/sec / 10^6 fission
				By Line E	By $\bar{E}$	Error Using $\bar{E}$		
	hr	N_f	kev			pct	$\times 10^6$	
Shot Tewa								
Standard cloud sample								
1	71.5	4.71×10^{13}	401.33	127.1	131.64	3.57	53.42	1.134
2	93.5		378.45	94.25	97.60	3.55	42.00	0.892
3	117.0		377.50	75.64	79.29	4.83	34.21	0.726
4	165.0		373.02	62.27	65.71	5.52	28.69	0.609
5	240.5		460.73	44.21	47.38	7.17	16.75	0.356
6	333.5		489.33	24.88	27.01	8.56	8.99	0.191
7	429.0		548.48	18.47	20.16	9.15	6.00	0.127
8	578.5		629.64	12.70	13.83	8.90	3.62	0.077
9	765.5		664.50	10.40	11.18	7.50	2.78	0.059
10	1,269.0		646.80	4.94	5.21	5.47	1.33	0.028
11	1,511.0		656.33	4.13	4.33	4.84	1.09	0.023
YAG 39-C-36								
1	173.0	1.77×10^{13}	345.84	16.78	17.41	3.75	8.2	0.463
2	237.0	(solid)	355.39	12.27	12.81	4.40	5.87	0.332
3	312.0		397.60	7.99	8.42	5.38	3.45	0.195
4	407.0		416.92	5.69	6.04	6.15	2.36	0.133
5	576.0		571.65	3.95	4.22	6.84	1.21	0.068
YFNB 13-E-56								
1	238	3.40×10^{13}	270.06	11.84	12.24	3.38	7.38	0.217
2	335	(solid)	295.56	7.16	7.46	4.19	4.11	0.121
3	413		327.78	4.85	5.07	4.54	2.52	0.074
4	578		434.03	3.82	4.00	4.71	1.50	0.044
5	1,270		542.00	1.64	1.67	1.83	0.50	0.015
6	1,512		563.09	1.16	1.17	0.86	0.34	0.010
Y3-T-1C-D	243	—	360.31	1.01	1.06	4.95	0.48	—
YFNB 13-E-54								
1	263	2.38×10^{13}	306.39	6.87	7.21	4.95	3.83	0.161
2	316		330.48	4.61	4.85	5.21	2.39	0.100
3	408.5		373.45	3.49	3.71	6.30	1.62	0.068
4	624.0		484.14	1.76	1.90	7.95	0.64	0.027
YAG 39-C-21								
1	287	1.82×10^{14}	427.26	68.72	73.34	6.72	27.96	0.154
3	411		465.32	40.67	43.65	7.33	15.28	0.084
4	626		564.53	23.70	25.53	7.72	7.40	0.041
5	767		605.21	17.33	18.66	7.67	5.07	0.028
6	1,271		672.61	9.75	10.18	4.21	2.51	0.014
7	1,513		669.95	7.83	8.08	3.19	2.00	0.011

TABLE B.22 COMPUTED DOGHOUSE DECAY RATES OF FALLOUT AND CLOUD SAMPLES

Activities are computed in units of (counts/sec)/10^4 fissions for a point source in a covered OCC tray on the floor of the counter. The product/fission ratio for the induced product activities (IP) appears directly below the nuclide symbol. Induced activities are summed and added to the fission product activity (FP) for the total computed count rate. Numbers in parentheses denote the number of zeros between the decimal point and the first significant figure, e.g., (3)291 = 0.000291.

Age		Na^{24}	Cr^{51}	Mn^{54}	Mn^{56}	Fe^{59}	Co^{57}	Co^{58}	Co^{60}	Cu^{64}	Sb^{122}	Sb^{124}
	hr	0.0109	0.00173	0.011	0.011 *	0.00041	0.0031	0.0036	0.00264	0.0090	0.0252 †	0.0084
Shot Zuni, Average Lagoon-Area Composition:												
45.8 min	0.763	(6)119	(10)419	(9)175	(6)544	(10)401	(10)921	(9)319	(10)111	(7)356	(7)335	(8)123
1.12 hrs	1.12	(6)117	(10)419	(9)175	(6)494	(10)401	(10)921	(9)319	(10)111	(7)347	(7)335	(8)123
1.64 hrs	1.64	(6)114	(10)419	(9)175	(6)430	(10)401	(10)920	(9)319	(10)111	(7)338	(7)333	(8)123
2.40 hrs	2.40	(6)110	(10)419	(9)175	(6)351	(10)400	(10)920	(9)319	(10)111	(7)326	(7)330	(8)123
3.52 hrs	3.52	(6)105	(10)419	(9)175	(6)260	(10)400	(10)920	(9)318	(10)111	(7)306	(7)328	(8)123
5.16 hrs	5.16	(7)970	(10)417	(9)175	(6)166	(10)400	(10)920	(9)318	(10)111	(7)280	(7)320	(8)123
7.56 hrs	7.56	(7)868	(10)415	(9)175	(7)874	(10)399	(10)920	(9)318	(10)111	(7)246	(7)312	(8)122
11.1 hrs	11.1	(7)738	(10)415	(9)175	(7)340	(10)398	(10)919	(9)318	(10)111	(7)203	(7)302	(8)122
16.2 hrs	16.2	(7)583	(10)412	(9)175	(8)861	(10)397	(10)919	(9)317	(10)111	(7)154	(7)285	(8)122
23.8 hrs	23.8	(7)409	(10)408	(9)175	(8)112	(10)395	(10)919	(9)316	(10)111	(7)103	(7)265	(8)121
1.45 days	34.8	(7)249	(10)405	(9)175	(10)581	(10)392	(10)917	(9)314	(10)111	(8)564	(7)235	(8)121
2.13 days	51.1	(7)117	(10)398	(9)175	(12)748	(10)388	(10)916	(9)312	(10)111	(8)234	(7)199	(8)120
3.12 days	74.9	(8)391	(10)388	(9)174		(10)382	(10)913	(9)309	(10)111	(9)651	(7)154	(8)118
4.57 days	109.7	(9)787	(10)374	(9)174		(10)374	(10)910	(9)305	(10)111	(10)936	(7)107	(8)116
6.70 days	160.8	(10)743	(10)353	(9)173		(10)362	(10)905	(9)299	(10)110	(11)629	(8)625	(8)113
9.82 days	235.7	(11)228	(10)327	(9)172		(10)345	(10)898	(9)290	(10)110	(12)112	(8)285	(8)109
14.4 days	345.6		(10)291	(9)169		(10)321	(10)887	(9)278	(10)110		(9)897	(8)104
21.1 days	506.4		(10)246	(9)167		(10)290	(10)872	(9)260	(10)110		(9)166	(9)958
30.9 days	741.6		(10)190	(9)164		(10)250	(10)851	(9)237	(10)109		(10)141	(9)857
45.3 days	1,087		(10)132	(9)158		(10)200	(10)820	(9)206	(10)109		(12)381	(9)727
66.4 days	1,594		(11)772	(9)151		(10)145	(10)777	(9)168	(10)108			(9)569
97.3 days	2,335		(11)351	(9)141		(11)902	(10)717	(9)125	(10)107			(9)398
143 days	3,432		(11)110	(9)126		(11)447	(10)638	(10)803	(10)105			(9)235
208 days	4,992		(12)211	(9)109		(11)165	(10)540	(10)432	(10)102			(9)111
301 days	7,224		(13)195	(10)882		(12)398	(10)425	(10)176	(11)990			(10)379

TABLE B.22 CONTINUED

Age	hr	Ta^{180} 0.0691‡	Ta^{182} 0.0326	Pb^{203} 0.050	Sum of FP
Shot Zuni, Average Lagoon-Area Composition					
45.8 min	0.763	(6)871	(8)355	(6)170	(4)6034
1.12 hrs	1.12	(6)850	(8)355	(6)170	(4)3946
1.64 hrs	1.64	(6)808	(8)355	(6)168	(4)2429
2.40 hrs	2.40	(6)760	(8)355	(6)167	(4)1469
3.52 hrs	3.52	(6)690	(8)355	(6)164	(5)8828
5.16 hrs	5.16	(6)599	(8)355	(6)161	(5)5243
7.56 hrs	7.56	(6)489	(8)355	(6)156	(5)3248
11.1 hrs	11.1	(6)362	(8)355	(6)148	(5)2210
16.2 hrs	16.2	(6)235	(8)355	(6)139	(5)1519
23.8 hrs	23.8	(6)123	(8)352	(6)126	(6)9903
1.45 days	34.8	(7)481	(8)352	(6)108	(6)5959
2.13 days	51.1	(7)121	(8)352	(7)870	(6)3336
3.12 days	74.9	(8)160	(8)349	(7)635	(6)1879
4.57 days	109.7	(10)829	(8)346	(7)400	(6)1133
6.70 days	160.8	(11)108	(8)342	(7)202	(7)6834
9.82 days	235.7		(8)336	(8)745	(7)4159
14.4 days	345.6		(8)326	(8)172	(7)2598
21.1 days	506.4		(8)313	(9)202	(7)1749
30.9 days	741.6		(8)295	(11)880	(7)1249
45.3 days	1,087		(8)270	(13)850	(8)9022
66.4 days	1,594		(8)238		(8)6424
97.3 days	2,335		(8)197		(8)4413
143 days	3,432		(8)149		(8)2726
208 days	4,992		(8)100		(8)1401
301 days	7,224		(9)570		(9)5868

TABLE B. 22 CONTINUED

Age		Na^{24}	Cr^{51}	Mn^{54}	Mn^{56}	Fe^{59}	Co^{57}	Co^{58}	Co^{60}	Cu^{64}	Sb^{122}	Sb^{124}
	hr	0. 0109	0. 00173	0. 011	0. 011*	0. 00041	0. 0031	0. 0036	0. 00264	0. 0090	0. 219	0. 073
Shot Zuni, Cloud Composition:												
45. 8 min	0. 763	(6)119	(10)419	(9)175	(6)544	(10)401	(10)921	(9)319	(10)111	(7)356	(6)291	(7)107
1. 12 hrs	1. 12	(6)117	(10)419	(9)175	(6)494	(10)401	(10)921	(9)319	(10)111	(7)347	(6)291	(7)107
1. 64 hrs	1. 64	(6)114	(10)419	(9)175	(6)430	(10)401	(10)920	(9)319	(10)111	(7)338	(6)289	(7)107
2. 40 hrs	2. 40	(6)110	(10)419	(9)175	(6)351	(10)400	(10)920	(9)319	(10)111	(7)326	(6)287	(7)107
3. 52 hrs	3. 52	(6)105	(10)419	(9)175	(6)260	(10)400	(10)920	(9)318	(10)111	(7)306	(6)285	(7)107
5. 16 hrs	5. 16	(7)970	(10)417	(9)175	(6)166	(10)400	(10)920	(9)318	(10)111	(7)280	(6)278	(7)107
7. 56 hrs	7. 56	(7)868	(10)415	(9)175	(7)874	(10)399	(10)920	(9)318	(10)111	(7)246	(6)272	(7)106
11. 1 hrs	11. 1	(7)738	(10)415	(9)175	(7)340	(10)398	(10)919	(9)318	(10)111	(7)203	(6)263	(7)106
16. 2 hrs	16. 2	(7)583	(10)412	(9)175	(8)861	(10)397	(10)919	(9)317	(10)111	(7)154	(6)247	(7)106
23. 8 hrs	23. 8	(7)409	(10)408	(9)175	(8)112	(10)395	(10)919	(9)316	(10)111	(7)103	(6)230	(7)105
1. 45 days	34. 8	(7)249	(10)405	(9)175	(10)581	(10)392	(10)917	(9)314	(10)111	(8)564	(6)204	(7)105
2. 13 days	51. 1	(7)117	(10)398	(9)175	(12)748	(10)388	(10)916	(9)312	(10)111	(8)234	(6)173	(7)104
3. 12 days	74. 9	(8)391	(10)388	(9)174		(10)382	(10)913	(9)309	(10)111	(9)651	(6)134	(7)103
4. 57 days	109. 7	(9)787	(10)374	(9)174		(10)374	(10)910	(9)305	(10)111	(10)936	(7)931	(7)101
6. 70 days	160. 8	(10)743	(10)353	(9)173		(10)362	(10)905	(9)299	(10)110	(11)629	(7)543	(8)985
9. 82 days	235. 7	(11)228	(10)327	(9)172		(10)345	(10)898	(9)290	(10)110	(12)112	(7)247	(8)949
14. 4 days	345. 6		(10)291	(9)169		(10)321	(10)887	(9)278	(10)110		(8)780	(8)905
21. 1 days	506. 4		(10)246	(9)167		(10)290	(10)872	(9)260	(10)110		(8)144	(8)832
30. 9 days	741. 6		(10)190	(9)164		(10)250	(10)851	(9)237	(10)109		(9)122	(8)745
45. 3 days	1, 087		(10)132	(9)158		(10)200	(10)820	(9)206	(10)109		(11)331	(8)631
66. 4 days	1, 594		(11)772	(9)151		(10)145	(10)777	(9)168	(10)108		(13)162	(8)494
97. 3 days	2, 335		(11)351	(9)141		(11)902	(10)717	(9)125	(10)107			(8)346
143 days	3, 432		(11)110	(9)126		(11)447	(10)638	(10)803	(10)105			(8)204
208 days	4, 992		(12)211	(9)109		(11)165	(10)540	(10)432	(10)102			(9)964
301 days	7, 224		(13)195	(10)882		(12)396	(10)425	(10)176	(11)990			(9)329

TABLE B.22 CONTINUED

Age		Ta^{180}	Ta^{182}	Pb^{203}	Sum of FP
hr		0.0411	0.0194	0.050	
Shot Zuni, Cloud Composition:					
45.8	min	0.763	(6)518	(8)211	(6)170	(3)1658
1.12	hrs	1.12	(6)506	(8)211	(6)170	(3)1068
1.64	hrs	1.64	(6)481	(8)211	(6)168	(4)6723
2.40	hrs	2.40	(6)452	(8)211	(6)167	(4)4223
3.52	hrs	3.52	(6)411	(8)211	(6)164	(4)2706
5.16	hrs	5.16	(6)356	(8)211	(6)161	(4)1788
7.56	hrs	7.56	(6)291	(8)211	(6)156	(4)1221
11.1	hrs	11.1	(6)215	(8)211	(6)148	(5)8454
16.2	hrs	16.2	(6)140	(8)211	(6)139	(5)5677
23.8	hrs	23.8	(7)732	(8)210	(6)126	(5)3650
1.45	days	34.8	(7)286	(8)210	(6)108	(5)2302
2.13	days	51.1	(8)719	(8)210	(7)870	(5)1428
3.12	days	74.9	(9)949	(8)208	(7)635	(6)8938
4.57	days	109.7	(10)493	(8)206	(7)400	(6)5891
6.70	days	160.8	(12)641	(8)204	(7)202	(6)3971
9.82	days	235.7		(8)200	(8)745	(6)2667
14.4	days	345.6		(8)194	(8)172	(6)1728
21.1	days	506.4		(8)186	(9)202	(6)1073
30.9	days	741.6		(8)175	(11)880	(7)6306
45.3	days	1,087		(8)161	(13)850	(7)3421
66.4	days	1,594		(8)141		(7)1734
97.3	days	2,335		(8)117		(8)9067
143	days	3,432		(9)889		(8)1954
208	days	4,992		(9)596		(8)2502
301	days	7,224		(9)340		(8)1114

TABLE B.22 CONTINUED

Age		Na^{24}	Cr^{51}	Nm^{54}	Nm^{56}	Fe^{59}	Co^{57}	Co^{58}	Co^{60}	Cu^{64}	Ta^{180}
	hr	0.0314	0.0120	0.10	0.094	0.0033	0.00224	0.00193	0.0087	0.0278	0.038 ¶
Shot Navajo, Average Fallout Composition:											
45.8	min	0.763	(6)342	(9)290	(8)159	(5)465	(9)322	(10)665	(9)171	(10)364	(6)110	(6)479
1.12	hrs	1.12	(6)336	(9)290	(8)159	(5)422	(9)322	(10)665	(9)171	(10)364	(6)107	(6)467
1.64	hrs	1.64	(6)330	(9)290	(8)159	(5)368	(9)322	(10)665	(9)171	(10)364	(6)104	(6)445
2.40	hrs	2.40	(6)317	(9)290	(8)159	(5)300	(9)322	(10)665	(9)171	(10)364	(6)101	(6)418
3.52	hrs	3.52	(6)301	(9)290	(8)159	(5)222	(9)322	(10)665	(9)171	(10)364	(7)945	(6)380
5.16	hrs	5.16	(6)279	(9)289	(8)159	(5)142	(9)322	(10)665	(9)171	(10)364	(7)865	(6)329
7.56	hrs	7.56	(6)250	(9)288	(8)159	(6)747	(9)321	(10)665	(9)170	(10)364	(7)759	(6)269
11.1	hrs	11.1	(6)213	(9)288	(8)159	(6)290	(9)320	(10)664	(9)170	(10)364	(7)628	(6)199
16.2	hrs	16.2	(6)168	(9)286	(8)159	(7)736	(9)319	(10)664	(9)170	(10)364	(7)475	(6)129
23.8	hrs	23.8	(6)118	(9)283	(8)159	(8)959	(9)318	(10)664	(9)169	(10)364	(7)317	(7)676
1.45	days	34.8	(7)716	(9)281	(8)159	(9)496	(9)316	(10)663	(9)168	(10)364	(7)174	(7)264
2.13	days	51.1	(7)336	(9)276	(8)159	(11)639	(9)313	(10)662	(9)167	(10)364	(8)723	(8)665
3.12	days	74.9	(7)113	(9)269	(8)158		(9)308	(10)660	(9)166	(10)364	(8)201	(9)878
4.57	days	109.7	(8)227	(9)259	(8)158		(9)301	(10)658	(9)163	(10)364	(9)289	(10)456
6.70	days	160.8	(9)214	(9)245	(8)157		(9)291	(10)654	(9)160	(10)363	(10)194	(12)593
9.82	days	235.7	(11)656	(9)227	(8)156		(9)278	(10)649	(9)156	(10)363	(12)348	
14.4	days	345.6		(9)202	(8)154		(9)259	(10)641	(9)149	(10)362		
21.1	days	506.4		(9)170	(8)152		(9)233	(10)630	(9)140	(10)361		
30.9	days	741.6		(9)132	(8)149		(9)201	(10)615	(9)127	(10)360		
45.3	days	1,087		(10)918	(8)144		(9)161	(10)592	(9)111	(10)358		
66.4	days	1,594		(10)535	(8)137		(9)116	(10)561	(10)901	(10)355		
97.3	days	2,335		(10)244	(8)128		(10)726	(10)518	(10)670	(10)351		
143	days	3,432		(11)760	(8)115		(10)360	(10)461	(10)430	(10)345		
208	days	4,992		(11)146	(9)992		(10)133	(10)390	(10)232	(10)338		
301	days	7,224		(12)136	(9)802		(11)319	(10)307	(11)942	(10)326		

TABLE B.22 CONTINUED

Age		Ta^{182}	Pb^{203}	Sum of FP
	hr	0.038	0.0993	
Shot Navajo, Average Fallout Composition:				
45.8	min	0.763	(8)414	(6)644	(3)1171
1.12	hrs	1.12	(8)414	(6)642	(4)7727
1.64	hrs	1.64	(8)414	(6)636	(4)4870
2.40	hrs	2.40	(8)414	(6)631	(4)3015
3.52	hrs	3.52	(8)414	(6)621	(4)1868
5.16	hrs	5.16	(8)414	(6)608	(4)1175
7.56	hrs	7.56	(8)414	(6)598	(5)7600
11.1	hrs	11.1	(8)414	(6)560	(5)5065
16.2	hrs	16.2	(8)414	(6)524	(5)3337
23.8	hrs	23.8	(8)410	(6)475	(5)2124
1.45	days	34.8	(8)410	(6)408	(5)1326
2.13	days	51.1	(8)410	(6)329	(6)8054
3.12	days	74.9	(8)407	(6)239	(6)4914
4.57	days	109.7	(8)403	(6)151	(6)3154
6.70	days	160.8	(8)399	(7)762	(6)2061
9.82	days	235.7	(8)391	(7)281	(6)1353
14.4	days	345.6	(8)380	(8)652	(7)8691
21.1	days	506.4	(8)365	(9)762	(7)5473
30.9	days	741.6	(8)344	(10)332	(7)3355
45.3	days	1,087	(8)315		(7)1968
66.4	days	1,594	(8)277		(7)1126
97.3	days	2,335	(8)229		(8)6652
143	days	3,432	(8)174		(8)3877
208	days	4,992	(8)117		(8)1989
301	days	7,224	(9)665		(9)8710

TABLE B. 22 CONTINUED

Age		Na^{24}	Cu^{64}	Co^{57}	Co^{58}	Sum of F?
	hr	0. 00145	0. 00217	0. 0036	0. 0053	
Shot Flathead, Average Fallout Composition:						
45. 8 min	0. 763	(7)158	(8)857	(9)107	(9)470	(3)1171
1. 12 hrs	1. 12	(7)155	(8)838	(9)107	(9)470	(4)7727
1. 64 hrs	1. 64	(7)152	(8)814	(9)107	(9)469	(4)4870
2. 40 hrs	2. 40	(7)146	(8)786	(9)107	(9)469	(4)3015
3. 52 hrs	3. 52	(7)139	(8)738	(9)107	(9)469	(4)1868
5. 16 hrs	5. 16	(7)129	(8)675	(9)107	(9)469	(4)1175
7. 56 hrs	7. 56	(7)115	(8)592	(9)107	(9)468	(5)7600
11. 1 hrs	11. 1	(8)982	(8)490	(9)107	(9)467	(5)5065
16. 2 hrs	16. 2	(8)776	(8)371	(9)107	(9)466	(5)3337
23. 8 hrs	23. 8	(8)544	(8)247	(9)107	(9)465	(5)2124
1. 45 days	34. 8	(8)331	(8)136	(9)107	(9)463	(5)1326
2. 13 days	51. 1	(8)155	(9)564	(9)106	(9)460	(6)8054
3. 12 days	74. 9	(9)521	(9)157	(9)106	(9)455	(6)4914
4. 57 days	109. 7	(9)105	(10)226	(9)106	(9)449	(6)3154
6. 70 days	160. 8	(11)989	(11)152	(9)105	(9)440	(6)2061
9. 82 days	235. 7	(12)303	(13)271	(9)104	(9)427	(6)1353
14. 4 days	345. 6			(9)103	(9)409	(7)8691
21. 1 days	506. 4			(9)101	(9)383	(7)5473
30. 9 days	741. 6			(10)988	(9)349	(7)3355
45. 3 days	1, 087			(10)952	(9)304	(7)1968
66. 4 days	1, 594			(10)902	(9)248	(7)1126
97. 3 days	2, 335			(10)833	(9)184	(8)6652
143 days	3, 432			(10)741	(9)118	(8)3877
208 days	4, 992			(10)627	(10)636	(8)1989
301 days	7, 224			(10)494	(10)259	(9)8710

TABLE B.22 CONTINUED

Age		Na^{24}	Cr^{51}	Mn^{54}	Fe^{59}	Co^{57}	Co^{58}	Co^{60}	Cu^{64}	Ta^{182}
	hr	(2)284	(3)297	(3)53	(3)167	(3)182	(3)289	(3)81	(2)228	(2)6
Shot Tewa, Average Lagoon-Area Composition:										
45.8 min	0.763	(7)310	(11)719	(11)843	(10)163	(11)541	(10)256	(11)339	(8)901	(9)654
1.12 hrs	1.12	(7)304	(11)719	(11)843	(10)163	(11)541	(10)256	(11)339	(8)880	(9)654
1.64 hrs	1.64	(7)298	(11)719	(11)843	(10)163	(11)540	(10)256	(11)339	(8)855	(9)654
2.40 hrs	2.40	(7)287	(11)719	(11)843	(10)163	(11)540	(10)256	(11)339	(8)825	(9)654
3.52 hrs	3.52	(7)273	(11)719	(11)843	(10)163	(11)540	(10)255	(11)339	(8)775	(9)654
5.16 hrs	5.16	(7)253	(11)716	(11)843	(10)163	(11)540	(10)255	(11)339	(8)709	(9)654
7.56 hrs	7.56	(7)226	(11)713	(11)843	(10)162	(11)540	(10)255	(11)339	(8)622	(9)654
11.1 hrs	11.1	(7)192	(11)713	(11)843	(10)162	(11)540	(10)255	(11)339	(8)515	(9)654
16.2 hrs	16.2	(7)152	(11)707	(11)843	(10)162	(11)540	(10)254	(11)339	(8)390	(9)654
23.8 hrs	23.8	(7)106	(11)701	(11)843	(10)161	(11)539	(10)253	(11)339	(8)260	(9)648
1.45 days	34.8	(8)648	(11)695	(11)843	(10)160	(11)539	(10)252	(11)339	(8)143	(9)648
2.13 days	51.1	(8)304	(11)683	(11)843	(10)158	(11)538	(10)251	(11)339	(9)593	(9)648
3.12 days	74.9	(8)102	(11)665	(11)837	(10)156	(11)536	(10)248	(11)339	(9)165	(9)642
4.57 days	109.7	(9)205	(11)642	(11)837	(10)152	(11)534	(10)245	(11)339	(10)237	(9)636
6.70 days	160.8	(10)194	(11)606	(11)832	(10)147	(11)531	(10)240	(11)338	(11)159	(9)630
9.82 days	235.7	(12)594	(11)561	(11)827	(10)140	(11)527	(10)233	(11)338	(13)285	(9)618
14.4 days	345.6		(11)499	(11)816	(10)131	(11)521	(10)223	(11)337		(9)600
21.1 days	506.4		(11)422	(11)806	(10)118	(11)512	(10)209	(11)336		(9)576
30.9 days	741.6		(11)327	(11)790	(10)102	(11)499	(10)190	(11)335		(9)542
45.3 days	1,087		(11)227	(11)763	(11)815	(11)481	(10)166	(11)333		(9)497
66.4 days	1,594		(11)132	(11)726	(11)590	(11)456	(10)135	(11)330		(9)437
97.3 days	2,335		(12)603	(11)678	(11)367	(11)421	(10)100	(11)327		(9)362
143 days	3,432		(12)188	(11)610	(11)182	(11)374	(11)644	(11)322		(9)275
208 days	4,992		(13)362	(11)526	(12)673	(11)317	(11)347	(11)314		(9)184
301 days	7,224		(14)336	(11)425	(12)161	(11)250	(11)141	(11)304		(9)105

TABLE B.22 CONTINUED

Age		hr	Pb^{203} (4)178	Sum of FP
Shot Tewa, Average Lagoon-Area Composition:				
45.8	min	0.763	(10)607	(4)6035
1.12	hrs	1.12	(10)605	(4)3947
1.64	hrs	1.64	(10)600	(4)2430
2.40	hrs	2.40	(10)594	(4)1470
3.52	hrs	3.52	(10)586	(5)8831
5.16	hrs	5.16	(10)573	(5)5246
7.56	hrs	7.56	(10)555	(5)3252
11.1	hrs	11.1	(10)529	(5)2214
16.2	hrs	16.2	(10)495	(5)1524
23.8	hrs	23.8	(10)449	(6)9968
1.45	days	34.8	(10)386	(6)6037
2.13	days	51.1	(10)310	(6)3427
3.12	days	74.9	(10)226	(6)1983
4.57	days	109.7	(10)142	(6)1243
6.70	days	160.8	(11)719	(7)7919
9.82	days	235.7	(11)265	(7)5126
14.4	days	345.6	(12)614	(7)3366
21.1	days	506.4	(13)719	(7)2287
30.9	days	741.6	(14)313	(7)1566
45.3	days	1,087		(7)1048
66.4	days	1,594		(8)6888
97.3	days	2,335		(8)4499
143	days	3,432		(8)2734
208	days	4,992		(8)1401
301	days	7,224		(9)5868

TABLE B.22 CONTINUED

Age	hr	Na^{24} (2)284	Cr^{51} (3)297	Mn^{54} (3)53	Fe^{59} (3)167	Co^{57} (3)182	Co^{58} (3)289	Co^{60} (3)81	Cu^{64} (2)228	Ta^{182} 0.01
Shot Tewa, Average Cloud and Outer Fallout Area Composition:										
45.8 min	0.763	(7)310	(11)719	(11)843	(10)163	(11)541	(10)256	(11)339	(8)901	(8)109
1.12 hrs	1.12	(7)304	(11)719	(11)843	(10)163	(11)541	(10)256	(11)339	(8)880	(8)109
1.64 hrs	1.64	(7)298	(11)719	(11)843	(10)163	(11)540	(10)256	(11)339	(8)855	(8)109
2.40 hrs	2.40	(7)287	(11)719	(11)843	(10)163	(11)540	(10)256	(11)339	(8)825	(8)109
3.52 hrs	3.52	(7)273	(11)719	(11)843	(10)163	(11)540	(10)255	(11)339	(8)775	(8)109
5.16 hrs	5.16	(7)253	(11)716	(11)843	(10)163	(11)540	(10)255	(11)339	(8)709	(8)109
7.56 hrs	7.56	(7)226	(11)713	(11)843	(10)162	(11)540	(10)255	(11)339	(8)622	(8)109
11.1 hrs	11.1	(7)192	(11)713	(11)843	(10)162	(11)540	(10)255	(11)339	(8)515	(8)109
16.2 hrs	16.2	(7)152	(11)707	(11)843	(10)162	(11)540	(10)254	(11)339	(8)390	(8)109
23.8 hrs	23.8	(7)106	(11)701	(11)843	(10)161	(11)539	(10)253	(11)339	(8)260	(8)108
1.45 hrs	34.8	(8)648	(11)695	(11)843	(10)160	(11)539	(10)252	(11)339	(8)143	(8)108
2.13 days	51.1	(8)304	(11)683	(11)843	(10)158	(11)538	(10)251	(11)339	(9)593	(8)108
3.12 days	74.9	(8)102	(11)665	(11)837	(10)156	(11)536	(10)248	(11)339	(9)165	(8)107
4.57 days	109.7	(9)205	(11)642	(11)837	(10)152	(11)534	(10)245	(11)339	(10)237	(8)106
6.70 days	160.8	(10)194	(11)606	(11)832	(10)147	(11)531	(10)240	(11)338	(11)159	(8)105
9.82 days	235.7	(12)594	(11)561	(11)827	(10)140	(11)527	(10)233	(11)338	(13)285	(8)103
14.4 days	345.6		(11)499	(11)816	(10)131	(11)521	(10)223	(11)337		(8)100
21.1 days	506.4		(11)422	(11)806	(10)118	(11)512	(10)209	(11)336		(9)960
30.9 days	741.6		(11)327	(11)790	(10)102	(11)499	(10)190	(11)335		(9)904
45.3 days	1,087		(11)227	(11)763	(11)815	(11)481	(10)166	(11)333		(9)828
66.4 days	1,594		(11)132	(11)726	(11)590	(11)456	(10)135	(11)330		(9)729
97.3 days	2,335		(12)603	(11)678	(11)367	(11)421	(10)100	(11)327		(9)603
143 days	3,432		(12)188	(11)610	(11)182	(11)374	(11)644	(11)322		(9)458
208 days	4,992		(13)362	(11)526	(12)673	(11)317	(11)347	(11)314		(9)307
301 days	7,224		(14)336	(11)425	(12)161	(11)250	(11)141	(11)304		(9)175

TABLE B.22 CONTINUED

Age		Pb^{203}	Sum of FP
	hr	(4)178	
Shot Tewa, Average Cloud and Outer Fallout Area Composition:			
45.8	min	0.763	(10)607	(3)1171
1.12	hrs	1.12	(10)605	(4)7727
1.64	hrs	1.64	(10)600	(4)4870
2.40	hrs	2.40	(10)594	(4)3015
3.52	hrs	3.52	(10)586	(4)1868
5.16	hrs	5.16	(10)573	(4)1175
7.56	hrs	7.56	(10)555	(5)7600
11.1	hrs	11.1	(10)529	(5)5065
16.2	hrs	16.2	(10)495	(5)3337
23.8	hrs	23.8	(10)449	(5)2124
1.45	days	34.8	(10)386	(6)1326
2.13	days	51.1	(10)310	(6)8054
3.12	days	74.9	(10)226	(6)4914
4.57	days	109.7	(10)142	(6)3154
6.70	days	160.8	(11)719	(6)2061
9.82	days	235.7	(11)265	(6)1353
14.4	days	345.6	(12)614	(7)8691
21.1	days	506.4	(13)719	(7)5473
30.9	days	741.6	(14)313	(7)3355
45.3	days	1,087		(7)1968
66.4	days	1,594		(7)1126
97.3	days	2,335		(8)6652
143	days	3,432		(8)3877
208	days	4,992		(8)1989
301	days	7,224		(9)8710

* Assumed same as Mn^{54} from ratio observed at Navajo.

† Based on ratio Sb^{122}/Sb^{124} for cloud sample.

‡ Based on ratio Ta^{180}/Ta^{182} for cloud sample.

§ Based on ratios U^{240}/U^{239} and U^{240}/U^{237} for cloud sample.

¶ Assumed same as Ta^{182}.

TABLE B.24 COMPUTED BETA-DECAY RATES

Beta-emission rates for fission products (FP) and induced products (IP) are computed and summed for the total emission rate in units of (β/sec)/10^4 fissions. Product/fission ratios are listed directly under the nuclide symbol. Conversion to counting rates, (counts/sec)/10^4 fissions, for a weightless mount and (point) source is made in the last column by means of the shelf factor G_n for comparison with experimental results (Table B.25). Numbers in parentheses indicate the number of zeros between the decimal point and the first significant figure, e.g., (2)200 = 0.00200.

Age	Na^{24}	Co^{57}	Co^{58} *	Cu^{64} †	Sum of FP	counts/sec / 10^4 fissions (G_1 = 0.2628)
hr	0.00145	0.0036	0.0053	0.00217		
Shot Flathead, Average Fallout Composition:						
45.8 min	0.763	(3)180	No β	(6)756	(3)178	1.544	0.5274
1.12 hrs	1.12	(3)177		(6)756	(3)174	1.009	0.3324
1.64 hrs	1.64	(3)173		(6)755	(3)169	0.634	0.1969
2.40 hrs	2.40	(3)167		(6)755	(3)163	0.398	0.1166
3.52 hrs	3.52	(3)158		(6)754	(3)153	0.255	(1)7335
5.16 hrs	5.16	(3)146		(6)754	(3)140	0.166	(1)4893
7.56 hrs	7.56	(3)131		(6)754	(3)123	0.109	(1)3364
11.1 hrs	11.1	(3)111		(6)752	(3)102	(1)716	(1)2343
16.2 hrs	16.2	(4)880		(6)751	(4)773	(1)456	(1)1615
23.8 hrs	23.8	(4)618		(6)748	(4)513	(1)282	(1)1103
1.45 days	34.8	(4)376		(6)745	(4)283	(1)176	(2)7640
2.13 days	51.1	(4)175		(6)740	(4)117	(1)109	(2)5256
3.12 days	74.9	(5)590		(6)733	(5)327	(2)674	(2)3564
4.57 days	109.7	(5)119		(6)723	(6)498	(2)452	(2)2430
6.70 days	160.8	(6)112		(6)708	(7)315	(2)309	(2)1580
9.82 days	235.7	(8)344		(6)688	(9)566	(2)212	(3)9708
14.4 days	345.6	(10)230		(6)658	(11)141	(2)145	(3)5770
21.1 days	506.4			(6)617		(3)972	(3)3374
30.9 days	741.6			(6)561		(3)637	(3)1957
45.3 days	1,087			(6)489		(3)411	(3)1145
66.4 days	1,594			(6)398		(3)262	(4)6968
97.3 days	2,335			(6)296		(3)170	(4)4478
143 days	3,432			(6)191		(3)105	(4)2765
208 days	4,992			(6)102		(4)590	(4)1553
301 days	7,224			(7)417		(4)311	(5)8184

TABLE B.24 CONTINUED

Age	hr	Na^{24}	Mn^{56}	Fe^{59}	Co^{58} *	Co^{60}	Cu^{64} †	Ta^{180} §	Ta^{182}
		0.0314	0.094	0.0033	0.00193	0.0087	0.0278	0.038	0.038
Shot Navajo, Average Fallout Composition:									
45.8 min	0.763	(2)389	(1)572	(5)585	(6)275	(6)363	(2)228	(2)840	(4)267
1.12 hrs	1.12	(2)383	(1)519	(5)585	(6)275	(6)363	(2)223	(2)817	(4)267
1.64 hrs	1.64	(2)374	(1)451	(5)585	(6)275	(6)363	(2)217	(2)779	(4)267
2.40 hrs	2.40	(2)361	(1)368	(5)585	(6)275	(6)363	(2)209	(2)733	(4)267
3.52 hrs	3.52	(2)342	(1)273	(5)584	(6)275	(6)363	(2)197	(2)655	(4)267
5.16 hrs	5.16	(2)317	(1)175	(5)584	(6)275	(6)363	(2)180	(2)578	(4)267
7.56 hrs	7.56	(2)284	(2)918	(5)583	(6)274	(6)363	(2)158	(2)471	(4)267
11.1 hrs	11.1	(2)241	(2)356	(5)581	(6)274	(6)363	(2)131	(2)349	(4)267
16.2 hrs	16.2	(2)191	(3)904	(5)580	(6)273	(6)363	(3)991	(2)226	(4)266
23.8 hrs	23.8	(2)134	(3)118	(5)577	(6)272	(6)363	(3)658	(2)119	(4)266
1.45 days	34.8	(3)813	(5)610	(5)573	(6)271	(6)363	(3)363	(3)464	(4)265
2.13 days	51.1	(3)380	(7)785	(5)567	(6)270	(6)363	(3)150	(3)116	(4)264
3.12 days	74.9	(3)128	(9)132	(5)558	(6)267	(6)362	(4)418	(4)154	(4)262
4.57 days	109.7	(4)257		(5)546	(6)263	(6)362	(5)639	(6)798	(4)260
6.70 days	160.8	(5)243		(5)529	(6)258	(6)362	(6)404	(7)104	(4)256
9.82 days	235.7	(7)744		(5)504	(6)250	(6)361	(8)726	(10)178	(4)252
14.4 days	345.6	(9)499		(5)470	(6)240	(6)361	(10)181		(4)245
21.1 days	506.4			(5)424	(6)225	(6)360			(4)235
30.9 days	741.6			(5)365	(6)204	(6)359			(4)222
45.3 days	1,087			(5)292	(6)178	(6)357			(4)203
66.4 days	1,594			(5)212	(6)145	(6)354			(4)179
97.3 days	2,335			(5)132	(6)108	(6)350			(4)148
143 days	3,432			(6)653	(7)694	(6)345			(4)112
208 days	4,992			(6)241	(7)372	(6)337			(5)752
301 days	7,224			(7)579	(7)152	(6)325			(5)429

TABLE B. 24 CONTINUED

Age hr	Sum of FP	Counts/sec per 10^4 fissions ($G_3 = 0.0958$)
Shot Navajo, Average Fallout Composition:		
45.8 min 0.763	1.544	0.172
1.12 hrs 1.12	1.009	0.113
1.64 hrs 1.64	0.634	(1)714
2.40 hrs 2.40	0.398	(1)455
3.52 hrs 3.52	0.255	(1)300
5.16 hrs 5.16	0.166	(1)201
7.56 hrs 7.56	0.109	(1)136
11.1 hrs 11.1	(1)716	(2)913
16.2 hrs 16.2	(1)456	(2)599
23.8 hrs 23.8	(1)282	(2)382
1.45 days 34.8	(1)176	(2)242
2.13 days 51.1	(1)109	(2)149
3.12 days 74.9	(2)674	(3)912
4.57 days 109.7	(2)452	(3)592
6.70 days 160.8	(2)309	(3)388
9.82 days 235.7	(2)212	(3)252
14.4 days 345.6	(2)145	(3)162
21.1 days 506.4	(3)972	(3)103
30.9 days 741.6	(3)637	(4)663
45.3 days 1,087	(3)411	(4)422
66.4 days 1,594	(3)262	(4)271
97.3 days 2,335	(3)170	(4)179
143 days 3,432	(3)105	(4)112
208 days 4,992	(4)590	(5)643
301 days 7,224	(4)311	(5)343

* 0.57 β^+/dis. † 0.128 β^+/dis. ‡ 0.21 β^-/dis. § Product ratio assumed same as Ta^{182}.

TABLE B.28 HOW ISLAND SURVEYS, STATION F

I. OBSERVED IONIZATION RATES

"Closed Window" readings 3 feet above ground at points shown on station layout (Figure 2.8).

Survey Time (Mike)		Hours Since ZU	FL	NA	TE	Ionization Rate, mr/hr F-B1	F-B2	F-B3	F-B4	F-B5	F-B6	F-B7	F-B8	F-B9	F-B10	F-B11	F-B12	Mean and σ	Instrument Type and Serial
6 May	1200	—	—	—	—	0.20	0.20	0.20	0.20	0.40	0.40	0.20	0.20	0.20	0.20	0.20	0.20	0.23	T1B 2443
21	1615	—	—	—	—	0.05	0.05	0.10	0.05	0.50	0.20	0.10	0.10	0.10	0.10	0.20	0.30	0.15	MX-5 17539
22	1120	—	—	—	—	0.10	0.10	0.20	0.15	0.30	0.20	0.15	0.10	0.10	0.10	0.20	0.25	0.16	MX-5 65008
23	1040	—	—	—	—	0.20	0.20	0.20	0.20	0.40	0.40	0.20	0.20	0.20	0.20	0.20	0.20	0.32	T1B 2443
26	0930	—	—	—	—	0.10	0.10	0.20	0.20	0.30	0.20	0.15	0.10	0.10	0.10	0.15	0.20	0.28	MX-5 65008
28	1710	11.2	—	—	—	—	1400	—	1600	1800	—	—	—	1800	1800	1800	1800	1714 ± 157	Cutie Pie 5028
29	1216	30.3	—	—	—	590	580	600	570	580	530	560	580	550	580	450	560	561	Cutie Pie 5028
30	1025	52.5	—	—	—	300	300	310	300	310	320	290	240	250	340	240	300	292	Cutie Pie 5501
1 June	1032	100.6	—	—	—	150	160	160	160	140	160	140	100	110	160	110	160	142	Cutie Pie 0325
2	1008	124.2	—	—	—	100	110	110	100	110	120	100	84	88	110	86	100	101	Cutie Pie 5501
3	1053	149.0	—	—	—	89	88	94	89	88	99	85	68	68	90	63	88	84.1	Cutie Pie 5501
5	1135	197.6	—	—	—	60	61	65	59	60	73	57	44	46	59	44	64	57.7	Cutie Pie 5501
7	1230	246.6	—	—	—	45	46	48	46	48	62	40	28	30	40	32	38	41.9 ± 9.4	Cutie Pie 5516
12	1620	370.4	9.9	—	—	22	20	21	22	—	31	24	14	16	21	15	24	20.9	Cutie Pie 5507
13	1015	388.3	27.8	—	—	20	22	22	20	20	30	22	18	18	20	18	20	20.8 ± 3.2	Cutie Pie 5516
14	1023	412.4	51.9	—	—	20	19	20	20	19	23	21	12	15	19	14	16	18.2	Cutie Pie 5501
9 July	1600	1,018	658	—	—	10	9	9	8	8	9	14	4	6	7	8	7	8.25 ± 2.4	T1B 580
11	1300	1,063	703	7.1	—	—	80	—	80	—	—	—	—	80	—	80	80	80.0	T1B 2058
11	1628	1,066	706	10.5	—	55	51	53	53	56	54	55	50	49	50	47	52	52.1	Cutie Pie 5501
12	1050	1,085	725	28.9	—	16	20	16	15	14	19	18	12	14	16	14	14	15.7	Cutie Pie 5516
13	1400	1,112	752	56.1	—	15	14	14	12	13	14	16	10	11	11	10	10	12.5	Cutie Pie 5502
21	1418	1,304	944	248.	8.5	240	—	—	260	—	—	180	—	240	—	210	240	228 ± 29	T1B 7234
21	1622	1,306	946	250	10.6	220	210	220	190	180	210	200	160	190	180	140	220	193 ± 25	Cutie Pie 5503
22	1022	1,324	946	268	28.6	95	86	94	88	90	110	91	75	79	82	71	89	87.5 ± 10.2	Cutie Pie 5516
23	1100	1,349	989	293	53.2	36	36	38	36	34	30	30	30	30	32	28	32	32.7 ± 3.2	T1B 7826
25	0836	1,395	1,035	339	98.8	21	21	22	20	20	25	23	16	15	19	16	18	19.7 ± 3.0	Cutie Pie 5507

TABLE B.28 HOW ISLAND SURVEYS, STATION F
II. RESOLUTION OF IONIZATION RATES BY EVENT

The ionization rates for Shots Zuni, Navajo, and Tewa are shown; Shots Flathead and Dakota produced negligible amounts of fallout.

Hours Since				Ionization Rate, mr/hr					
						TE			
ZU	FL	NA	TE	ZU *	Na †	By Diff. ‡	By Relative Decay §	Mean Observed and σ	Residual Error
								pct	pct
11.2	—	—	—	1,714	—	—	—	1,714 ± 9.18	—
30.3	—	—	—	561	—	—	—	561	—
52.5	—	—	—	292	—	—	—	292	—
100.6	—	—	—	142	—	—	—	142	—
124.2	—	—	—	101	—	—	—	101	—
149.0	—	—	—	84.1	—	—	—	84.1	—
197.6	—	—	—	57.7	—	—	—	57.7	—
246.6	—	—	—	41.9	—	—	—	41.9 ± 22.5	—
370.4	9.9	—	—	20.9	—	—	—	20.9	—
388.3	27.8	—	—	20.8	—	—	—	20.8 ± 15.6	—
412.4	51.9	—	—	18.2	—	—	—	18.2	—
1,018	658	—	—	8.82	—	—	—	8.25 ± 29.3	—
1,063	703	7.1	—	8.60	71.4	—	—	80.0	—
1,066	706	10.5	—	8.60	43.5	—	—	52.1	—
1,085	725	28.9	—	8.46	7.24	—	—	15.7	—
1,112	752	56.1	—	8.32	4.18	—	—	12.5	—
1,304	944	248	8.5	7.55	0.463	220	199.2	228 ± 12.5	−9.45
1,306	946	250	10.6	7.55	0.456	185	161.7	193 ± 13.2	−12.6
1,324	964	268	28.6	7.48	0.410	79.6	64.3	87.5 ± 11.7	−19.2
1,349	989	293	53.2	7.48	0.364	24.9	34.5	32.7 ± 9.88	+38.5
1,395	1,035	339	98.8	7.34	0.293	12.1	15.3	19.7 ± 15.4	+26.4

* Computed from ZU + 1018 hr and later by 4-π gamma relative ionization decay of How F-64 ZU, Tray 856.

† Computed from difference, observed ZU, to NA + 56.1 hours; thereafter by 4-π gamma relative ionization decay of YAG 40-A-1, Tray P-3753.

‡ Computed from difference, observed (ZU + NA).

§ Computed from best fit of 4-π gamma relative ionization decay of YFNB 13-E-57, Tray 1973.

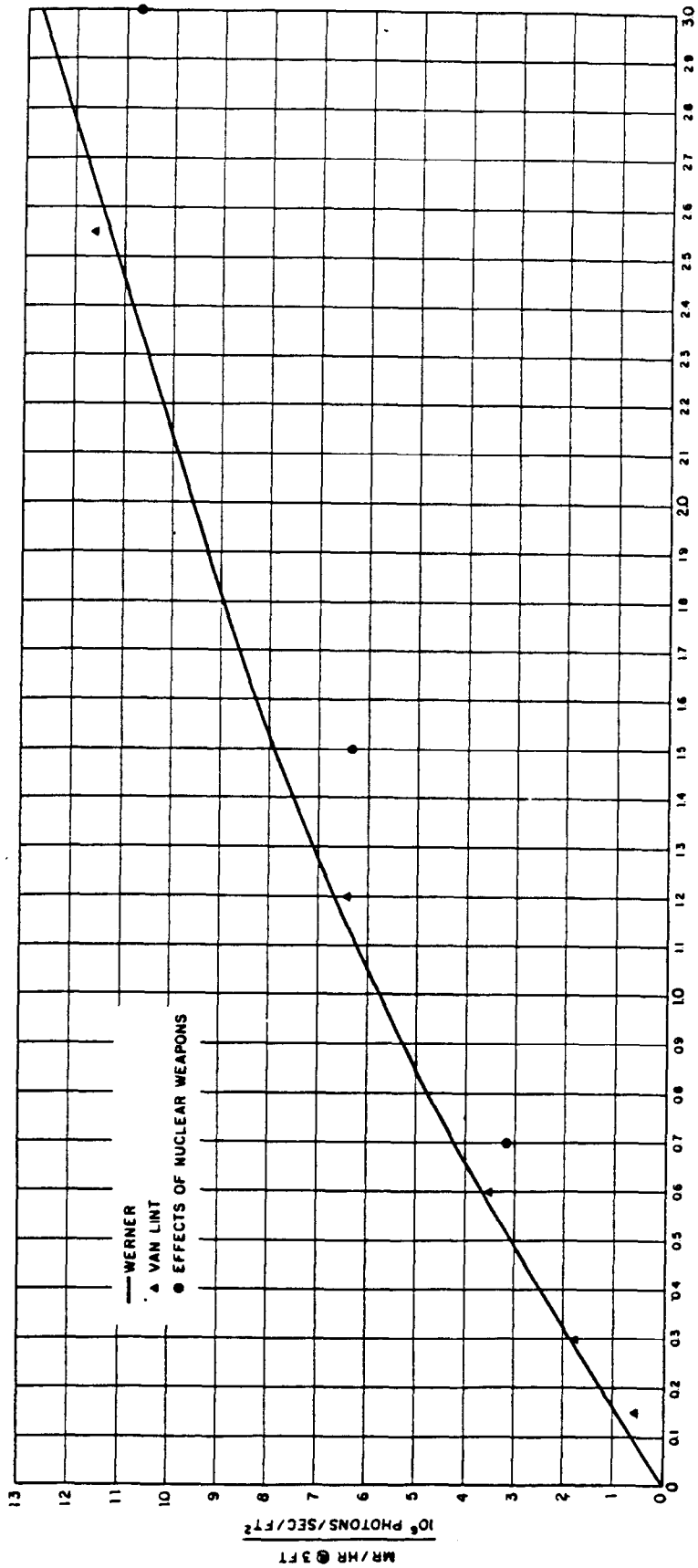

Figure B.6 Computed gamma-ionization rate above a uniformly contaminated smooth infinite plane.

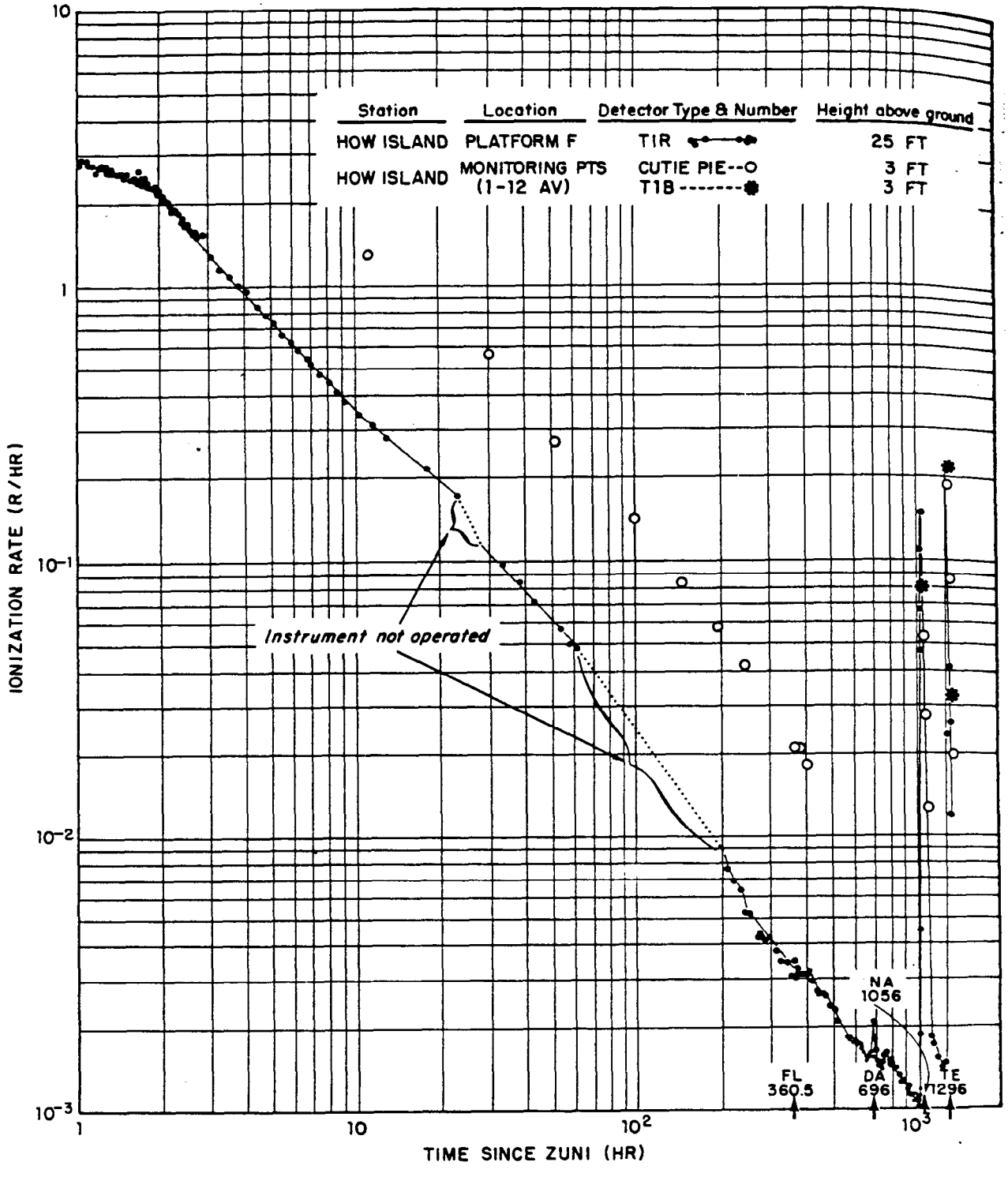

Figure B.7 Gamma-ionization-decay rate, Site How.

TABLE B.30 RADIOCHEMICAL ANALYSIS OF SURFACE SEA WATER AND YAG-39 DECAY-TANK SAMPLES

Shot	Bottle Number	Designator	Time of Collection	Location		Fission/ml	Fission/ft^3
				Latitude N	Longitude E		
			H+hr	deg min	deg min		
Zuni	8030	Y3-S-1B	26.1	13 00	165 11	1.94×10^{7}	5.49×10^{11}
	8035	Y3-T-1B	26.4	—	—	3.28×10^{7}	9.29×10^{11}
	8254	Y4-S-1B	16.1	12 25	165 26	8.20×10^{7}	2.32×10^{12}
Flathead	8544	Y3-S-1B	13.8	12 04	165 26	3.85×10^{6}	1.09×10^{11}
	8549	Y3-T-1B	14.1	—	—	3.29×10^{7}	9.32×10^{11}
Navajo	8052	M-MS-5A	43.0	12 44.3	162 40	4.72×10^{6}	1.34×10^{11}
	8053	M-MS-5B	43.0	12 44.3	162 40	5.97×10^{6}	1.69×10^{11}
	8241	M-MS Sta. 10	−39.6	11 41	165 11.5	2.88×10^{6}	8.16×10^{10}
	8242	M-MS Sta. 11	34.4	11 34.5	164 44.1	5.62×10^{5}	1.59×10^{10}
	8581	Y3-S-3B	18.2	11 59.5	165 15.5	4.16×10^{7}	1.18×10^{12}
	8585	Y3-T-3B	18.3	—	—	1.64×10^{6}	4.64×10^{12}
Tewa	8289	Y4-S-2B-T	18.0	12 06.0	165 00.5	9.97×10^{8}	2.82×10^{13}
	8326	Y3-S-1B-T	11.0	12 00.5	165 18	6.84×10^{8}	1.94×10^{13}
	8350	Y3-T-1B-T	52.0	—	—	1.15×10^{10}	3.26×10^{14}

* Estimated reliability ± 25 to 50 pct.